AIR/GAS SYSTEM DYNAMICS AND IMPLOSION CONTROL OF FOSSIL FUEL POWER PLANTS

by

Shang Zhi Wu

M.S., Massachusetts Institute of Technology, 1981

M.S. in Management of Technology, M.I.T., 1984

SUBMITTED TO THE DEPARTMENT OF MECHANICAL ENGINEERING IN PARTIAL FULFILLMENT OF THE REQUIREMENTS FOR THE DEGREE OF

DOCTOR OF PHILOSOPHY

at the

MASSACHUSETTS INSTITUTE OF TECHNOLOGY

October 1984

Signature of Author _____
Department of Mechanical Engineering
October 19, 1984

Certified by _____
David N. Wormley
Thesis Supervisor

Accepted by _____
Ain Sonin
Chairman, Department Committee

AIR/GAS SYSTEM DYNAMICS AND IMPLOSION CONTROL
OF FOSSIL FUEL POWER PLANTS

by

Shang Zhi Wu

Submitted to the Department of Mechanical Engineering on October 19, 1984 in partial fulfillment of the requirements for the degree of DOCTOR OF PHILOSOPHY.

Abstract

A computer-based mathematical model for analyzing power plant air/gas system transient dynamics has been developed. The model is formulated by representing power plant air/gas system components as a set of generic elements. This set of generic elements can be connected by generalized junction structures to represent a variety of plant configurations. The response of pressure, flow, temperature and heat transfer rate at any point in air/gas systems subjected to a wide range of fluid, mechanical and thermal disturbances can be determined by computer simulations. Such a formulation and simulation of air/gas system is particularly useful for studies of air/gas pressure dynamics coupled with thermal transients in the same time frame, such as boiler furnace implosions.

To validate the mathematical model and illustrate the use of the computer code, basic plant models for a coal-fired plant and an oil-fired plant have been developed. System responses to main fuel trips are simulated for both plants. The simulation predictions of furnace pressure excursions are in close agressment with the experimental data from field test results.

The computer simulation of the coal-fired plant has been used to evaluate various control systems for furnace and stack implosion protection. The simulation results have shown that a well designed draft control system can limit furnace pressure excursions to an acceptable level. The limitations of present control systems are the actuator speed and possible negative pressure

excursions in the stack during control actions. A preliminary study indicates that discharging steam into the furnace after fuel trip implosion condition may be an effective alternative solution, and the implementation of such a scheme merits further investigation.

Thesis Supervisor: David N. Wormley
Title: Professor of Mechanical Engineering

Acknowledgments

I am very fortunate to have had Professor David N. Wormley supervise both my master's and doctor's thesis. His insight, experience and careful guidance have made our association extremely rewarding for me. I also wish to thank Professors Peter Griffith, Henry M. Paynter and Derek Rowell for serving on my thesis committee. I am grateful for their valuable suggestions, criticism and encouragement.

Special thanks go to James Roseborough, Bruce Eason and John Samon for their technical assistance and helpful discussions, and to Leslie Regan for her help during my five years schooling at M.I.T.

I wish to extend my gratitute to my wife Xiao-xing and my parents for their love and support.

My education at M.I.T. is supported by a scholarship from Chinese Ministry of Educatoin and a research grant from Electric Power Research

Table of Contents

List of Figures

List of Tables

NOMENCLATURE

a - ash deposit absorptivity

A - duct cross section area, ft^2

A_a - cross section area of axial fan chamber, ft^2

A_h - heat transfer area, ft^2

A_i - heat transfer area of furnace compartment i, ft^2

A_r - flow resistance geometry coefficient

A_s - steam discharge valve area, ft^2

B - fuel activation energy

C - fuel concentration, lbm/ft^2

c - specific heat for solid, Btu/lbm F

c_c - heat exchanger cold side fluid specific heat, Btu/lbm F

c_h - heat exchanger hot side fluid specific heat, Btu/lbm F

C_o - speed of sound in fluid, ft/sec

C_{ox} - oxygen concentration, lbm/ft^3

C_p - gas specific heat at constant pressure, Btu/lbm F

C_v - gas specific heat at constant volume, Btu/lbm F

C_{st} - specific heat for steam, Btu/lbm F

C_w - specific heat for water, Btu/lbm F

d - fan impeller diameter, ft

D_o - diffusion coefficient

E_c - combustion energy generated, Btu/sec

E_w - energy needed to evaporate fuel moisture, Btu/sec

E_v - rate of energy release, Btu/sec.ft^3

f - fuid friction coefficient

G - control gain

h_i - energy flow rate at the ith branch of general junction, Btu/sec

h_{fg} - latent heat value for water, Btu/lbm

h_J - net energy flow into junction, But/sec

HT - ash hemispherical temperature, F

H_v - fuel heat value, Btu/lbm

I - flow inertance of axial fan element, 1/ft

k - thermal conductivity, Btu/ft^2,hr,F/ft

K - combustion rate constant

k_1 - conductivity of primary layer, Btu/hr ft F

k_2 - conductivity of secondary layer,Btu/hr ft F

k_c - reaction collison frequency constant

k_g - modification coefficient for resistance

l - heat transfer material thickness, in

L - length of transmission line, ft

l_1 - thickness of primary ash deposit layer, in

l_2 - thickness of secondary ash deposit layer, in

L_a - length of axial fan chamber, ft

l_f - mass transfer film thickness, in

M - gas mass, lbm

M_s - solid mass, lbm

P - pressure (inches of H_2O or lbf/ft^2)

P_J - pressure at general junction, inches of H_2O

PD - transmission line downsteam pressure, inches of H_2O

PU - transmission line upsteam pressure, inches of H_2O

ΔP_f - pressure drop acoss fans, inches of H_2O

Q - heat transfer, Btu/sec

Q_f - volume flow rate, ft^3/sec

q - heat transfer rate, Btu/sec. ft^2

q_i - average heat transfer rate in compartment i, Btu/sec, ft^2

r - critical pressure ratio

R - ideal gas constant (=53.3 lbf-ft/lbm R)

R_i - flow resistance at ith branch of general junction, (inches of H_2O sec/lbm)

R_t - combustion rate, lbm/sec.ft^3

r_c - chemical reaction controlling rate, 1/sec

r_m - mass transfer controlling rate, 1/sec

S - laplace operator

t - time, sec

T - temperature, ^oR

T_D - wave propagation delay time, sec

T_s - ash deposit surface temperature, ^oR

T_{is} - initial slag temperature, ^oF

T_{tb} - water tube temperature, ^oR

T_{st} - saturated steam temperature, ^oR

T_f - initial fuel temperature, ^oR

T_J - junction temperature, ^oR

T_{cv} - critical temperature for ash, ^oF

u - fan impeller tip speed, ft/sec

U - internal energy, Btu

U_i - reflected wave variable of ith transmission line at junction, inches of H_2O

U_c - convection film conductivity, Btu/hr R ft^2

UD - transmission line downstream right wave inches of H_2O

UU - transmission line upstream right wave inches of H_2O

v - flow velocity, ft/sec

V - volume, ft^3

VD - transmission line downstream left wave inches of H_2O

VU - transission line upstream left wave inches of H_2O

W - gas mass flow rate, lbm /sec

W_c - heat exchanger cold side flow rate, lbm/sec

W_h - heat exchanger hot side flow rate, lbm/sec

W_J - net mass flow into junction, lbm/sec

W_i - incoming mass flow, lbm/sec

W_o - outgoing mass flow, lbm/sec

WU - transmission line upstream flow

WD - transmission line down stream flow

W_f - fuel flow rate, lbm/sec

W_{fs} - initial fuel flow rate, lbm/sec

W_s - steam flow rate, lbm/sec

x - distance long transmission line, ft

Z_c - transmission line characteristic impedance (sec inches of H_2O/lbm)

α - fan imlet guide vane or blade angle, degrees

α_q - quadratic resistance coefficient, inches of $H_2O/(lbm/sec)^2$

α_d - damper angle, degrees

β - fluid bulk modulus

β_f - fraction of ash in fuel

ρ - fluid density, lbm/ft^3

λ - fuel moisture fraction

ϵ - ash deposit emissivity

ϵ_f - flame emissivity

σ - Stefan - Boltzmann constant for radiation

Φ - fan flow coefficient

Ψ - fan pressure coefficient

η - slag viscosity, poise

τ - time constant, sec

Chapter 1
INTRODUCTION

1.1 Background

Several dynamic problems are associated with the combustion air, flue and gas recirculation systems of fossil fuel electric power plants. These problems may be broadly classified as (1) steady state pulsation problems resulting in noise or duct and equipment vibration, and (2) transient and control problems leading to a possible implosion condition or instability.

Pulsation problems may generate sufficient noise to represent a health problem, sufficient vibration to result in structural damage or in the case of large amplitude low frequency pressure surging, sufficient pressure variation to cause equipment to trip or fail.

The transient control problem leading to a possible implosion is usually caused by a fuel trip or misoperation of the forced draft or induced draft fans in which the general fan-duct-furnace response leads to an excessively low furnace pressure. In an extreme transient response, the air/gas system may sustain structual damage.

A principal cause of a potential implosion results from a flameout after a main fuel trip (MFT). The basic physical factors resulting in a drop in pressure after a MFT are illustrated in Figure 1-1. Following a MFT, the temperature in the radiant furnace typically decreases from 2500 ^{o}F to approximately 1000 ^{o}F in a matter of a few seconds following the cutoff of

fuel. Since the airflow can not change instantaneously and increase the gas density in the furnace, the furnace pressure drops approximately as described by the ideal gas law. This drop in pressure may be large enough to cause structural damage.

Other potential causes of substantial negative pressure excursions include control system failures and incorrect fan operating procedures. For example, if an FD fan damper is suddenly closed while the ID fan is operating, a drop in furnace pressure occurs as a result of continuous ID fan suction of furnace gas. On the other hand, the negative pressure excursion may occur in the stack if the ID fan damper is suddenly closed.

A number of implosion incidents have been recorded in the past few years. The cost of such incidents from loss of generation and structural damage can be significant. Because of the trends to install larger balanced draft steam generating units, and the increased draft losses of flue gas cleaning units required for environmental control, ID fans with significant head are required. These factors have led to requirements for detailed evaluation of implosion conditions prior to plant construction or alteration.

1.2 Research Objectives

Research has been initiated to aid in developing solutions to air/gas system dynamic problems in fossil fuel plants. The specific objectives of this research are:

1. To develop a mathematical basis for understanding air/gas system dynamics for steady state and transient conditions.

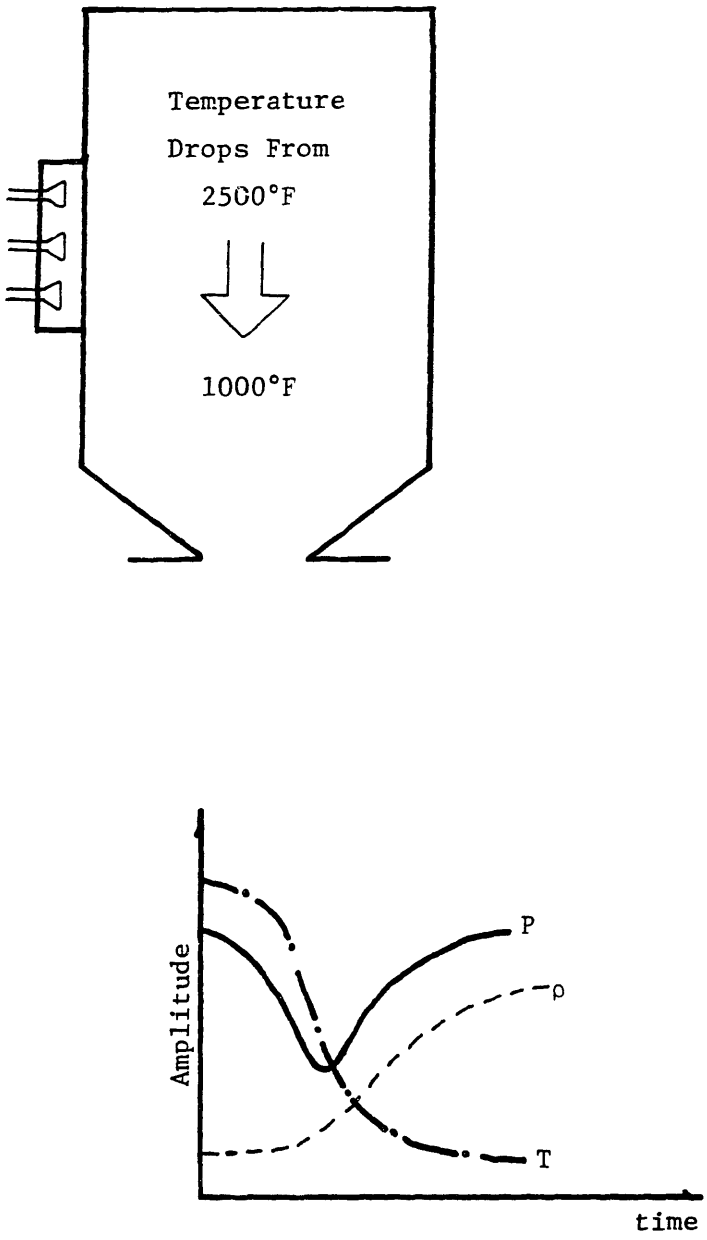

Figure 1-1: Furnace Implosion after a Main Fuel Trip

a. Define a set of generic elements to represent air/gas systems which are derived from fluid mechanic and thermodynamic laws. The elements can be either lumped- or distributed- parameter model for the thermofluid process representations.

b. Define a lumped - distributed parameter system structure using the generic elements and junction structures to form a variety of different air/gas system configuration for dynamic analysis. The system model should be capable of simulating coupled air/gas pressure dynamics with thermal energy transients.

c. Evaluate the capacity of the mathematical model to predict and analyze system dynamic behavior by comparison with experimental plant data.

2. To characterize the implosion phenomenon and evaluate the present and proposed implosion control systems through computer simulations.

a. Predict pressure and temperature responses at any point of an air/gas system after a thermofluid or mechanical disturbance

b. Characterize the implosion phenomenon for both coal and oil fired plants

c. Evaluate the effectiveness of implosion control systems including recently proposed bypass and steam discharge control systems

3. To develop general guidelines in air/gas system dynamic analysis and design for fossil fuel power plants

a. For existing plants, identify and evaluate solutions to the system dynamic problems, including passive and active damping systems.

b. For new plants, provide a basis for selection of system components to avoid system dynamic problems.

c. Provide simplified models for initial analysis and preliminary design.

1.3 Previous Work

Research on transient dynamics in power plant air/gas systems has been primarily motivated by implosion problems in utility boiler furnaces where sufficient negative pressure force developes to exceed the furnace structural strength. The cost of implosion incidents from loss of generation and structural damage can be significant. Probably the most conservative and expensive long term solution for furnace implosion prevention is to strengthen the boiler structure to withstand the maximum possible negative pressure in the transient. However, recent draft requirements such as the addition of stack gas scrubbers may require boiler structural design to withstand negative pressure as low as -50 inches of water. Thus, evaluation of control systems to prevent implosion has been of interest.

Electric utility companies have conducted many field tests to evaluate the potential implosion damage to both coal and oil fired plants [14] [15] [60] [55]. These test results usually include a set of pressure responses at different locations in the air/gas system after a fuel trip from various load conditions. These test data have provided important information in the field and have been used extentively for computer model calibration. One of the most useful pieces of information taken by Commonwealth Associates [31] at a field test was flame decay data, which can be used to estimate the actual flame energy release rate in the furnace zone after a main fuel trip. This estimated energy release rate has been used as fuel trip disturbances in most implosion computer

simulations.

Based on the field test results, computer simulation techniques have been used to characterize furnace implosions and to pursue control solutions. Laskowski [37] has shown that slowing down fuel shut-off rate is the most effective mechanism for reducing the furnace pressure excursions. This is so only because controls are given time to move FD and ID dampers. It has been noted that slowing down the fuel shut-off does not reduce pressure excursions if damper control are not in an automatic mode.

Leithner et al. [38] have simulated the pressure vibrations in the flue air/gas path with and without ID fans. They have demonstrated that the flow inertance and capacitance effects as well as fan characteristics together determine the pressure oscillations in air/gas systems.

Kirchmeier [32] [33] investigated the damper and fan characteristics along with furnace - ductwork dynamics in implosion conditions. He [34] also described the operating dynamics for both axial and centrifugal fans after a main fuel trip. An axial ID fan may stall when the furnace pressure drops after a MFT. The stall condition leads to an immediate flow reduction which reduces the drop in furnace pressure. However, the fan stall may be too late to be any help for implosion prevention and the simulation results show that oscillations may be present throughout the draft system in fan stall conditions.

The ID fan head has been recognized by Euchner and Undrill [13] as an important parameter in implosion. On the basis of reported incidents and field tests, the maximum negative furnace pressure is not likely to exceed the low gas flow maximium head capacity of the ID fan. A major objective of the final design is to limit draft equipment maximum head capacity to that required for

satisfactory operation. Euchner has defined an ID fan control scheme that keeps the fan operating within a head limit. Special consideration is given to selection of the fan and the duct arrangement to limit the negative head developed before the ID fan sustains to low flue gas flow rates.

The simulation results of many plant models have shown that feedback control alone may be too slow for the furnace implosion control after a MFT. The National Fire Protection Association (NFPA) has issued a general guideline for furnace implosion protection called Standards for Prevention of Furnace Implosions [42]. Several methods for controlling implosions have been proposed to meet the standards.

A three mode control system was suggested by Kirchmeier [34] to include a feed forward loop which can use a MFT signal directly to move the control devices even before the negative furnace excursion occurs. After the furnace pressure excursion phenomena are well documented by field tests and model simulation, a predesigned function may be used for the forward control signal generation.

An ID fan bypass control system for implosion control has been described in reference [35] by Koennman. Small and fast acting dampers are installed in parallel with the ID fans. When these dampers are modulated open, they provide an additional flow path for the fans. The flow through the fan itself is in the forward direction while the flow into the bypass path is in the backward direction. The flow into and flow out of the bypass system are equal by the continuity principle. The objective of the bypass control system is to decrease the net flow through the bypassed ID fan system while limiting or even decreasing the pressure rise across the ID fan. This objective can not be accomplished without a bypass path due to the downward slope of the fan

characteristics. When the furnace negative pressure occurs, the control command signal from the controller opens the bypass damper. The backward flow through the bypass damper increases at a faster rate than the flow through the fan. The sum of these two flows are reduced even though the flow through the ID fan may have increased. The major advantage in using the ID fan bypass control system is that the bypass damper is much smaller and faster acting than the damper installed in the main ducts. After a MFT the flow of the flue gas from the furnace can be reduced faster because of this fast damper action. This in turn provides a more effective implosion control.

A review of the literature on implosion and other thermal transients related air/gas dynamics studies indicates that there is a need for a systematic approach to the problems -- both on the modeling of the coupled thermofluid processes and the evaluation of proposed control systems. While power plants may differ considerably in detail, the basic types of components are similiar in most plants. It is desirable to characterize such components as generic elements and to construct the plant model using the generic elements as building blocks.

The general concept of such a system approach has been developed and demonstrated by theories of Linear Graphs [52] and Bond Graphs [43]. The analytical development of the generic elements in this research has built upon the publications on thermofluid process by H. Paynter [44] and R. Franks [17]; the gas and water transmission systems by F. Ezekiel and H. Paynter [46], R. Sidell and D. Wormley [54], F. Goldschmied, D. Wormley and D. Rowell [21] and Pseudo Bond Graphs by D. Karnopp [27] [28] [29].

The development of the Modular Modeling System (MMS) [41] has taken a systematic approach for power plant dynamics modeling and simulation. A model of a power plant of any arbitary configuration may be assembled from

pre-programmed generic MMS component models. Each significant physical component of the plant is represented by an element module. The user merely defines component data and interconnections while MMS will construct system equations and simulate the system dynamics. Although MMS includes practically all components in the flue air/gas path from the pulverizer through the furnace to the air heater, its main application is for the steam/water side. In the MMS code, the air/gas side is decoupled from the steam/water side for efficient execution. It retains only the energy dynamics on the air/gas side but not the pressure dynamics.

Also taking a systematic approach, M.I.T has performed research on power plant air/gas dynamics since 1980. The research has led to the development of a mathematical model which characterizes the propagation of disturbances from a source to any point in a plant, to measurement and analysis of pulsation data at 125 MW and 500 MW plants, and to evaluation of the mathematical model with experimental data. The general results of the study have identified from field test data that air preheaters and fans are primary system sources of disturbance. In both plants tested, the strongest disturbances were generated in system recirculation loops and resulted from operation of the recirculation fans at low flow rates corresponding to a stall condition. Characterization of fan stall-related disturbances have been performed through laboratory studies. These research results have been summarized in references [20] [21] [22] [23] [24]. A further development from the pulsation studies at M.I.T. was the establishment of a user-friendly computer code DUCSYS [51] which uses a well defined set of generic elements to represent different system configurations. The code DUCSYS simplifies plant modeling and increases the potential use of the computer model for

air/gas dynamic analysis. The elements developed in DUCSYS are isothermal elements. They can simulate neither the interaction of internal energy with pressure and kinetic energy in an element nor the heat transfer between elements.

In between MMS and DUCSYS, there is an absence of modeling and simulation capability which represents the coupled air/gas pressure dynamics with system thermal energy transients.

1.4 Summary of Results

A computer-based mathematical model for analyzing power plant air/gas system transient implosions has been developed. The responses of pressure, flow, temperature, and heat transfer rate at any point of the system can be determined by the simulation model subject to a wide range of fluid, mechanical and thermal disturbances.

The mathematical model is formulated by representing a plant as a set of generic elements. These elements are coupled together by junction structures to represent the air/gas thermofluid system configurations. The model can analyze the air/gas system responses to a variety of fluid, mechanical and thermal disturbances. It is particularly useful in studies of air/gas pressure dynamics coupled with thermal transients in the same time frame such as furnace implosions. The model has been implemented in a modular computer program which can be utilized to represent a wide variety of plant configurations.

In order to conduct a complete implosion study using the mathematical model, the fuel combustion process has been included in the model and the

fuel mass flow is represented as a direct disturbance to the system.

The model includes an initial steady state analysis capability. Two alternative approaches can be selected according to the application. One is primarily for new plant design when all the plant design parameters are assumed as known. In this case the system parameters such as flow resistances and heat transfer coefficients are then calculated from their analytical expressions. For an existing plant, initial steady state pressures and temperatures at points in the plant may be measured and used as a baseline. The system parameters, including flow resistances, heat transfer coefficients and slag or ash deposit quantity, can then be estimated from this measured data.

To validate the mathematical model and illustrate use of the computer code, basic system models for the Detroit Edison coal fired St. Clair Unit 3 and the oil fired Greenwood Unit 1 plants have been developed. Main fuel trip simulations have been conducted for both plants. The simulation predictions of the furnace pressure excursion for the two plants are in close agreement with the data from the field implosion tests in terms of magnitude and time delay after a MFT. The applicability of the model for both predicting the furnace pressure excursion and designing an implosion control system has been demonstrated.

In the coal fired plant, the coal-ash deposit on the waterwall tubes has been identified as an important factor in determining the maximum pressure excursion after the main fuel trip. This is due to the fact that the ash deposit may have a larger heat capacity than the combustion gas inside the furnace. After the fuel trip, the furnace gas temperature may drop below the ash deposit temperature causing heat transfer from the ash deposit to the flue gas inside the furnace. An analytical model is developed to represent the ash

deposit and a formal procedure is also outlined to estimate the steady state heat transfer rate and the amount of deposition.

The system models used for the St. Clair and Greenwood plants are detailed, nonlinear models. For preliminary design studies, one simplified simulation model and its linearized version have been developed. If only furnace pressure is of interest and the control action is slow, their use for implosion studies is acceptable.

The detailed mathematical model has been used to evaluate various implosion control system designs. A set of damper and fan inlet guide vane positions can be modeled as control actions. The basic control scheme was formulated according to furnace protection standards [42]. Different physical control system implementations and actuator designs have been investigated using the computer model. These simulation results have shown that well designed draft control systems can limit pressure excursions in the furnace to an acceptable level. The limitations of these systems are the control actuator speed and the maximum negative pressure excursion in stack during the control actions. A steam discharge implosion control system has been proposed to overcome the above limitations. Preliminary study has shown that the steam discharge control system can be very effective, and further evaluation of implementattion of such a scheme is merited.

Chapter 2
MATHEMATICAL REPRESENTATION OF PLANT AIR/GAS ELEMENTS

2.1 General Concept

The air/gas system of a typical fossil fuel power plant consists of a number of common components as illustrated in Figure 2-1 and cited below:

1. A forced-draft fan system which supplies ambient air through the ductwork and air preheater to the furnace.

2. A furnace where combustion occurs to increase the temperature of the gas in the furnace and heat is transfered to the boiler tubes to generate steam.

3. A high temperature flue gas system including a superheater, reheater, economizer and an air preheater.

4. A low-temperature flue gas system consisting of the induced-draft fans, precipitator and scrubbers, ductwork and the stack.

5. An optional recirculation system consisting of a recirculation fan and duct which recirculates the hot gases from the economizer outlet into the furnace bottom to aid in controlling steam temperature.

While plants may differ considerably in detail, the basic types of components shown in Figure 2-1 are typical of the components in most plants, thus the representation of air/gas system dynamics must include the characteristics of these components.

A system model to represent plants containing these components may be

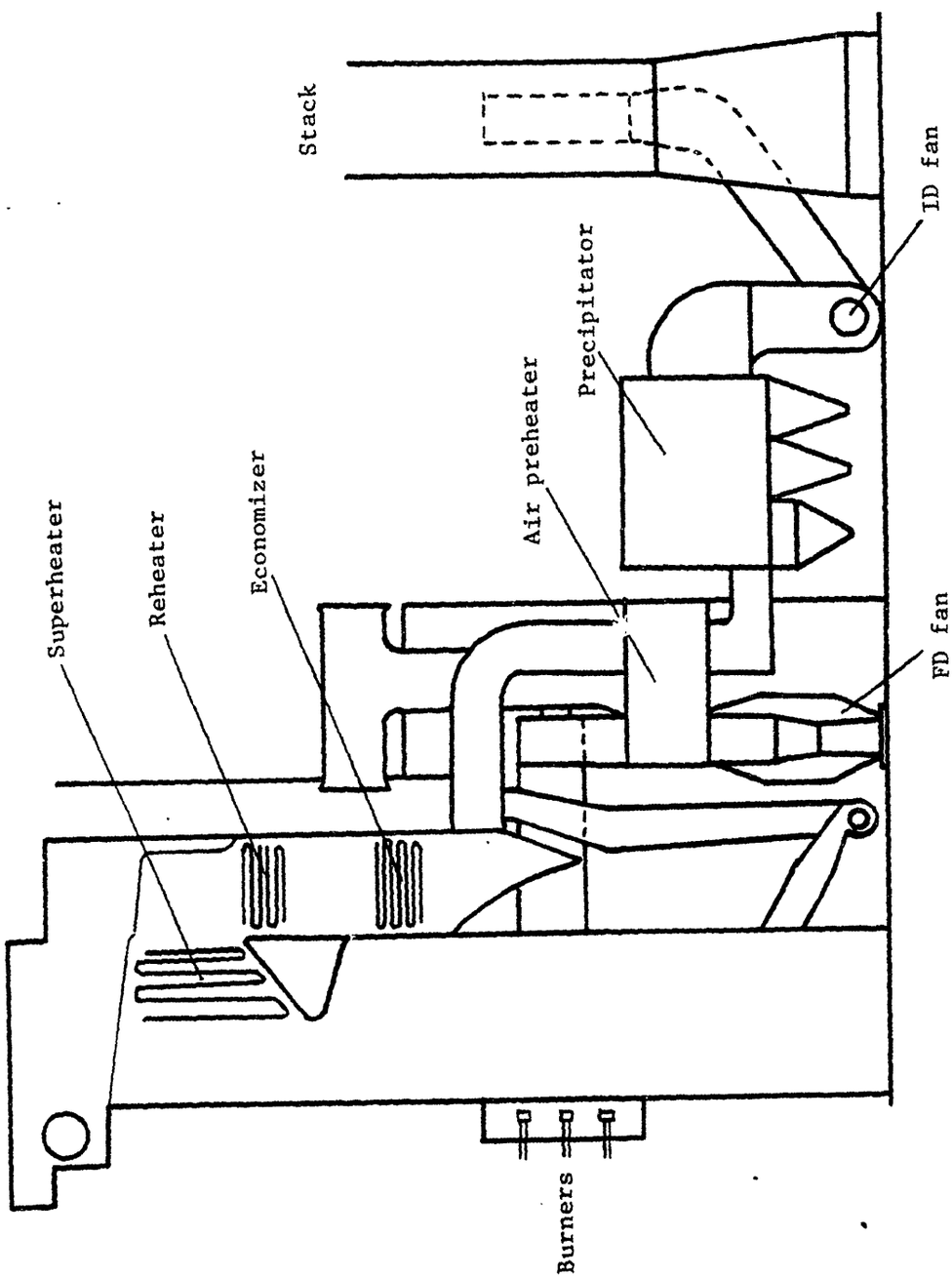

Figure 2-1: A Typical Power Plant Air/Gas System Configuration

constructed using a finite set of generic elements which are interconnected through junction structures to represent a given plant configuration.

2.2 Element Development

In this study, lumped parameter elements (plenum volume, flow resistance and thermal heat exchanger) are coupled with distributed parameter elements(uniform duct sections) to represent power plant thermo-fluid systems. This coupled analysis technique has been sucessfully applied to the analysis of liquid and gas piping systems, water distribution systems and power plants as described in references [46], [56], [54] and [19]. In the representation, each element is derived from basic principles of thermodynamics and fluid mechanics including the conservation laws of mass, energy and momentum and the equations of state for the operating fluid. Lumped parameter elements in the model are assumed to have spatially uniform pressures, densities and temperatures. Distributed parameter transmission line elements are one-dimensional and represent pressure and flow waves with wavelengths which are long compared to the duct width and height. Thus, highly localized flows are represented only in terms of their influence on the primary one-dimensional flow.

In the analysis, the pressures, flows and temperatures at any point in the system are computed resulting from a disturbance at any specified point in the system.

The principal elements included in this study are:

1. A plenum volume element represents the mass and energy balance in a large gas volume.

2. A furnace element which represents the radiant furnace gas volume where combustion of the fuel occurs.

3. A transmission line element which represents ductworks by one-dimensional pressure and flow waves with an internal energy balance over the duct vloume which determines a uniform but temperature dependent propagation speed in ducts.

4. A centrifugal fan element which represents the normalized fan pressure - flow characteristics in terms of the inlet guide vane or damper angle, motor speed and gas density as independent parameters.

5. An axial fan element which represents the normalized fan pressure - flow characteristics in terms of the blade angle, motor speed and gas density as independent parameters. The gas flow inertance through the fan chamber is also included.

6. A flow resistance element which represents the flow - pressure drop characteristics in a general temperature dependent quadratic form.

7. A mechanical damper element which represents flow - pressure drop characteristics across the damper as function of damper angle.

8. A family of heat transfer elements which represent the heat transfer in forms of conduction, convection and radiation.

9. A solid thermal element which represents energy storage in metals, slags and ashes.

10. A heat exchange element which represents the energy balance at superheaters, economizers and air heaters.

2.2.1 Plenum Volume Element

The plenum volume element represents the gas dynamics inside a structural volume. The gas is assumed to be ideal and spatially uniform with respect to temperature and pressure. A schematic representation of the element is shown in Figure 2-2.

The mathematical equations representing the element may be derived from mass and energy conservation principles and ideal gas laws as:

$$dM/dt = W_i - W_o \tag{2.1}$$

$$dU/dt = c_p T_i W_i - c_p T W_o - Q \tag{2.2}$$

$$T = VP/RM = U/c_v M \tag{2.3}$$

where: M = gas mass in plenum, lbm

T = temperature in plenum, ^{o}R

U = internal energy in plenum, Btu

V = plenum volume, ft^3

W = mass flow rate, lbm/sec.

R = gas constant, (= 53.3 lbf-ft/lbm R)

c_v = specific heat of ideal gas at constant volume

Q = rate of heat transfer leaving the plenum, Btu/sec.

Although the schematic and mathematical representations of the plenum element developed here include only a single inlet and outlet flow, an extension to general multiple inlet and outlet flows is straightforward.

2.2.2 Combustion Furnace Element

The combustion furnace element equations are formulated utilizing perfectly stirred reactor (PSR) theory. The steady state characteristics of a combustion chamber have been successfully represented, as described in

reference [11] using the PSR model. The extension of the PSR model for transient analysis is developed here for representation of combustion after a fuel trip.

In a perfectly stirred reactor as illustrated in Figure 2-3 incoming fuel is assumed to be dispersed uniformly throughout the reactor. The uniform fuel distribution assumption within a PSR reduces the theoretical requirements to an overall mass and energy balance on the reactor, plus a reaction rate equation per unit of reactor volume. The simplicity of the perfectly stirred model results from the neglect of spatial variations. The fuel concentration and temperature gradients in a large boiler furnace space thus must be represented by a number of PSR elements.

Both gas mass flow and fuel mass flow may be injected into a PSR. By the PSR assumption, the incoming materials are distributed instantaneously and uniformly throughout the PSR. In the process, they are mixed with and diluted by the materials already present. A unique gas density and an unburnt fuel concentration represent the mass states of the PSR. The unburnt fuel mass conservation can be expressed with the assumption that the unburnt fuel particles or droplets leave the PSR at the same speed as the exiting gas. The equation (2.4) implies that the rate of accumulation of unburnt fuel is equal to fuel flow into the PSR minus the fuel burning rate.

$$dC/dt = W_f/V + C_iW_i/\rho_iV - CW_o/\rho V - R_t \qquad (2.4)$$

where: C = concentration of unburnt fuel, lbm/ft^3

W_f = fuel mass flow rate, lbm/sec.

V = volume of PSR, ft^3

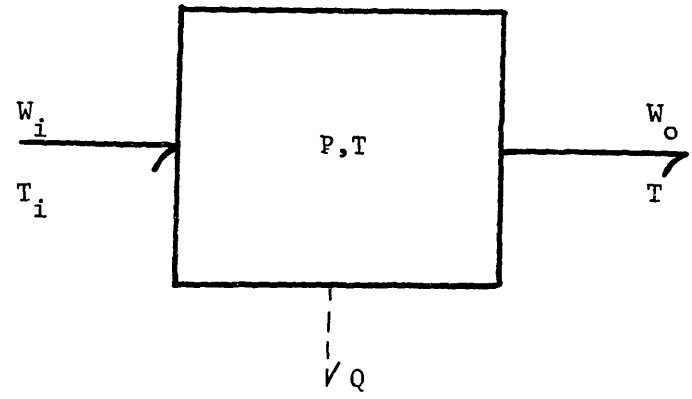

Figure 2-2: Plenum Volume Element

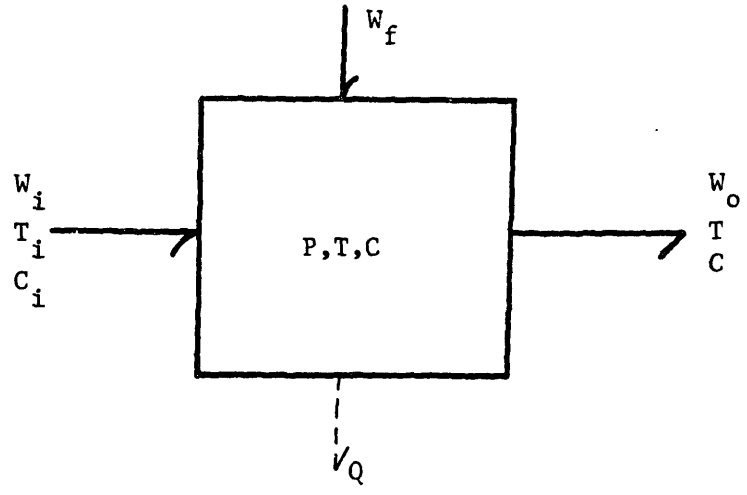

Figure 2-3: Perfect Stirred Reactor (PSR) Model for Combustion Furnace

W_o = gas mass flow rate, lbm/sec.

ρ = gas density, lbm/ft^3

R_t = combustion rate, $lbm/(sec.ft^3)$

After combustion, part of the burnt fuel changes to a gaseous state according to the chemical reaction stoichiometry of the combustion process.

$$dM/dt = W_i + (1-\beta_f)VR_t - W_o \tag{2.5}$$

where: M = mass of gas in PSR, lbm

W_i = gas flow rate entering PSR, lbm/sec.

β_f = fraction of ash in fuel

Application of first law of thermodynamics to the PSR results in the energy conservation equation:

$$dU/dt = E - Q + c_pW_iT_i - c_pW_oT \tag{2.6}$$

where: T_i = temperature of inlet gas flow, ^oR

T = temperature of PSR, ^oR

E = rate of energy conversion into gas, Btu/sec.

Q = heat transfer rate leaving PSR, Btu/sec.

U = internal energy in the PSR, Btu

c_p= specific heat of gas at constant pressure

If the ideal gas law is assumed for the PSR combustion gas, then the internal energy U is a function of temperature T:

$$U = c_v MT \tag{2.7}$$

where: M = the mass of the gas in the PSR

c_v = the specific heat of the combustion gas.

The specific heat of the combustion gas can be obtained from the Rosin-Fehling I.T. diagram shown in Figure 2-4 from reference [58]. The ideal gas law also defines the following relations, with the traditional qausi-static assumption for thermodynamics:

$$PV = RMT \tag{2.8}$$

$$c_p = 1.4c_v \tag{2.9}$$

where: P = pressure in the PSR, lbf/ft^2

R = ideal gas constant, $lbf\text{-}ft/lbm^{\circ}R$

The energy into the combustion furnace gas model is equal to the energy generated by combustion minus the energy needed to heat and evaporate the moisture content in the fuel and gas:

$$E = E_c - E_w \tag{2.10}$$

where: E_c = energy generated by combustion.

E_w = energy needed to heat and evaporate moisture.

It has been shown that the combustion properties of normal commercial fuels can be fairly accurately specified by two parameters, namely, the caloric value and type of fuel. When the fuel burn rate is defined, the local rate of energy generation then may be defined as the product of fuel caloric value and

its burn rate. The total combustion rate in a PSR volume then becomes:

$$E_c = H_v V R_t \tag{2.11}$$

A reaction rate equation which is a function of temperature and composition may be written as:

$$R_t = r(T)\ C_1\ C_2 \tag{2.12}$$

where: C_1 = concentration of reactant 1

C_2 = concentration of reactant 2

r(T) = temperature dependency function

Since oil and pulverized coal are mainly of interest here, the general rate expressions are derived for these two cases in the following paragraphs.

(1) Oil Fired Combustion Rate Equation

In reference [4] Bragg and Holliday have derived the rate equation for oil combustion assuming that the concentration of two species participating in the oxidation of carbon monoxide are proportional to the concentration of the unburnt fuel and oxygen respectively as:

$$E_v = k_c P^2 T^{-3/2} C_{ox} C\ e^{-B/RT} \tag{2.13}$$

where: E_v = local rate of energy release, Btu/sec.ft^3

C = unburnt fuel concentration, lbm/ft^3

C_{ox} = Oxygen concentration, lbm/ft^3

k_c = collison frequency constant, 1/sec.

T,P = local temperature and pressure

B = activation energy

R = gas constant

Based on experimental results, a procdure to evaluate the value of B/R has been proposed in reference [4].

For implosion studies, the rate equation may be simplified. After a MFT, the fuel supply is reduced to zero in approximately one to two seconds, the fuel concentration change dominates the rate change during this process. When the the temperature drops as a result of the disturbance, the exponential term $e^{-B/RT}$ dominates the combustion rate and a simple rate equation can be written in the form:

$$R_t = K\ e^{-B/RT}\ C \tag{2.14}$$

This expression is combined with state equations (2.4),(2.5),(2.6) to simulate combustion dynamics after a MFT in oil fired plants.

(2) Pulverized Coal Fired Combustion Rate Equation

Pulverized coal combustion may be described as a five step reaction process:

- Step 1. Diffusion of gaseous reactant through the film surrounding the coal particle surface.
- Step 2. Penetration and diffusion of gas through the blanket of ash to the surface of the unreacted core, the reaction surface.
- Step 3. Chemical reaction of the gaseous reactant with the coal.
- Step 4. Diffusion of the gaseous products through the film back into the surface of the coal.

- Step 5. Diffusion of the gaseous reaction product through the film back into the main gas body.

Since these steps must occur successively for the reaction to occur, they may be considered as resistances in series and whenever one of the steps offers the major resistance, that step may be considered as the rate controlling step. One important characteristic of the combustion rate is its temperature dependency. In different temperature ranges, different processes control the rate. The temperature dependency of pulverized coal combustion has been discussed in reference [58] and illustrated in Figure 2-5 where chemical reaction is rate controlling in the low temperature range and film and ash diffusion are rate controlling at higher temperatures. For low temperatures where the chemical reaction is controlling, the rate temperature dependency has been derived in reference [58] as:

$$r_c = k_2 \, e^{-B/RT} \tag{2.15}$$

For high temperatures where mass transfer rate is controlling, the rate temperature dependency has been derived in reference [58] as:

$$r_m = (P_o D_o / l_f)(T/T_o)^m \qquad m < 2 \tag{2.16}$$

where: D_o = diffusion coefficient at a standard temperature T_o

l_f = film thickness

If a large temperature range is of interest, both mass transfer and chemical reaction require consideration and an overall rate may be derived as shown in reference [39] as:

$$1/R_t = 1/R_{t1} + 1/R_{t2} \tag{2.17}$$

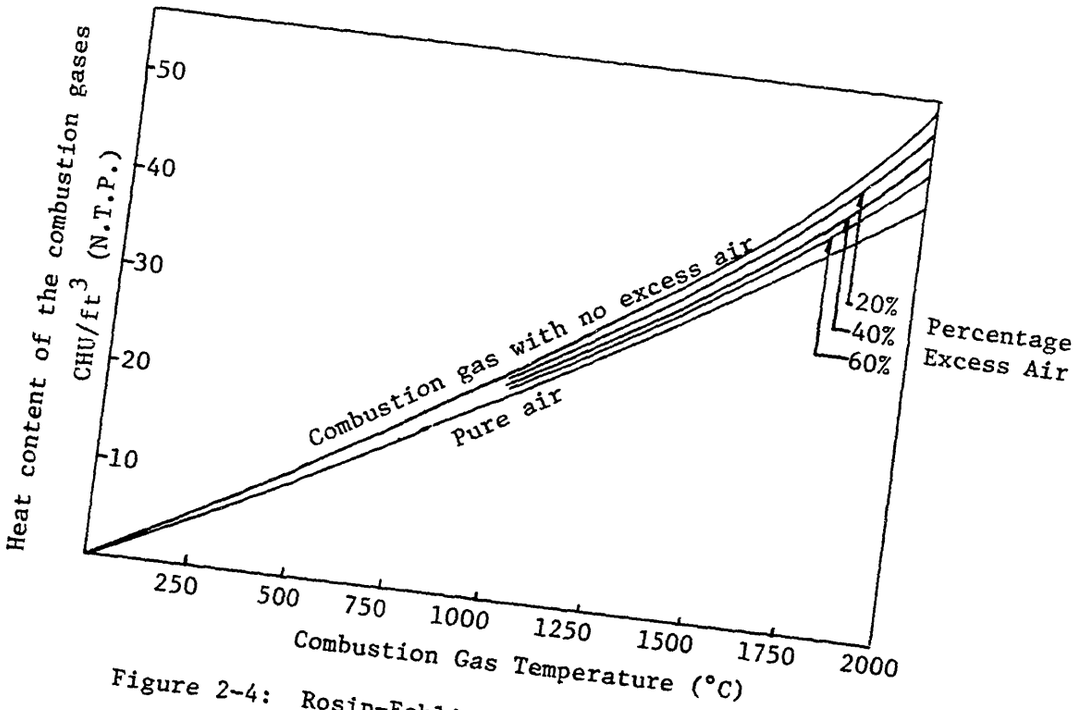

Figure 2-4: Rosin-Fehling I.T. Diagram Ref. [55]

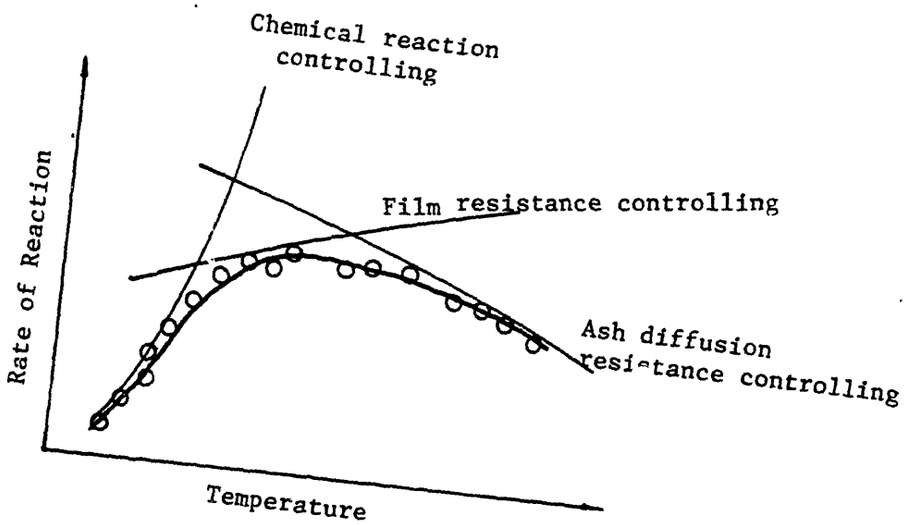

Figure 2-5: Reaction Rate as a Function of Temperature

if the rate of the chemical reaction alone is R_{t1} and the rate of mass transfer alone is R_{t2}.

In implosion studies, both mass transfer and chemical reaction are considered for coal fired combustion and the overall rate equation is used combining (2.15), (2.16) and (2.17) in the PSR model.

2.2.3 Transmission Line Element

Transmission line elements are used to represent wave propagation due to distributed inertance and capacitance of the fluid in the duct. A distributed parameter model of a lossless fluid transmission line is developed which represents the dominant longitudinal wave transmission modes in ducts. The model is derived for a duct of uniform cross section with rigid walls and assumes the flow is lossless with a fluid velocity small compared with the acoustic velocity of sound in the fluid. In most plant duct sections the average flow velocities are less than 5% of the acoustic sound velocity and the assumption that the flow velocity is small compared with the velocity of sound is valid. The model for a single line assumes that the temperature in the line is uniform. In sections of a plant where temperature varies significantly along the duct length, several lines each with a different temperature may be required to represent the complete line.

The application of the continuity and momentum equations to the elemental control volume of a fluid transmission line may lead to the derivation of two classical wave equations for pressure and mass flow rate representing the dynamic behavior of a single line.

$$\partial^2 P/\partial^2 X = \rho/\beta \; \partial^2 P/\partial^2 t \qquad (2.18)$$

$$\partial^2 W/\partial^2 X = \rho/\beta \; \partial^2 W/\partial^2 t \tag{2.19}$$

The detailed derivation of equations (2.18) and (2.19) is summarized in Appendix A. For the time domain solution to these equations the pressure and flow in the line can be represented by an alternate set of variables called wave scattering variables. The pressure waves in the line are partitioned into waves which travel in the flow direction, represented by U, and waves which travel opposite to the flow direction, represented by V. The pressure and flow at upstream and downstream ends of the line can be defined in terms of the wave scattering variables and charateristic impedance Z_c:

$$PU = UU + VU \tag{2.20}$$

$$WU = (UU - VU)/Z_c \tag{2.21}$$

$$PD = UD + VD \tag{2.22}$$

$$WD = (UD - VD)/Z_c \tag{2.23}$$

If the pressure is in inches of water and the mass flow rate is in pounds per second, the characteristic impedance is defined as:

$$Z_c = \frac{C_o}{A(32.2)(5.3)} \tag{2.24}$$

The velocity of the sound C_o can be expressed as function of the duct line temperature as:

$$C_o = \sqrt{RT} \tag{2.25}$$

Using the scattering wave variables, the solutions to the wave equations (2.18) and (2.19) can be expressed in a very convenient form [21]. The

detailed derivation of this solution is also included in Appendix A.

$$UD(t) = UU(t-T_D) \tag{2.26}$$

$$VU(t) = VD(t-T_D) \tag{2.27}$$

The wave propagation delay is:

$$T_D = L/C_o \tag{2.28}$$

The pressures and flows of the transmission line are expressed in terms of pure time delays. The time delay, T_D, represents the time required for a pressure wave to travel the length of the line. Equation (2.26) shows that for the wave which travels downstream the downstream value of UD at time t is equal to the upstream value UU at time (t - T_D) where the time difference is the time required for the wave to travel the length of the line. Similarly, for the upstream traveling wave, the upstream value of VU at time t is equal to the downstream value of VD at time (t - T_D).

A diagram of the transmission line model is shown in Figure 2-6. The wave variables UD and VU are considered quasi-state variables for the system since they define the state of the system and are related to the values of UU and VD by the delay T_D. The characteristic impedance determines in part the portion of the wave reflected and transmitted when a line is coupled with another element and relates the wave variables to the pressures and mass flows at each end of the line. The delay T_D and characteristic impedance Z_c, which represent the characteristics of the transmission line, are function of transmission line parameters. In the thermal transient, the temperature of the duct changes with time. T_D and Z_c also vary with time according to

equations (2.25), (2.28) and (2.24). These temperature (convective energy) dynamics of the duct are modeled by a global energy balance equation over the duct volume. The model is equavilent to coupling a plenum element with the volume size of the duct to the pressure - flow wave model. The flow rate input to this "duct plenum" is determined by the wave equations. Although it is not appropriate to assume a perfectly mixed fluid to compute the thermodynamic states in this dynamic situation, integration of the net mass and energy flows into this "duct plenum" will approximate the average gas density and temperature for the duct. In this type of the model formulation, a uniform but possibly time varying temperature is defined for a single transmission line.

The numerical solution of the wave equations, the values of UU and VD are established at time t by the equations coupling the line to the other elements in the system. Both pressure and flow are related to the scattering variables at the end of the transmission line as shown in Figure 2-6. The values of UD and VU at time t are then established directly from the values of UU and VD by the delay operator. The average temperature of the duct is obtained by integrating the net incoming energy flow. The parameters T_D and Z_c also vary with temperature and are updated when a thermal disturbance occurs upstream. However, the heat transfer along the duct is not considered, such a topic is discussed with other dispersion effects in references [25] [5] and [6].

2.2.4 Centrifugal Fan Element

The generic representation of a centrifugal fan element is by a steady state pressure-flow relation :

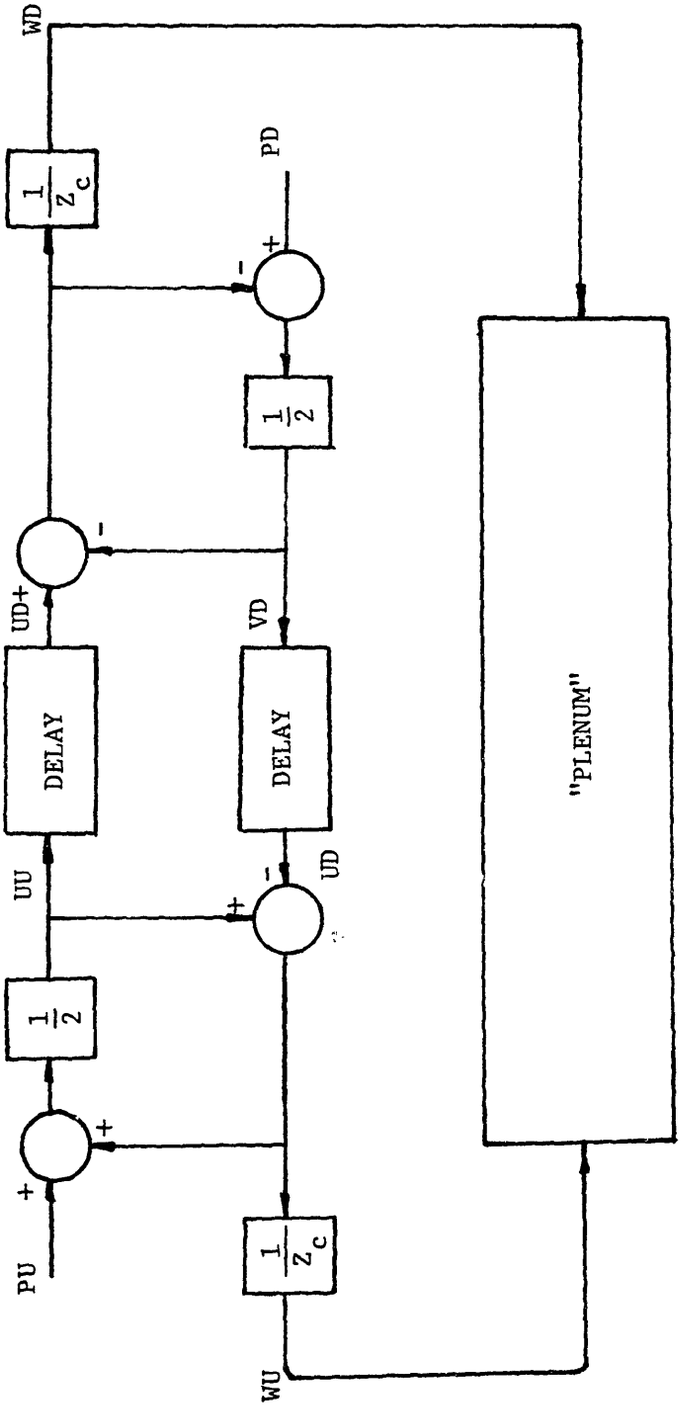

Figure 2-6: Transmission Line Element Representation

$$\Delta P = F_f(W, \alpha) \tag{2.29}$$

where $F_f(W,\alpha)$ is the functional relationship relating flow W and fan inlet guide vane or damper angle α to pressure rise ΔP.

This fan relation may be defined in general in terms of a dimensionless flow coefficient Φ and a dimensionless pressure coefficient Ψ. These coefficients are derived by dimensional analysis to fans with geometric similarity. When the Reynolds number does not vary significantly, the functional relationship

$$\Psi = f_f(\Phi,\alpha) \tag{2.30}$$

represents the general characteristics of geometricaly similar fans, where the coefficients are defined as:

$$\Phi = \frac{4Q_f}{\pi d^2 u} \tag{2.31}$$

$$\Psi = \frac{2\Delta P}{\rho u^2} \tag{2.32}$$

where: d = fan impeller diameter

u = impeller tip speed

Q_f = volume flow rate

ρ = fluid density

ΔP = pressure rise across the fan

The symbolic representation and typical centrifugal fan characteristics are shown in Figure 2-7 and Figure 2-8 respectively. The normalized fan curves in Figure 2-8 are characterized at M.I.T. [59].

For numerical work the function $f_f(W,\alpha)$ is either represented as a table with pairs of values of ΔP and W for fixed α or with a polynomial fit to

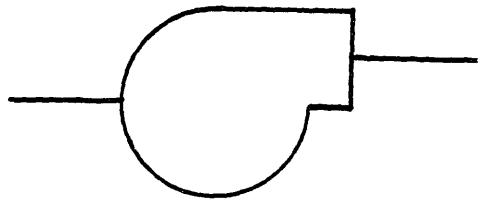

Figure 2-7: Centrifugal Fan Symbolic Representation

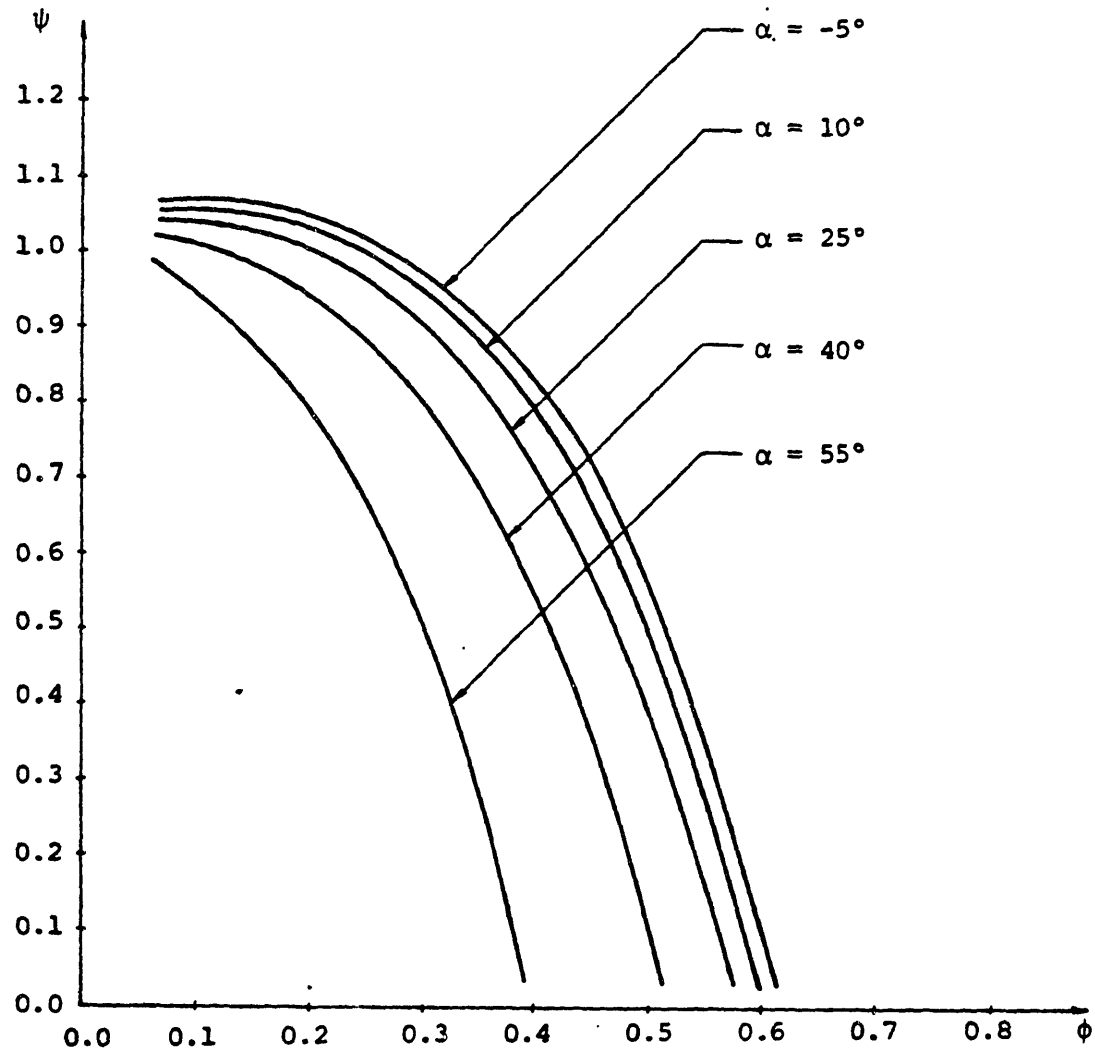

Figure 2-8: Typical Centrifugal Fan Characteristics

equation (2.33). For each fixed angle α, a polynomial can be determined by the least squares method:

$$\Psi = \sum C_i \Phi^i \tag{2.33}$$

For different angles α, a different set of coefficients C_i are obtained so that the polynomial coefficients in (2.33) are functions of the angle α. This functional relation can also be approximated as polynomials:

$$C_i = \sum b_{ij} \alpha^j \tag{2.34}$$

By substituting equation (2.34) into (2.33), the numerical approximation of the fan characteristics is established as:

$$\Psi = \sum\sum b_{ij} \alpha^j \Phi^i \tag{2.35}$$

2.2.5 Axial Fan Element

The generic representation of an axial fan element is by a steady state pressure-flow relation:

$$\Delta P = F_a(W, \alpha) \tag{2.36}$$

where $F_a(W,\alpha)$ is the functional relationship relating flow W and fan blade or damper angle α to pressure rise ΔP.

This fan relation may be defined in general in terms of a dimensionless flow coefficient Φ and a dimensionless pressure coefficient Ψ. These coefficients are derived by dimensional analysis to fans with geometrical similarity. When the Reynolds number does not vary significantly, the functional relationship

$$\Psi = f_f(\Phi,\alpha) \tag{2.37}$$

represents the general characteristics of geometrical similar fans, where the coefficients are defined as:

$$\Phi = \frac{4Q_f}{\pi d^2 u} \tag{2.38}$$

$$\Psi = \frac{2\Delta P}{\rho u^2} \tag{2.39}$$

where: d = fan impeller diameter

u = impeller tip speed

Q_f = volume flow rate

ρ = fluid density

ΔP = pressure rise across the fan

The symbolic representation of an axial fan and typical axial fan characteristics are shown in Figure 2-9 and Figure 2-10 respectively.

For numerical work the function $f_a(W,\alpha)$ is either represented as a table with pairs of values of ΔP and W for fixed α or with a polynomial fit to the fan curves. Because of the stall characteristic of the axial fan curve, a piecewise curve fit is usually preferred rather than a full range one. For each fixed angle α, a polynomial can be determined by the least squares method just as shown in the centrifugal fan case.

Since the mass flow passes through a relative long ring-section chamber of an axial fan, the gas flow inertance effect becomes important and should be included in the model by the following equation:

$$I(dW/dt) = \Delta P_I \tag{2.40}$$

where:

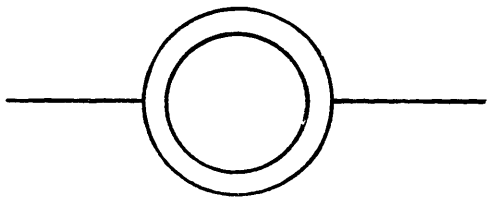

Figure 2-9: Axial Fan Symbolic Representation

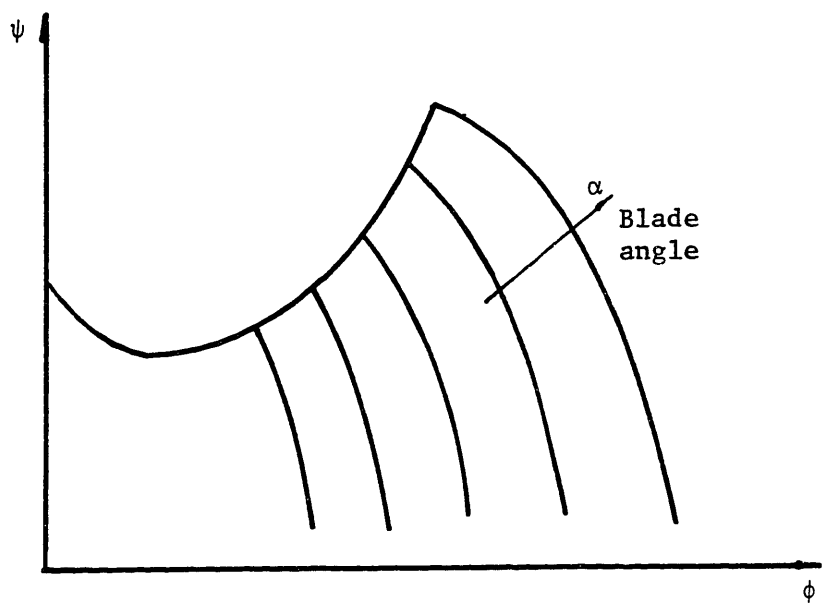

Figure 2-10: Typical Axial Fan Characteristics

$I = L_a/A_a$

L_a = length of the axial fan chamber

A_a = cross section area of axial fan chamber

2.2.6 Flow Resistance Element

The symbolic representation of the resistance element is shown in Figure 2-11, it represents the quasi-steady pressure-drop/flow characteristics of ducts, bends and other equipment and may be represented as the functional relationship:

$$\Delta P = f(W) \tag{2.41}$$

The functional relation of equation (2.41) for a straight duct can be expressed as:

$$\Delta P = fA_rT|W|W \tag{2.42}$$

where f is the friction coefficient and is a function of the flow Reynolds number, and A_r is a geometry coefficient and is a function of duct length and cross section area. For most power plant applications A_r is constant, and f is assumed constant since most flows are in the turbulent region. The temperature T is the weighted average of the upstream temperature and the downstream temperature of the duct representing the effect of the gas density change due to compressibility and heat transfer along the duct. Under these conditions, the pressure drop ΔP is proportional to fluid absolute average temperature T (^oR) and mass flow squared |W|W:

$$\Delta P = k_g \, T \, |W|W \tag{2.43}$$

Equation (2.43) is valid not only for straight ducts but also for bends, tube banks, dampers, airheaters and other equipment with some modifications of the coefficient k_g. Analytical and empirical expressions for k_g are given in reference [7].

2.2.7 Mechanical Damper Element

A mechanical damper is one type of fluid resistance which deserves attention because of its relation to draft control. The symbolic representation of a mechanical damper is shown in Figure 2-12. The generic characteristic is represented by a pressure-flow relation with the damper angle as a parameter:

$$\Delta P = D_f(W, \alpha_d) \tag{2.44}$$

The particular functional relation in (2.44) is provided by manufacturers curves or tables where pairs of values for ΔP and W for a fixed α_d are listed.

For numerical work the function (2.44) can be approximately represented by a polynomial using the least squares method:

$$\Delta P = \sum r_i(\alpha_d) W^i \tag{2.45}$$

2.2.8 Heat Transfer Resistance Element

The heat transfer resistance element represents heat transfer between two objects. The symbolic representation is shown in Figure 2-13.

$$Q = F(T_1, T_2) \tag{2.46}$$

Figure 2-11: Symbolic Representation of Resistance Element

Figure 2-12: Symbolic Representation of Mechanical Damper

There are three recognized modes of heat transfer, conduction, convection and radiation. All the varied phases of heat transfer involve one or more of these modes. For the conduction mode:

$$Q = \frac{k}{l} A_h (T_1 - T_2) \tag{2.47}$$

where: Q = rate of heat flow, Btu/hr

k = thermal conductivity, Btu/ft^2,hr,F/ft

A_h = heat transfer area, ft^2

l = thickness, ft

Convection heat transfer between a fluid and a solid is expressed as

$$Q = U_c A_h (T_1 - T_2) \tag{2.48}$$

where U_c is the convection film conductance, Btu/ft^2,hr,F.

Radiation heat transfer in combustion furnaces is defined as:

$$Q = A_h (\sigma \epsilon_f a T^4 - \sigma \epsilon T_s^4) \tag{2.49}$$

where:

σ = Stefan-Boltzmann constant

ϵ_f = flame emissivity

ϵ = ash deposit emissivity

a = ash deposit absorptivity

2.2.9 Solid Thermal Element

In order to study the thermal transient problem after a MFT, a good estimation of the energy storage in plant structures and in slag is important. These metal structures and ash slags can be modeled as solid thermal elements illustrated in Figure 2-14. The consitutive equation for this element is:

$$cM_s dT/dt = \sum Q \tag{2.50}$$

where: c = specific heat for the solid

M_s = mass of the solid

Q = heat transfer into the element

T = solid temperature

2.2.10 Heat Exchanger Element

The heat transfer and energy exchange at the superheater, economizer and airpreheater can be modeled with heat exchanger elements. The symbolic representation of the heat exchanger element is shown in Figure 2-15. The exact heat transfer solutions are available for both counter-flow and parallel-flow exchangers as given in reference [50].

$$Q = UA\frac{\Delta T_a - \Delta T_b}{Ln(\Delta T_a/\Delta T_b)} \tag{2.51}$$

The hot side energy flow is:

$$h_h = c_h W_h[T_{h1}+T_{h2}]/2 + c_h|W_h|[T_{h1}-T_{h2}]/2 - Q \tag{2.52}$$

The cold side energy flow is:

Figure 2-13: Heat Transfer Element

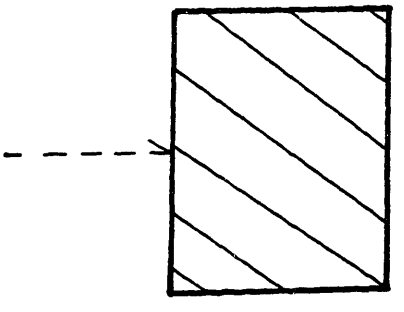

Figure 2-14: Solid Thermal Element

$$h_c = c_c W_c[T_{c2}+T_{c1}]/2 + c_c|W_c|[T_{c2}-T_{c1}]/2 + Q \tag{2.53}$$

The heat exchanger element described here can simulate the flow reverse situation in either side. The flow reveral formulation was introduced in reference [47]. Care must also be taken for Equation (2.51) during a dynamic simulation since it is unstable when $c_h W_h = c_c W_c$. An alternative model has been developed to approximate the heat exchanger element as shown in Figure 2-16. The heat transfer rate in this model is approximated as:

$$Q = UA[(T_{h1}+T_{h2})/2 - (T_{c2}+T_{c1})/2] \tag{2.54}$$

This formulation ensures a stable dynamic simulation. If the detailed spatial variation of the temperature is of interest, a compartmented model can be constructed using the basic cell in Figure 2-16. An advantage of this heat exchanger model is its capability to incorporate dynamic elements to represent energy storage at either side of an exchanger. More complete treatments of heat exchanger modeling can be found in reference [40].

One requirement for this capability is that the temperatures at both ends of the exchanger are known before equations (2.51) (2.52) and (2.53) can be solved. However, if flow reversal is not considered, the causality of a counter-flow heat exchanger can be simplified using only upstream temperatures as indenpendent variables. The element energy equations become a simple matrix [47]:

$$\begin{bmatrix} T_{h2} \\ T_{c1} \end{bmatrix} = \begin{bmatrix} \Gamma & 1-\Gamma \\ 1-\Delta & \Delta \end{bmatrix} \begin{bmatrix} T_{h1} \\ T_{c2} \end{bmatrix}$$

(2.55)

where

$$\Gamma = \frac{2c_h c_c W_h W_c + UAc_h W_h - UAc_c W_c}{2c_h c_c W_h W_c + UAc_h W_h + UAc_c W_c}$$

$$\Delta = \frac{2c_h c_c W_h W_c - UAc_h W_h + UAc_c W_c}{2c_h c_c W_h W_c + UAc_h W_h + UAc_c W_c} \qquad (2.56)$$

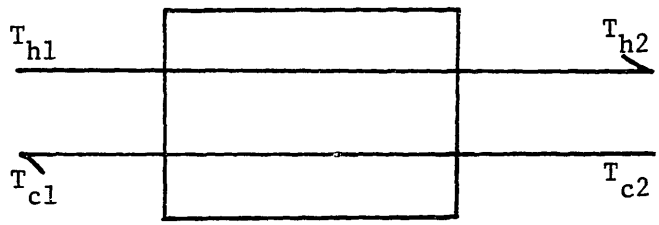

Figure 2-15: Symbolic Representation of Heat Exchanger

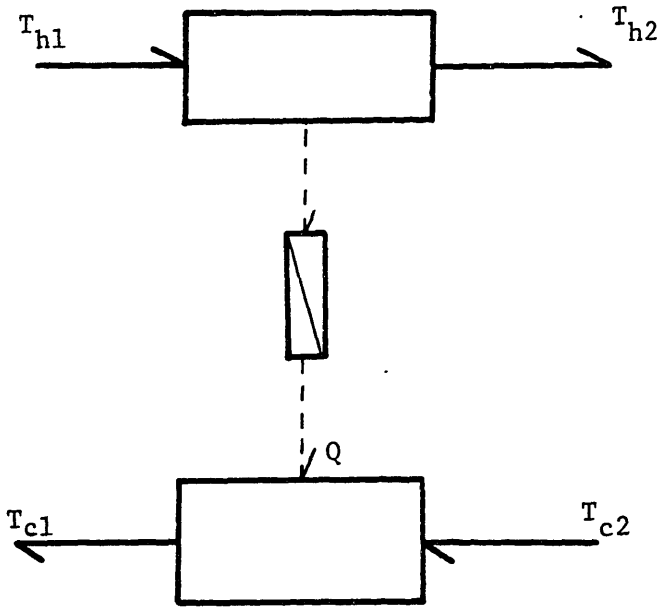

Figure 2-16: Heat Exchange Element Model

Chapter 3
SYSTEM STRUCTURE AND PARAMETER ESTIMATION

3.1 Introduuction

To represent a power plant configuration using the generic mathematical elements developed in Chapter 2, a criterion must be developed for partitioning the system into a finite number of elements to approximate the continuous thermofluid process; a system structure must also be developed that couples the divided elements for system representation. In this section, a compartmental furnace model is developed to demonstrate a general procedure for compartmental modeling of thermofluid processes; a family of junction elements is also developed to link the elements together to form system configurations.

3.2 Compartmental Furnace Model

An ideal PSR model for the combustion chamber is developed. For simplicity, it is restricted to the assumption that the gas density, fuel concentration, and temperature in the chamber are uniform. These assumptions are no longer valid when a large boiler furnace is to be modeled. The fuel concentration near the burner should be much higher than that near the furnace outlet. A similar temperature gradience is expected as well [9]. A compartment model for the large furnace is necessary. The question then

becomes how to divide the furnace into regions. The goal is to use the PSR to model each region, and to connect these PSRs to represent the overall characteristics of the furnace.

Shieh and Essenhigh [53] developed a compartment incinerator furnace model according to a physical zone basis. Four zones are identified as combustion and gasification, pyrolysis, ignition, and final burn-out. Each of the zones can be modeled by a PSR with the appropriate rate equation in the zone. The analysis was suported by experimental results [36]. The application of the theory to a large industrial furnace was demonstrated by the authors. However a compartment model by zonal analysis is only valid at steady state. It is not an easy task to define the zone boundries for a particular furnace.

An alternative approach to development of a furnace compartment model is to use the theory of residence time distribution (RTD), by which the model formulation is valid for both transient and steady state conditions. The compartment boundaries can be determined by a simple tracer test on any particular furnace, although the physical phenomenon in different regions is not so clearly analyzed as with the zonal approach. However, if our primary interest is the overall characteristics of the furnace or that of the entire air/gas system dynamics, the residence time distribustion analysis is certainly advantageous.

The theory of residence time distribution in a reactor was developed by Levenspiel [39]. The application of the theory is, through a tracer response test, to decide the optimal number of compartments needed to model a continuous thermofluid process such as a furnace; and to determine where the compartment boundaries should be. The compartmental model so developed should represent the dynamic characteristics of the total system.

A helium-tracer was used in an isothermal test incinerator by Rao [48]. A typical F curve (see reference [39]) is shown in Figure 3-1. The response contains two regions, the first is approximately a pure delay, the second region is a exponential decay. This shape of reponse is relatively general. It has been observed by many researchers, [36], [11].

Bragg [3] mathematically proved that this is a general pattern. He defined a furnace compartment model as a stirred reactor region followed by a plug-flow region. The exponential time constant is associated with the stirred reactor hold-up time, while the delay in tracer response is associated with the plug-flow region delay. This is called the Bragg Criterion, illustrated in Figure 3-2.

Since the hold-up time of the PSR and the delay time of the plug flow region are functions of the region volumes for a particular steady state, the size of these two region can be calculated based on the tracer test result.

We have already developed a PSR model for the first region. The plug-flow region can be approximated as a series PSR. Figure 3-3 can be used to show how the approximation is achieved.

Since both fuel concentration C and temperature T are monotone variables [45] at a steady gas flow condition, if the entire region has a mean hold-up time τ, then each PSR element will have a mean hold-up time τ/n. General expressions of T_n in terms of T_0 and C_n in terms of C_0 in the Laplace domain are:

$$T_n(S) = \frac{T_0(S)}{(\tau/n\ S + 1)^n} \tag{3.1}$$

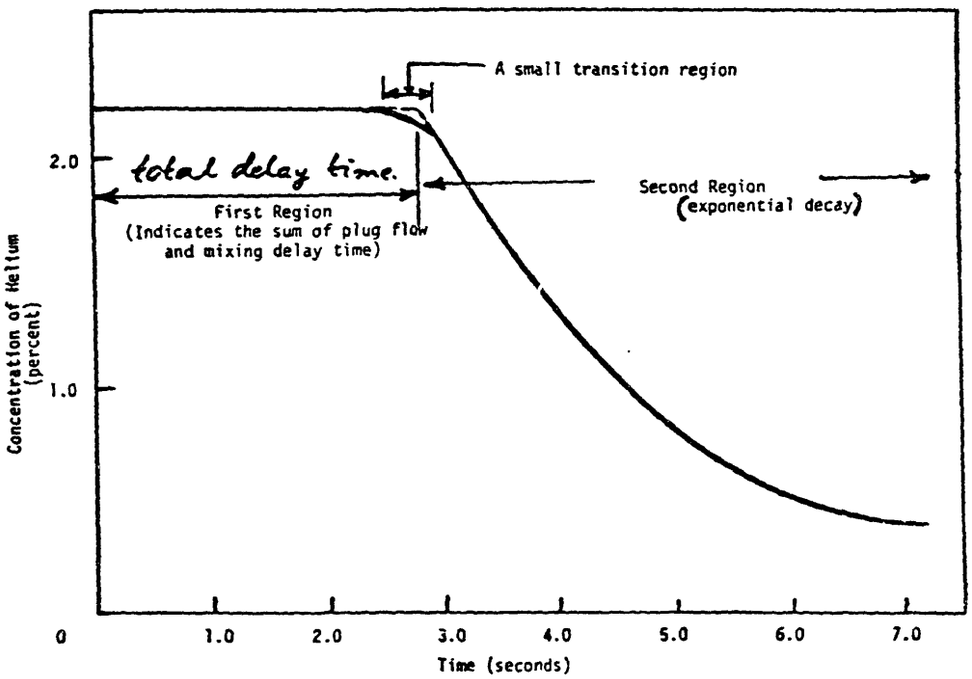

Figure 3-1: Typical Decay of Tracer after a Cutoff Injection Ref. [46]

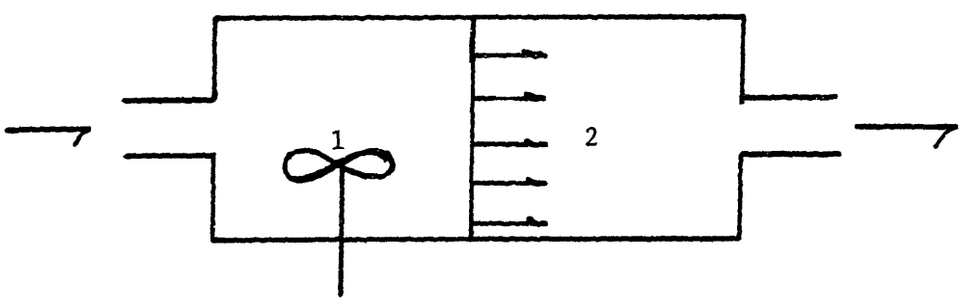

Figure 3-2: Bragg's Idealized Combustion Chamber Illustrating the Bragg Criterion, 1-a PSR; 2- a Plug-flow Region Ref. [3]

$$C_n(S) = \frac{C_0(S)}{(\tau/n\ S + 1)^n} \tag{3.2}$$

The time domain responses of T_n to T_0 and C_n to C_0 when T_0 and C_0 are unit steps are plotted in Figure 3-4 taking n as a parameter. When n=1, the entire region is modeled as a PSR; when n -> ∞, the region is modeled as a plug-flow element. The conclusion is that the plug-flow region can be approximated as a finite PSR set in series, and the entire furnace can be modeled as a finite PSR set in series.

3.3 General Junction

The basic elements developed in Chapter 2 are coupled together through junctions to represent a power plant configuration. At any junction three conditions must be satisfied - (1) the net mass flow rate into the junction is zero:

$$\sum W_i = 0 \tag{3.3}$$

(2) the net energy flow into the junction is zero:

$$\sum h_i = 0 \tag{3.4}$$

(3) the pressure and temperature at the center of the junction satisfy compatibility conditions.

A general junction is shown in Figure 3-5. There are a number of

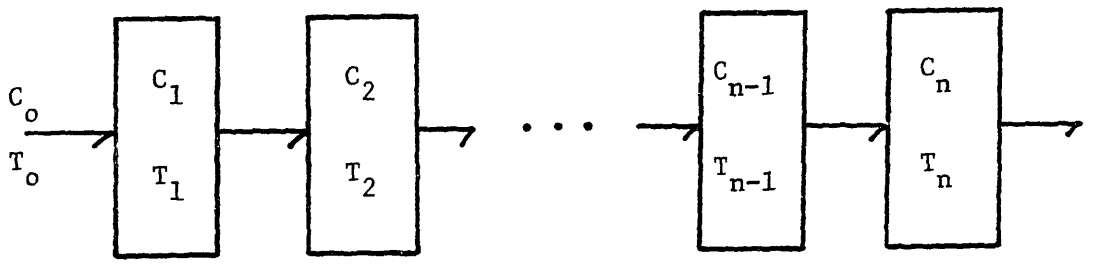

Figure 3-3: PSR Versus Plug-Flow Model

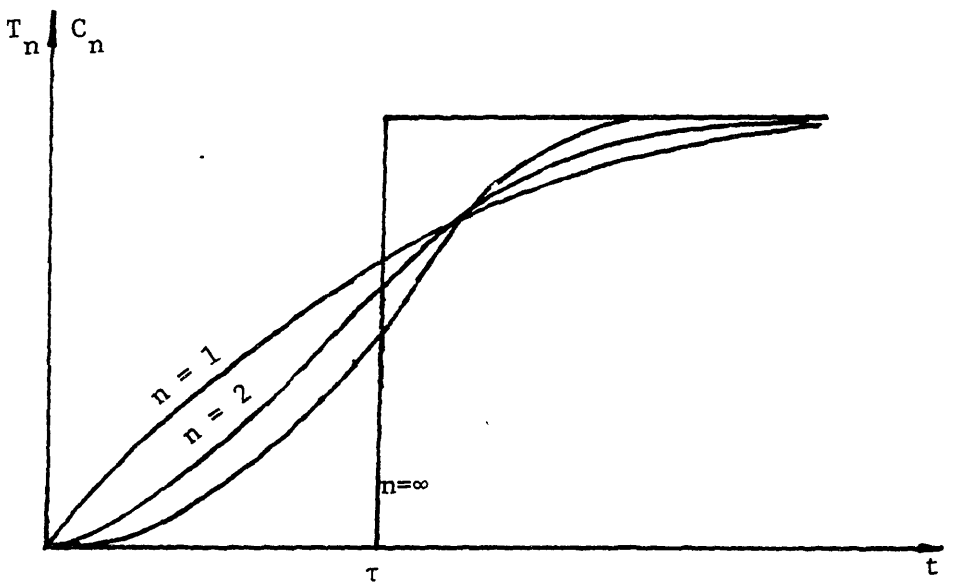

Figure 3-4: Step Response of N- PSR Models

assumptions on this general junction which connects any number of transmission lines and plenum elements or pressure sources. The flow momentum into and out of the junction is neglected so that the angle of connecting ducts is not a variable in consideration. The internal energy is considered decoupled from pressure and kinetic energy, it then becomes possible to solve the fluid balance equations independently of the energy balance equations. The energy balance equations are solved when the flow rates are known from the solution of the fluid balance equations.

Because wave scattering variables are used to simulate transmission line dynamics, the end of transmission lines represent the location of one independent variable (the incident wave U_i) to the general junction element and one dependent variable (the reflected variable V_i) from the general junction element. A plenum element also has an independent variable, pressure, and a dependent variable, flow, for the fluid balance equation.

There are n+m+1 dependent variables to solved for in the fluid balance equations at general juntions, one for each branch plus the pressure at the node. For constraint equuations, there are n+m equations which represent the pressure - flow relations across the resistance and Equation (3.3). Because of the quadratic representation of the resistance element, n+m+1 nonlinear algebric equations are required in its solution.

One way of simulating this set of equations is to assign an approximate linear resistance value to each quadratic resistance at each timestep based on the last calculated operating condition. The junction equations are then solved using ordinary matrix methods. With the appproximate solution known, a new approximate linear resistance can be calculated and iteration may be applied until a tolerance is satisfied. If $W_{i,t}$ is the last calculated operating flow

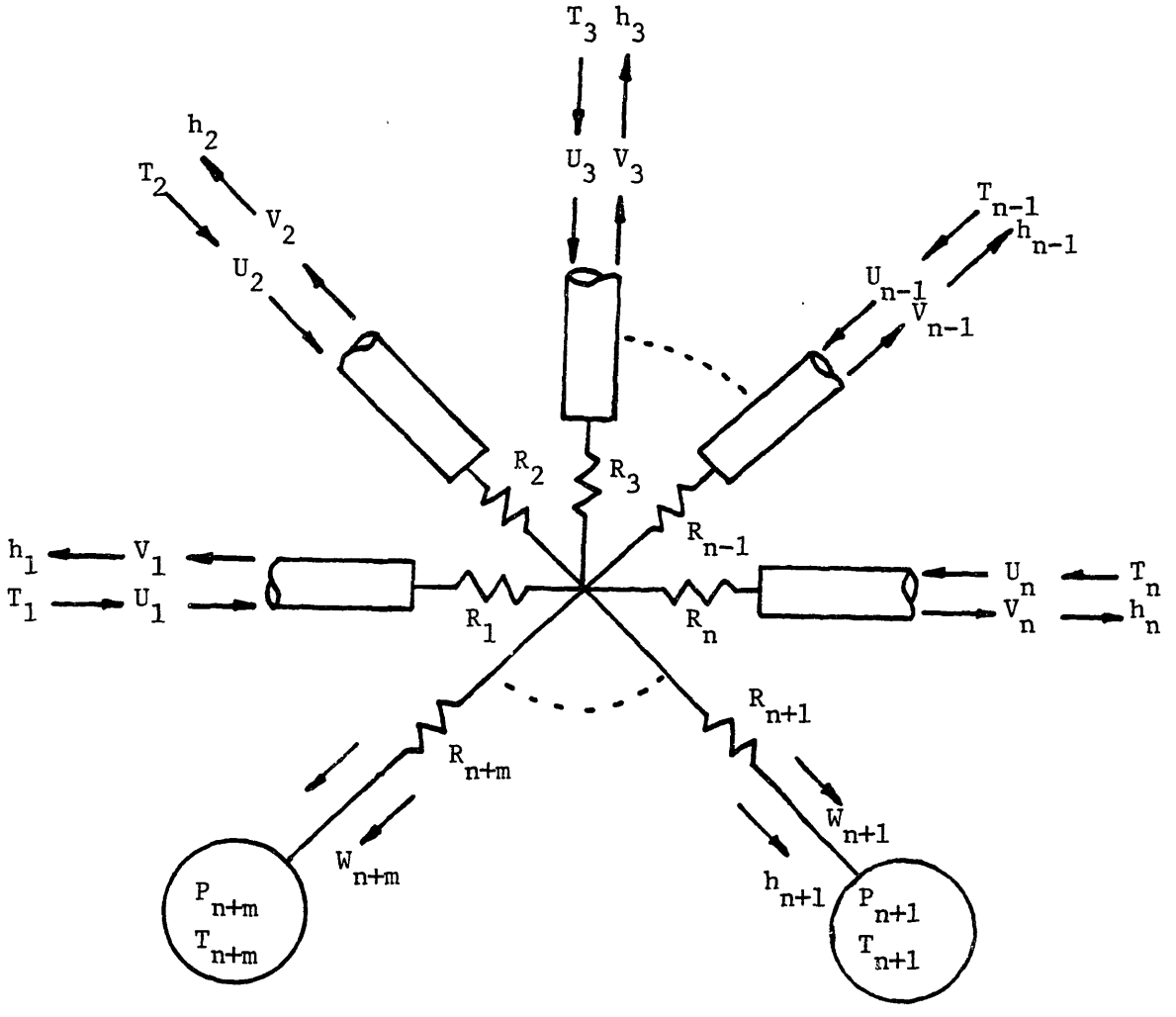

Figure 3-5: General Junction

condition, the appropriate value for the linearized resistance, $R_{i,t+\Delta t}$, is then given by:

$$R_{i,t+\Delta t} = \alpha_q |W_{i,t}| \tag{3.5}$$

In certain cases, using the value of $R_{i,t+\Delta t}$ according to (3.5) may result in a slow converging or oscillating iteration. To enhanee the speed and stability of the iteration procedure when dealing with unknown conditions, the following method of updating the quasi-linear resistance at each iteration has been suggested [51]:

$$R_{i,t+\Delta t} = 0.65\alpha_q |W_{i,t}| + 0.35R_{i,t} \tag{3.6}$$

After the resistances at a junction are linearized, the junction fluid balance equations can be cast into a simple matrix formulation and solved [51]. If the pressure at the node of the junction is unknown, the general junction matrix is described in equation (3.7).

If a plenum exists at the center of the general junction, the pressure of that junction is an independent variable for a given timestep and the junction equations become equation (3.8).

$$
\left[\begin{array}{ccccc|ccc|c}
1+\frac{R_1}{Z_1} & & & & 0 & & & & -1 \\
& 1+\frac{R_2}{Z_2} & & & & & & & -1 \\
& & \ddots & & & & 0 & & \vdots \\
0 & & & & & & & & \\
& & & 1+\frac{R_n}{Z_n} & & & & & -1 \\
\hline
 & & & & & R_{n+1} & & & 1 \\
 & & & & & & 0 & & \\
 & & & & & R_{n+2} & & & 1 \\
 & & 0 & & & & & & \vdots \\
 & & & & & 0 & & & \\
 & & & & & & & R_{n+m} & 1 \\
\hline
\frac{1}{Z_1} & \frac{1}{Z_2} & \cdots & \frac{1}{Z_n} & & -1 & -1 & \cdots -1 & 0
\end{array}\right]
\left[\begin{array}{c} V_1 \\ V_2 \\ \vdots \\ V_n \\ \hline W_{n+1} \\ \\ W_{n+2} \\ \vdots \\ W_{n+m} \\ \hline P_J \end{array}\right] =
$$

$$
\left[\begin{array}{ccccc|ccc|c}
1-\frac{R_1}{Z_1} & & & & 0 & & & & \\
& 1-\frac{R_2}{Z_2} & & & & & & & \\
& & \ddots & & & & 0 & & 0 \\
0 & & & & & & & & \\
& & & 1-\frac{R_n}{Z_n} & & & & & \\
\hline
 & & & & & 1 & & & \\
 & & & & & & 0 & & \\
 & & & & & 1 & & & 0 \\
 & & 0 & & & & \ddots & & \\
 & & & & & 0 & & & \\
 & & & & & & & 1 & \\
\hline
\frac{1}{Z_1} & \frac{1}{Z_2} & \cdots & \frac{1}{Z_n} & & & 0 & & 1
\end{array}\right]
\left[\begin{array}{c} U_1 \\ U_2 \\ \vdots \\ U_n \\ \hline P_{n+1} \\ \\ P_{n+2} \\ \vdots \\ P_{n+m} \\ \hline W_J \end{array}\right]
$$

$(W_J = 0)$

(3.7)

$$
\left[\begin{array}{cccc|ccc|c}
1+\frac{R_1}{Z_1} & & & & & & & V_1 \\
 & 1+\frac{R_2}{Z_2} & 0 & & & 0 & & V_2 \\
 & & \ddots & & & & & \vdots \\
0 & & & 1+\frac{R_n}{Z_n} & & & & V_n \\
\hline
 & & & & R_{n+1} & & 0 & W_{n+1} \\
 & & & & & R_{n+2} & & W_{n+2} \\
 & 0 & & & & 0 & & \vdots \\
 & & & & 0 & & R_{n+m} & W_{n+m} \\
\hline
\frac{1}{Z_1} & \frac{1}{Z_2} & \cdots & \frac{1}{Z_n} & -1 & -1 & \cdots\ -1 & W_J
\end{array}\right]
$$

$$
\left[\begin{array}{cccc|ccc|c}
1-\frac{R_1}{Z_1} & & & & & & 1 & U_1 \\
 & 0 & & & & & 1 & U_2 \\
 & & 1-\frac{R_2}{Z_2} & & & 0 & \vdots & \vdots \\
 & & & \ddots & & & 1 & U_n \\
0 & & & 1-\frac{R_n}{Z_n} & & & & \\
\hline
 & & & & 1 & & -1 & P_{n+1} \\
 & & & & & 0 & -1 & P_{n+2} \\
 & 0 & & & 1 & & \vdots & \vdots \\
 & & & & 0 & & 1\ \ -1 & P_{n+m} \\
\hline
\frac{1}{Z_1} & \frac{1}{Z_2} & \cdots & \frac{1}{Z_n} & & 0 & 0 & P_J
\end{array}\right]
$$

(3.8)

For the energy balance at the general junction element, there are n+m temperatures at each connecting element as independent variables, and n+m transport energy flows through each branch plus temperature at the node as dependent variables. To solve this set of n+m+1 dependent variables, n+m energy transport equations and the energy balance equation in (3.4) have to be employed.

Since the fluid flow at each branch of the junction element has been calculated by fluid balance equations for a given timestep, based on the flow directions shown in Figure 3-5, the energy transport eqaution at branch i becomes:

$$h_i = c_p W_i T_i \tag{3.9}$$

where T_i is the temperature at the element connected at branch i. However, Equation (3.9) is correct only if the flow direction at branch i is indeed from the connecting element to the general junction. The notion that temperatures upstream determine the temperatures downstream in a dynamic sense has always caused problems if it is possible for flow directions to reverse at the junction. The reverse of the flow direction requires a change in causality and thus a complicated reformulation of the system equations at certain points of time. In order to avoid such a complication, a scheme of constant causality is developed for the general junction element in which thermal energy transport flows is alway based on the "true" upstream temperatures regardless the flow signs. For a single branch, such a causality is [47]:

$$h_i = c_p W_i[T_i + T_J]/2 + c_p|W_i|[T_i - T_J]/2 \tag{3.10}$$

The general junction energy balance equations can similarly formulated in

matrix form. If there is no plenum element at the center of the junction, the temperature T_J is unknown and has to be calculated as:

$$T_J = - \frac{\sum (W_i + |W_i|) T_i}{\sum (W_i - |W_i|)} \tag{3.11}$$

in both summations i = 1,2,...,N+M assuming all flows signs are positive when they go into the junction.

The energy transport flow h_i at each branch can be calculated in a matrix (3.12).

If there is a plenum element at the center of the general junction element, the temperature T_J at that plenum is known at a given timestep, the energy transport flow h_i and the net energy transport flow into that plenum can be determined by the matrix (3.13).

For general thermofluid network simulation, heat transfer rates should be incorporated into the general junction. A general junction including N transmission lines, M plenums or pressure sources and L heat transfer branches is shown in Figure 3-6. The dashed lines represent the heat transfer branches where the mass flows of gas are zero. The mass balance equations for this junction are the same as Equations (3.7) and (3.8). However, the inclusion of heat transfer does alter the energy balance equations. If there is no plenum element at the center of the junction, the energy flow and heat transfer rates at junction can be calculated by Equation (3.14); while if there is a plenum element at the center of the junction, the energy flows and heat transfer rates are then calculated by Equation (3.15).

$$
\begin{bmatrix} h_1 \\ \\ h_2 \\ \vdots \\ h_i \\ \vdots \\ h_{n+m} \end{bmatrix}
= \frac{c_p}{2}
\left[\begin{array}{ccccc:c}
W_1 + |W_1| & & & & & W_1 - |W_1| \\
& W_2 + |W_2| & & 0 & & W_2 - |W_2| \\
& & \ddots & & & \vdots \\
& & & W_i + |W_i| & & W_i - |W_i| \\
& & & & \ddots & \vdots \\
& 0 & & & & W_{n+m} + |W_{n+m}|
\end{array}\right]
\begin{bmatrix} T_1 \\ T_2 \\ \\ \vdots \\ T_i \\ \vdots \\ T_{n+m} \\ \hline T_J \end{bmatrix}
$$

$(h_J = 0)$

(3.12)

$$\begin{bmatrix} h_1 \\ h_2 \\ \vdots \\ h_i \\ \vdots \\ h_{n+m} \\ \hline h_J \end{bmatrix} = \frac{C_p}{2} \left[\begin{array}{ccccc|c} W_1+|W_1| & & & & 0 & W_1-|W_1| \\ & W_2+|W_2| & & & & W_2-|W_2| \\ & & \ddots & & & \vdots \\ & & & W_i+|W_i| & & W_i-|W_i| \\ & & & & \ddots & \vdots \\ 0 & & & & W_{n+m}+|W_{n+m}| & W_{n+m}-|W_{n+m}| \\ \hline W_1+|W_1| & W_2+|W_2| & \cdots & W_i+|W_i| & \cdots W_{n+m}+|W_{n+m}| & \sum_{i=1}^{n+m}(W_i-|W_i|) \end{array}\right] \begin{bmatrix} T_1 \\ T_2 \\ \vdots \\ T_i \\ \vdots \\ T_{n+m} \\ \hline T_J \end{bmatrix}$$

(3.13)

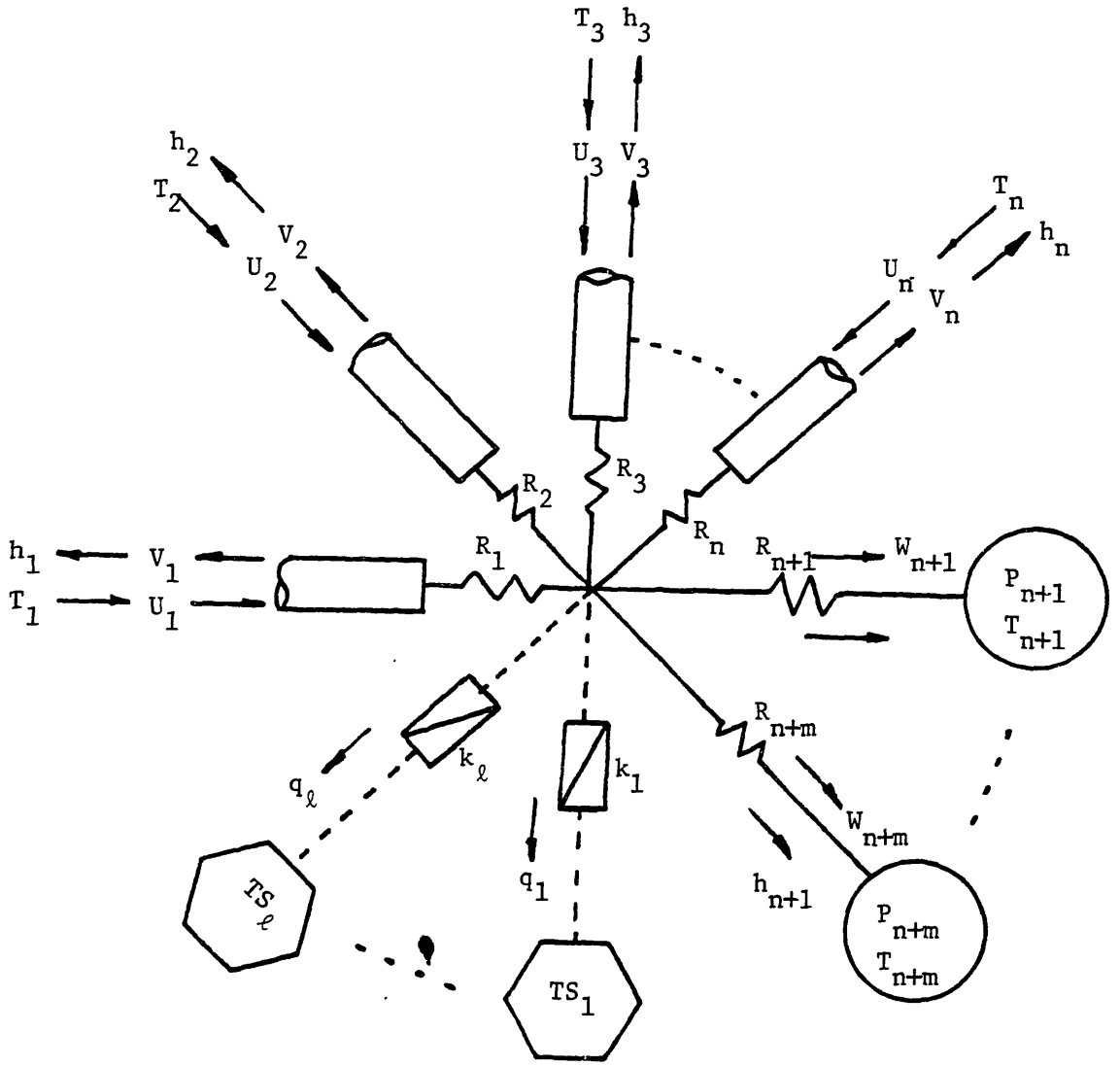

Figure 3-6: General Junction with Heat Transfer

$$
\begin{bmatrix}
1 & & & \frac{C_p}{2}(|W_1|-W_1) \\
 & \ddots & 0 & \frac{C_p}{2}(|W_2|-W_2) \\
 & 1 & & \frac{C_p}{2}(|W_{n+m}|-W_{n+m}) \\
\hline
 & 1 & & -K_1 \\
 & 1 & & -K_2 \\
0 & \ddots & & \vdots \\
 & & 1 & -K_L \\
\hline
1\ 1\ \ldots\ 1 & & -1\ -1\ \ldots\ -1 & 0
\end{bmatrix}
\begin{bmatrix} h_1 \\ h_2 \\ \\ h_{n+m} \\ \hline q_1 \\ q_2 \\ \vdots \\ q_L \\ \hline T_J \end{bmatrix}
$$

$$
=
\begin{bmatrix}
\frac{C_p}{2}(W_1+|W_1|) & & & 0 \\
 & \frac{C_p}{2}(W_2+|W_2|) & 0 & 0 \\
 & \ddots & & \vdots \\
 & & \frac{C_p}{2}(W_{n+m}+|W_{n+m}|) & 0 \\
\hline
 & & -K_1 & 0 \\
0 & & -K_2 & 0 \\
 & & \ddots & \vdots \\
 & & & -K_L \quad 0 \\
\hline
0\ 0\ \ldots\ 0 & & 0\ 0\ \ldots\ 0 & 1
\end{bmatrix}
\begin{bmatrix} T_1 \\ T_2 \\ \vdots \\ T_{n+m} \\ \hline TS_1 \\ TS_2 \\ \vdots \\ TS_L \\ \hline h_J \end{bmatrix}
\tag{3.14}
$$

$$
\begin{bmatrix} h_1 \\ h_2 \\ \vdots \\ h_{n+m} \\ \hline q_1 \\ q_2 \\ \vdots \\ q_L \\ \hline h_J \end{bmatrix} =
\left[\begin{array}{ccc|c|c}
\frac{C_p}{2}(W_1+|W_1|) & & 0 & & \frac{C_p}{2}(W_1-|W_1|) \\
& \frac{C_p}{2}(W_2+|W_2|) & & 0 & \frac{C_p}{2}(W_2-|W_2|) \\
0 & \ddots & & & \vdots \\
& & \frac{C_p}{2}(W_{n+m}+|W_{n+m}|) & & \frac{C_p}{2}(W_{n+m}-|W_{n+m}|) \\
\hline
& & & -K_1 \quad 0 & K_1 \\
& 0 & & -K_2 \quad \ddots & K_2 \\
& & & 0 \quad \ddots & \vdots \\
& & & \quad -K_L & K_L \\
\hline
\frac{C_p}{2}(W_1+|W_1|) & \frac{C_p}{2}(W_2+|W_2|) & \cdots \frac{C_p}{2}(W_{n+m}+|W_{n+m}|) & -K_1 \quad -K_2 \cdots -K_L & \sum_{i=1}^{n+m} \frac{C_p}{2}(W_i-|W_i|) - \sum_{j=1}^{L} K_j
\end{array}\right]
\begin{bmatrix} T_1 \\ T_2 \\ \vdots \\ T_{n+m} \\ \hline TS_1 \\ TS_2 \\ \vdots \\ TS_L \\ \hline T_J \end{bmatrix}
\tag{3.15}
$$

3.4 Fan Junctions

The general junction is able to connect basic elements for system configurations in most cases. However, when some nonlinear elements require special causalities, a special junction is required to include that particular element in the system structure. Fan elements are such special nonlinear elements. Figure 3-7 shows typical fan junction configurations. In general, a fan will be between two transmission lines or between some combinations of transmission lines and plenums or pressure sources. Since the pressure rise across the fan is a single function of flow through the fan, imposition of a flow input causality is needed for fan junction general solutions.

For centrifugal fans, one branch of the solution covers most of the operating range. It becomes possible to approximate the fan characteristic by a quadratic function and solve the higher flow solution for the fan junction. Such junction equations are formulated in reference [21] for all four configurations in Figure 3-7.

An alternative way to solve the centrifugal fan junction is to approximate the fan characteristic by several linear segments [51]. In the method that is used, the appropriate segment which matches the system resistance associated with the fan is determined first, and then the solution is computed using that segment as the fan characteristic.

In an axial fan element, when considered over its full range of operation, flow input causality must be imposed since the axial fan flow is a multi-branch function of the fan pressure head over a wide range. A dynamic axial fan element and the junction associated with it has been developed. Its schematic and associated bond graph representations are shown in Figure 3-8 and Figure

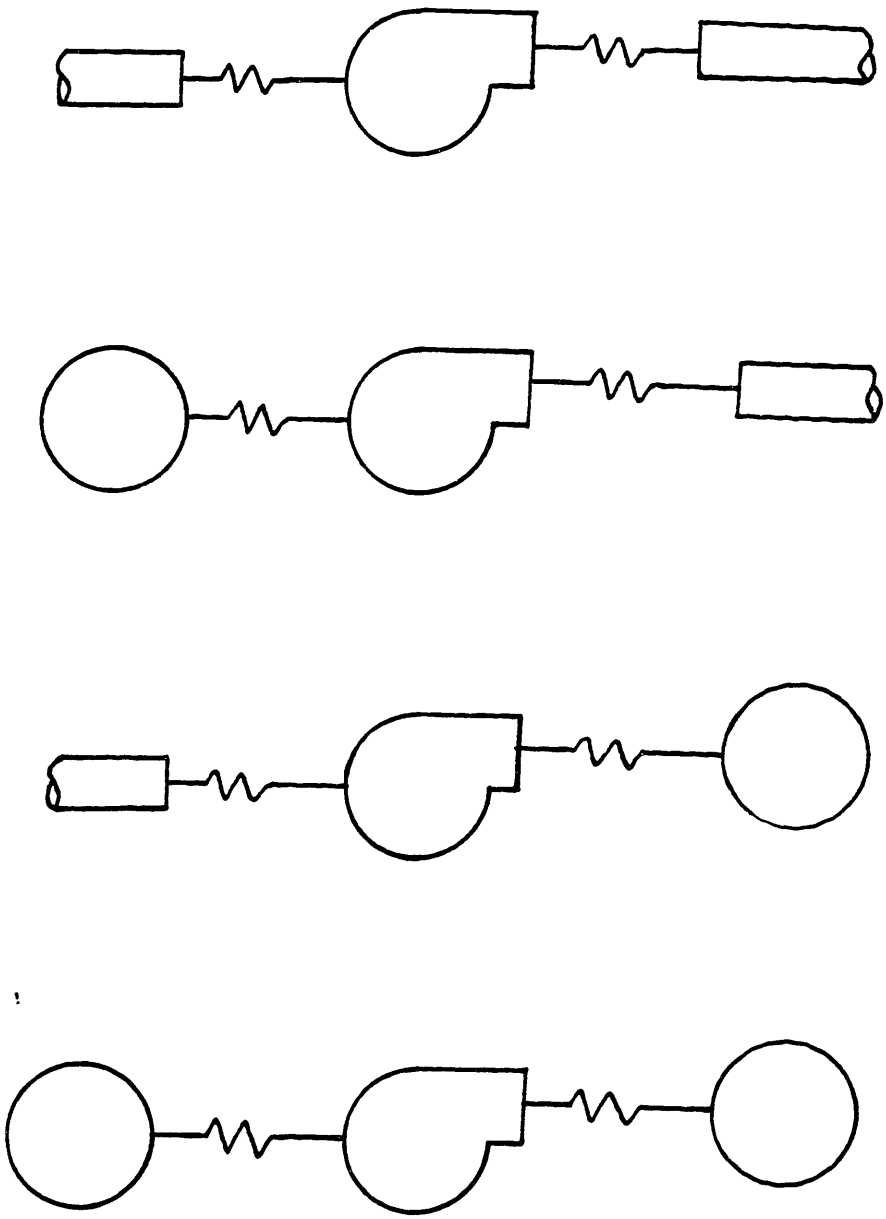

Figure 3-7: Fan Junction Configurations

3-9.

The pressure drops at fan inlet and at fan outlet are modeled by two resistance elements R_1 and R_2:

$$\Delta P_1 = R_1 W^2 \tag{3.16}$$

$$\Delta P_2 = R_2 W^2 \tag{3.17}$$

The fan static characteristic is defined in the dimensionalized form:

$$\Delta P_f = \sum B_i W^i \tag{3.18}$$

Since the mass flow goes through a long ring chamber in an axial fan, the inertance effect becomes important and should be included in the model,

$$I\frac{dW}{dt} = \Delta P_I \tag{3.19}$$

$$I = \frac{L}{A_c} \tag{3.20}$$

where:

L = length of axial fan chamber

A_c = cross section area of axial fan chamber

The equations for axial fan junction system in Figure 3-9 then can be formulated as:

$$I\frac{dW}{dt} = \Delta P_I \tag{3.21}$$

$$\Delta P_I = (2UD_1 - 2VU_2 + B_0) + (B_1 - Z_1 - Z_2)W + (B_2 - R_1 - R_2)W^2 + \sum B_i W^i \tag{3.22}$$

$$VD_1 = UD_1 - Z_1W \tag{3.23}$$

$$UU_2 = VD_2 + Z_2W \tag{3.24}$$

where i = 3,...,N, if the fan characteristic is approximated to second order, the summation term can be neglected.

The energy balance equation for the fan junction is straightforward, the notion that the temperature upstream determine the temperature downstream still applies. The transport energy flow through the fan is:

$$h_{fan} = c_pW[T_u + T_d]/2 + c_p|W|[T_u - T_d]/2 \tag{3.25}$$

Although the reverse flow fan characteristic is not known for most of the fans, the energy balance equation is still formulated as if reverse flow may occur to maintain structural uniformity.

3.5 Heat Exchanger Junction

The general junction does not include heat exchanger elements in its connections. A special junction has to be developed for heat exchangers.

The mass flow on either side of a heat exchanger is independent from the other side, and it can be solved seperately. In general, the fluid flow path of either side of the heat exchanger is between two transmission lines or some combination of transmission lines and plenums or pressure sources. Figure 3-10 shows some typical configurations of the heat exchanger junction. The fluid mass flow equations for either side of the heat exchanger junction are summarized in reference [21]. After the fluid mass flow equations are solved,

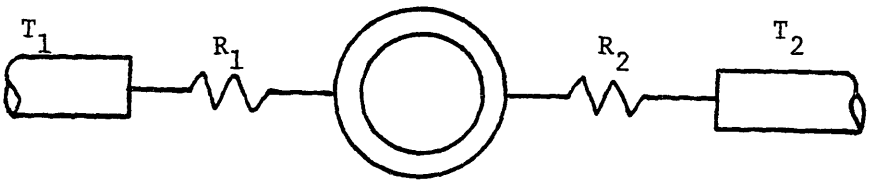

Figure 3-8: An Axial Fan Junction

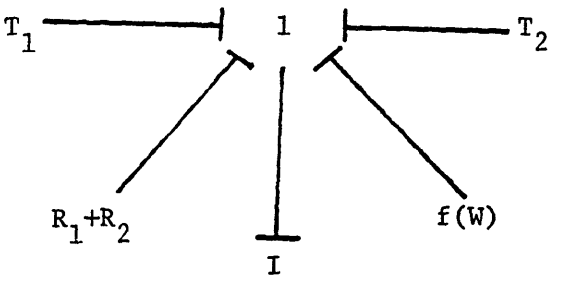

Figure 3-9: Axial Fan Junction Bond Graph Representation

the energy balance can be solved by the following equations.

$$Q = UA\frac{\Delta T_a - \Delta T_b}{Ln(\Delta T_a/\Delta T_b)} \tag{3.26}$$

$$h_h = c_h W_h[T_{h1}+T_{h2}]/2 + c_h|W_h|[T_{h1}-T_{h2}]/2 - Q \tag{3.27}$$

$$h_c = c_c W_c[T_{c2}+T_{c1}]/2 + c_c|W_c|[T_{c2}-T_{c1}]/2 + Q \tag{3.28}$$

3.6 Furnace Coal-Ash Deposit Estimation

In a coal fired plant, the coal-ash deposit on the waterwall tube may be an important factor in determining the maximum presure excursion after a main fuel trip. This is due to the fact that the ash deposit may have larger heat capacity than the combustion gas inside the furnace. After a MFT, the temperature of the combustion gas may decrease much faster than the temperature of the ash deposit on the waterwall tubes. The temperature of the gas becomes lower than the temperature of the ash deposit, resulting in heat transfer from the ash deposit back to the furnace combustion gas. The amount of heat transfer depends on the amount and characteristics of the ash deposit.

Substantial amount of research work has been devoted to establishing methods for analyzing coal-ash behavior for pulverized coal furnaces, some of which are cited in Appendix B in order to form a basis to characterize the ash deposit.

An analytical model is developed to represent the ash deposit and a formal procedure is also outlined to estimate the steady state heat transfer rate and the amount of deposition.

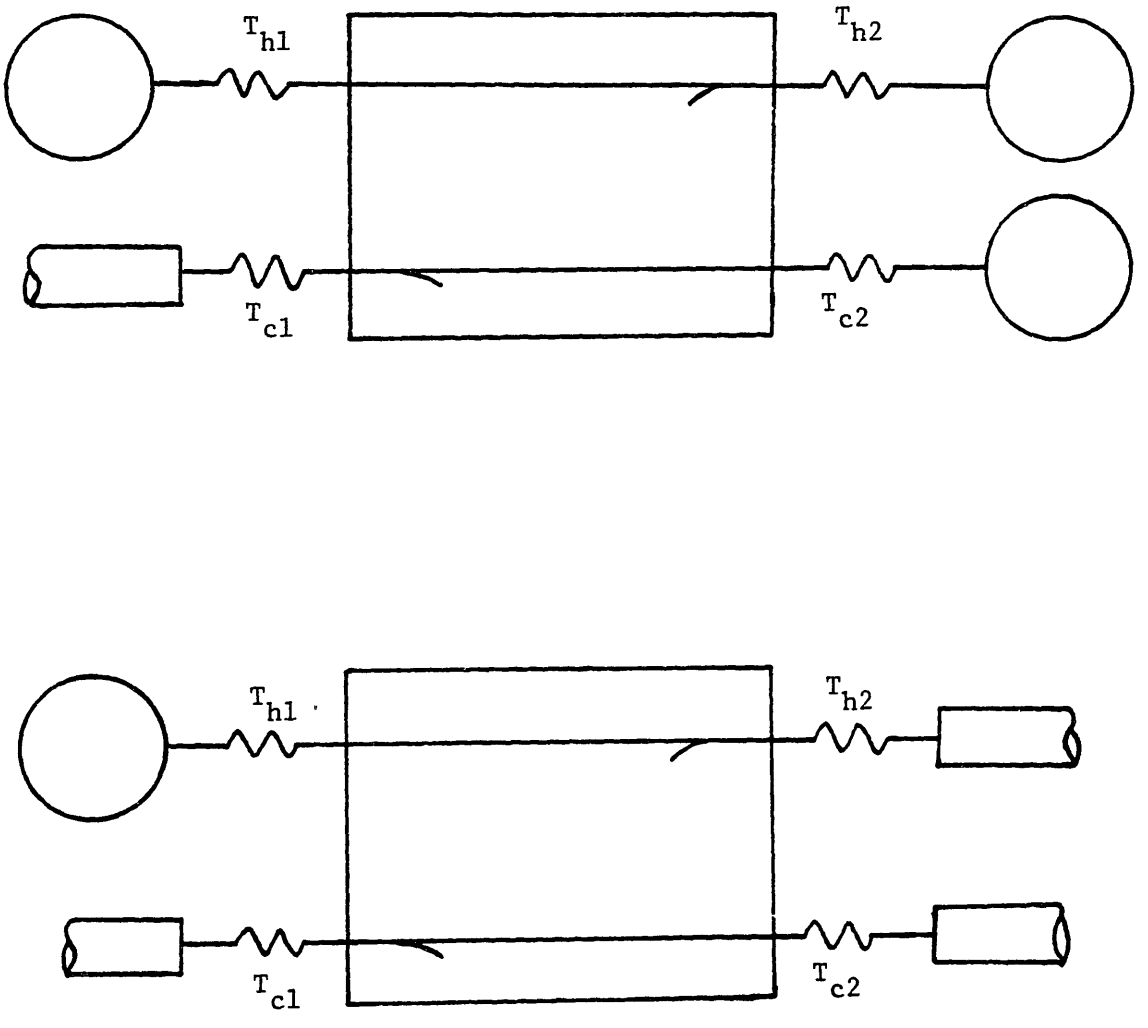

Figure 3-10: Heat Exchanger Junction Configurations

The unit element coal-ash deposit heat transfer model has been described in Appendix B. However, the thickness of the deposit is not directly measurable and varies over time during operation. Different operating schedules of the soot-blower may produce various possible deposit distribution at any particular time of day. The furnace heat-absorbing surface may, when clean, have absorption rates in excess of 175,000 Btu/sq ft,hr. When slag accumulations reach equilibrium, the absorption rates may be reduced to 50,000 Btu/sq ft,hr. or lower. Since the ash deposit accumulation is the dominant varible for heat absorption rate, it is reasonable to estimate the ash deposit thickness from the measured or calculated steady state heat transfer rate and other operating parameters. The thickness of the ash deposits can be computed if the heat transfer rate through the deposit and the thermal conductivity of the deposit is known. A formal procedure for the deposit estimation is developed which includes the following steps.

1. Estimate Furnace Total Heat Absorption Rate:

The heat transfer rate may be measured directly by installing thermal probes at different elevations of the furnace. A typical heat transfer rate distribution is shown in Figure 3-11 for a Babcock & Wilcox furnace [7]. However such directly measured data may not available, and an analytical solution of the problem of heat transfer in the entire furnace is extremely complex. Operating information is needed to supplement theoretical calculations.

Figure 3-12 shows a model for the estimation of total heat transfer in a furnace. It is assumed that the furnace outlet temperature is constantly monitored and is a known parameter for the calculation. Such an assumption is based on the fact that the furnace outlet temperature, to a large extent,

has been the dominant factor in the design of downstream components, particularly the superheater.

The total heat transfer in a furnace can be calculated by using the steady state energy blance equation on the model shown in Figure 3-12.

$$Q = E_c - E_w + c_p W_i T_i - c_p W_o T_o \tag{3.29}$$

$$E_w = \lambda W_f \left[c_w(T_{st}-T_f) + h_{fg} + c_{st}(T_o-T_{st})\right] \tag{3.30}$$

$$E_c = H_v W_f \tag{3.31}$$

where:

Q = total heat transfer rate

E_c = energy generated by combustion

E_w = energy to evaporate the moisture in the fuel

c_p = specific heat of the gas

T_i = inlet air temperature

T_o = furnace outlet temperature

W_i = inlet air flow rate

W_o = outlet gas flow rate

λ = fuel moisture fraction

W_f = fuel flow rate

c_w = specific heat of water

c_{st} = specific heat of steam

T_{st} = saturation temperature of water

T_f = fuel input temperature

h_{fg} = water latent heat value

H_v = heat value of the fuel

2. Average Heat Transfer Rate in a Furnace Compartment:

With the total heat transfer known, the local heat transfer rate per unit area can be calculated if the heat transfer distribution is known. It is assumed, that the heat transfer rate follows the pattern shown in Figure 3-11. In most practical cases, a furnace is modeled by a number of compartments, each one of which is a combustion furnace element developed in Chapter 2. It is convenient to assume that the heat transfer rate within each compartment is uniform. An average heat transfer rate can be calculated in the following equation to represent heat transfer for each compartment.

$$q_i = \frac{1}{Ai} \int_{Ai} q dA \tag{3.32}$$

where:

q_i = average heat transfer rate in compartment i

Ai = heat transfer area of compartment i

3. Calculate Ash Deposit Surface Temperature:

The ash deposit surface temperature can be calculated by iterating the following equation with q_i as a known variable from step 2.

$$q_i = \sigma \epsilon_f a T^4 - \sigma \epsilon T_s^4 + U_c(T-T_s) \tag{3.33}$$

where:

σ = Stefan-Boltzmann constant

ϵ_f = flame emissivity

ϵ = ash deposit emissivity

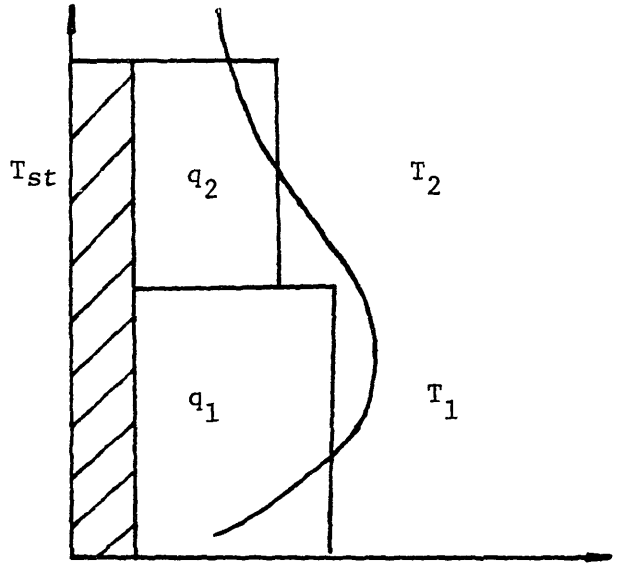

Figure 3-11: Typical Heat Absorption Distribution

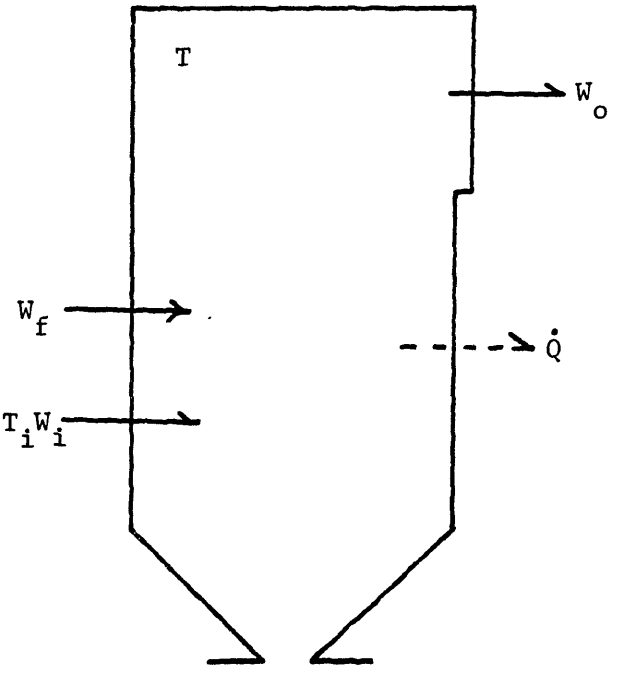

Figure 3-12: Steady State Furnace Energy Balance Model

a = ash deposit absorptivity

U_c = surface convective heat transfer coeffecient

The numerical values of ash deposit emissivity and absorptivity can be found in Appendix B. Large confidence intervals exist for these two parameters, choosing upper or lower bound for the data may result in quite different surface temperatures. Engineering judgements must be made after the surface temperature is computed.

First of all, the surface temperature should never be higher than the flow temperature of the ash deposit. The means that the slag viscosity η should be less than 80 when the surface temperature T_s is substituted into the viscocity equation in Appendix B.

If the secondary deposit layer is assumed to exist and corresponding surface parameters are chosen, the resultant surface temperature should be higher than the initial slagging temperature defined in Appendix B.

4. Estimate Ash Deposit Thickness:

After the ash deposit surface temperature is computed, and the existence or non-existence of the secondary deposit layer is confirmed from step 3. It is easy to estimate the deposit thickness from the following conduction equations.

$$l_1 = k_1(T_{is} - T_{tb})/q_i \tag{3.34}$$

$$l_2 = k_2(T_s - T_{is})/q_i \tag{3.35}$$

where:

l_1 = thickness of the primary deposit layer

l_2 = thickness of the secondary deposit layer

k_1 = thermal conductivity of primary deposit layer

k_2 = thermal conductivity of secondary deposit layer

T_s = deposit surface temperature

T_{is} = initial slagging temperature

T_{tb} = watertube temperature

q_i = heat transfer rate

The thermal conductivities k_1 and k_2 are provided in Appendix B when the initial slagging temperature is defined. The watertube temperature is assumed to be close to the saturated water temperature inside the tube due to the high thermal conductivity of the metal tube when compared to that of the ash deposits.

5. Estimate Ash Deposit Heat Capacity:

The steady state energy storage in the primary and secondary ash deposits can be calculated from the following equations.

$$U_1 = (c_s A_i l_1 \rho)\frac{T_{is} + T_{tb}}{2} \tag{3.36}$$

$$U_2 = (c_s A_i l_2 \rho)\frac{T_s + T_{is}}{2} \tag{3.37}$$

The specific heat of the ash deposit c_s can be computed in reference to Appendix B. The density of the ash deposits is from the density table in Appendix B.

The ash deposit estimation procedure outlined in this section is used to establish necessary initial conditions for any implosion simulation.

Chapter 4
PLANT DESCRIPTIONS AND MATHEMATICAL REPRESENTATIONS

4.1 Introduction

The representation of a plant with the foregoing generic basic elements and the junctions defined in previous chapters requires the following assumptions and considerations.

First, the selection of a basic element to represent a particular portion of a plant must be based on careful engineering judgement. For example, when the Plenum Element is used to represent the convective furnace, the momentum effect of the flowing gas is neglected since it is not included in the plenum element formulation. Similarly, when the transmission line is used to represent ductwork, neither attenuation nor dispersion is considered in the model. This is true for most power plant ductwork when hot gas flows in large cross section ducts, they are practically in the turbulent region and the pressure drop is very small when compared with bends and other connections.

Beside Plenum and Combustion Furnace Elements, there is an implicit assumption for all the rest of thermofluid elements that the internal energy is decoupled from the other forms of energy. Under this assumption, the internal energy and the other forms of energy couple and transform only at Plenum and Furnace Elements. The rest of the system can be represented by a fluid model coupled with a thermal transport model in an active manner. The fluid

model represents the energy conservation relation except for the internal energy terms. Its system structure and causality have been developed and described in references [54] [21]. The thermal side of the model accounts for internal energy transport and determines the temperature. This thermal model approximates transport delay when steady flows are involved, and also produces rational models when the fluid flows vary. A causality scheme has been developed to remain valid for all flow directions at the expense of additional nonlinear consititutive laws for junction elements. In this thesis, such a thermal causality is used whenever it is appropriate. In the event that it is known that the flows do not reverse, such as in the combustion furnace, the simple causality is used.

The equations defining the set of junctions coupling the elements must be written as defined in Chapter 3.

Two power plants are characterized in this chapter to demonstrate the system modeling structure. The models are also used in the next two chapters to simulate the furnace implosion dynamics, and the results are to be compared with field test data to validate the model. The descriptions of the plants are given in the following paragraphs.

4.2 Detroit Edison St. Clair Unit 3

4.2.1 Plant Description

Each St. Clair Unit 1-4 is rated at 156 MW and consists of a balanced draft coal fired boiler. The forced draft side of each unit has two variable speed FD fans operating in parallel, each capable of delivering 210,500 CFM at

12.5 inches of water head and 855 RPM. The induced draft side of each unit at the time of test had two variable speed ID fans operating in parallel, each capable of delivering 268,000 CFM at 16.6 inches of water head and 865 RPM.

Extensive implosion tests were conducted in the plant before the plant was converted to fire low sulfur Decker coal. The significance of the conversion was that the low sulfur Decker coal has a much lower BTU content (higher moisture) requiring larger induced draft (ID) fans. Unit 3 was selected to perform the tests.

A schematic representation of the plant is shown in Figure 4-1.

4.2.2 Plant Model

A simulation model for the St. Clair plant Unit 3 has been formulated which includes a characterization of the following:

- Radiant Furnace
- Convective Furnace
- Centrifugal FD and ID fans
- Superheaters, Reheaters and Economizers
- Air Preheaters
- Precipitator
- Duct Work
- Fuel and Ash Properties

The model for this plant is shown in Figure 4-2. Due to the large temperature and fuel concentration gradients in the radiant furnace, it has

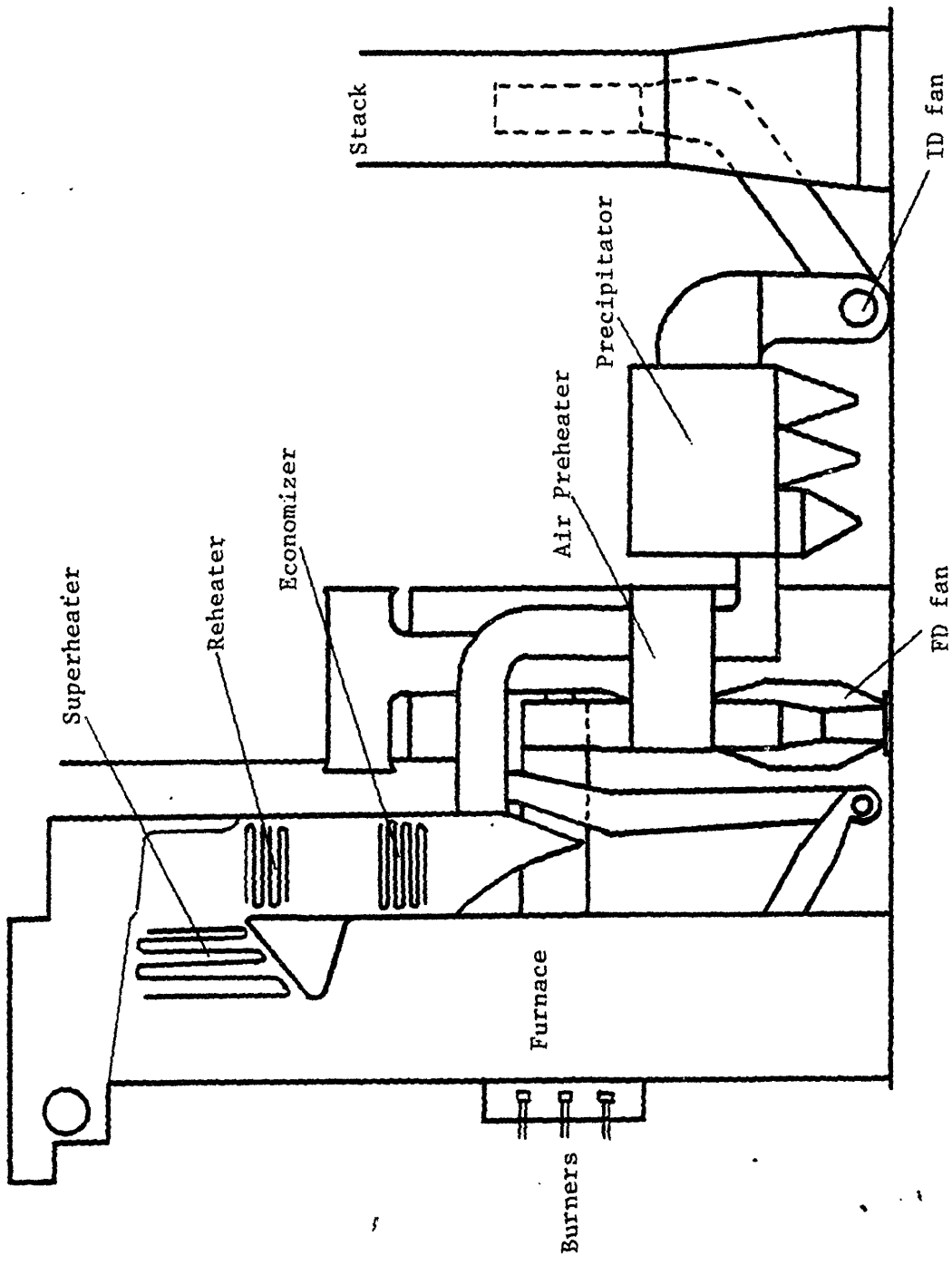

Figure 4-1: The Detroit Edison St. Clair Unit 3

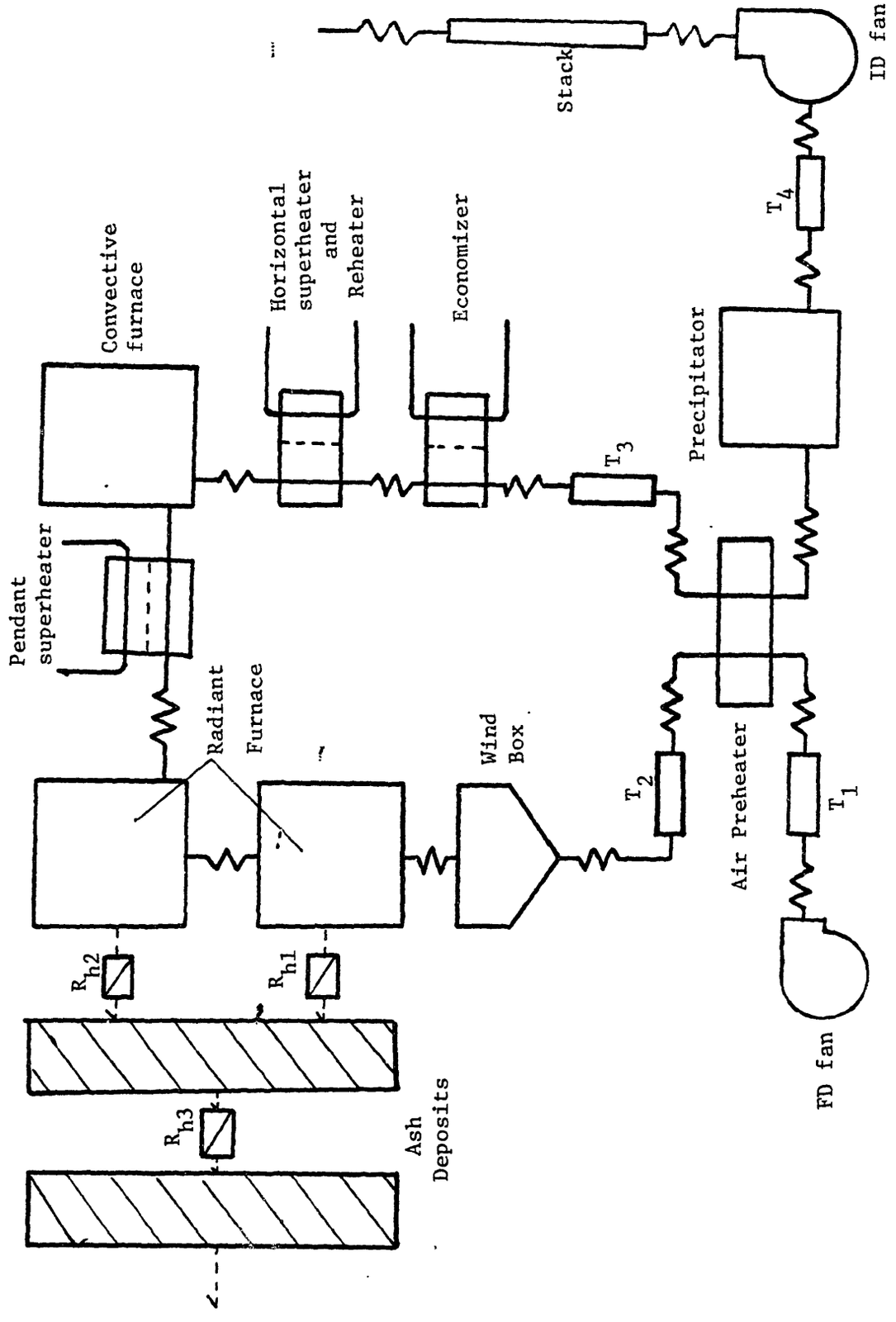

Figure 4-2: Mathematical Model for St. Clair Unit 3

been represented as a compartmental model by two combustion furnace elements F_1 and F_2 of proper sizes to represent the fuel average residue time in the radiant furnace. The procedure to determine the residue time distribution of a furnace is outlined in Chapter 3. Since a tracer test is not available for this particular furnace, two equally divided furnaces elements are used.

The heat transfer resistance elements R_{h1} and R_{h2} represent the heat transfer between radiant furnace gas and the slag deposit on the furnace wall. Both radiative and convective heat transfer modes are considered. The heat transfer element R_{h3} represents the conduction heat transfer from the ash deposits.

The ash deposits on the furnace walls are modeled as solid thermal elements. Their primary function is to represent the energy storage in ash deposits. Since these solid thermal elements may store much more energy than the gaseous elements, their time constants may be longer. However, in the time frame of implosion, the heat transfer between the gas in the furnace and ash deposit may change rapidly, even in its direction, because of the large time constant of the ash deposit. Therefore, the inclusion of these elements in the model is important for transient analysis of furnace implosion after a main fuel trip. Since the water tubes have very high thermal conductivity, the temperature of the tube is essentially that of the saturated steam. The temperature drop across the ash deposits is usually as high as a few hundred degrees. Although it may be a very thin layer, a fraction of a inch, the ash deposit is more accurately represented dynamically by two solid thermal elements instead of one.

Significant heat transfer and pressure drop take place as the flue gas

passes through the pendant superheater and reheater. Heat Exchanger H_1 is used to represent the energy transfer from the gas side to the steam side.

Plenum elements are utilized to represent the windbox, the convective furnace and the precipitator where the gas accumulated in each of these large volumes has essentially uniform pressure and temperature.

The long ducts are modeled by transmission line elements. The transmission line elements in the model include T_1 representing the duct work from the FD fan to the air preheater, T_2 from the air preheater to the windbox, T_3 from the furnace outlet to the air preheater and T_4 from the precipitator to the ID fan. Since these duct lengths are much longer than their cross section dimensions, their dynamic behavior is well represented by one-dimensional pressure and flow waves in the transmission line element.

Since the two parallel centrifugal FD fans and the ducts connected to them are identical, an equivalent fan element and an equivalent transimission line are used to represent the overall forced draft pressure and flow characteristics. Two parallel ID fans and the ducts connected to them are represented by an equivalent fan and an equivalent transmission line element. Second order polynomials are used to represent the fan pressure-flow characteristics.

The heat exchanger elements are also used to represent the temperature drops across the horizontal superheater H_2, economizer H_3 and air preheater H_4.

The elements have been coupled by the junction structures to represent the plant configuration.

4.2.3 Plant Parameters

The baseline parameters for the plant including lengths and area of transmission lines, volume and effective heat transfer areas for furnaces and plenums are summarized in Table 4-I. These geometric parameters are estimated from plant drawings. Also indicated in the table are the initial steady state pressure, flow and temperature data at a partial load of 132 MW. Along with the heat exchanger input and output temperatures, these data are used to compute the flow resistances and heat transfer coefficients for the plant. The equivalent FD and ID fan initial conditions are also included in the table.

The amount of ash deposit in the furnace is not directly available, and may vary from time to time during operation. However the importance of the effect of ash deposits on the pressure excursion after a MFT has been shown in the simulation. A formal procedure to estimate the ash or slag deposit on the furnace walls has been developed in Chapter 3. The ash deposits estiamation for the St. Clair plant is summarized in Chapter 6.

Table 4-1. St. Clair Unit 3 Plant Parameters

Transmission Line Elements

	T_1	T_2	T_3	T_4	T_5
Length (ft)	50	50	100	75	75
Area (ft^2)	100	100	75	75	75
Initial Pressure (inches of H_2O)	8	5	-6	-10	1
Initial Temperature (°R)	540	900	1060	720	720
Initial Flow (lbm/sec)	328	328	328	328	328

Combustion Furnace Elements/Plenum Volume Elements

	F_1	F_2	P_1	P_2	P_3
Volume (ft^3)	45750	45750	30,000	53,000	33,000
Projected Area (ft^2)	8500	8500	——	——	——
Initial Temperature (°R)	2600	2400	900	1,800	720
Initial Pressure inches of H_2O)	3.5	3	4.5	0	-9

Table 4-1. Continued

Equivalent Fans

	Diameter (ft)	RPM	Initial IGV
FD	8	855	25
ID	8	865	40

Heat Exchanger Elements

Temperature (°R) \ Element	H_1	H_2	H_3	H_4
TH1	2400	1800	1360	1060
TH2	1800	1860	1060	720
TC2	1100	900	700	540
TC1	1500	1250	1000	900

4.3 Detriot Edison Greenwood Unit 1

4.3.1 Plant Decription

The Detroit Edison Greenwood Unit 1 is an 800 MW oil fired unit which is capable of fast fuel cut off. The unit design is quite compact and has no precipitators and therefore no large unheated gas volumes. The axial induced draft fans have high suction capability.

4.3.2 Plant Model

The mathematical model of Greenwood Unit 1 is shown is Figure 4-3. The model consists 39 elements:

```
2 Combustion Furnaces
   F1 -- Compartment 1 of radiant furnace
   F2 -- Compartment 2 of radiant furnace

2 Plenum Volumes
   P1 -- Windbox
   P2 -- Convective Furnace

2 Fans
   FD -- Forced draft centrifugal fan
   ID -- Induced draft axial fan

5 Transmission Lines

19 Fluid Flow Resistances

2 Solid Thermal Elements
   TH1 -- Slag or ash deposit on tube walls
   TH2 -- Boiler tubes

4 Heat Exchangers
   H1 -- Pendant superheater
   H2 -- Horizontal superheater
```

H3 -- Economizer
H4 -- Air preheater

3 Heat Transfer Resistances

The basic considerations and techniques for modeling the furnace, plenums and transmission lines are essentially similiar to the St. Clair plant. Since detailed information about FD and ID fans is not available, generic centrifugal FD fan and axial ID fan characteristics have been assumed. In the plant, six holes, each measuring twelve square feet, were cut in the FD fan outlet duct to bypass part of the flow to atmosphere. At full load 25% of the FD fan air flow is vented to the atmosphere. The resistance R_o in Figure 4-3 represents these holes. The purpose of cutting these holes is to avoid excessive negative pressures in the forced draft ductwork during implosion conditions.

4.3.3 Plant Parameters

The plant parameters are summarized in Table 4-II. Only geometric parameters are included in the table. Since the tests conducted in the Greenwood plant were at different load levels, there are no single nominal values for pressure, flow and temperature to compute flow resistances and heat transfer coefficients. Instead, a formal steady state analysis capability has been built into the computer model which uses the initial pressure, flow and temperature values at a load level to compute the system parameters such as flow resistances and heat transfer coefficients corresponding to the load level.

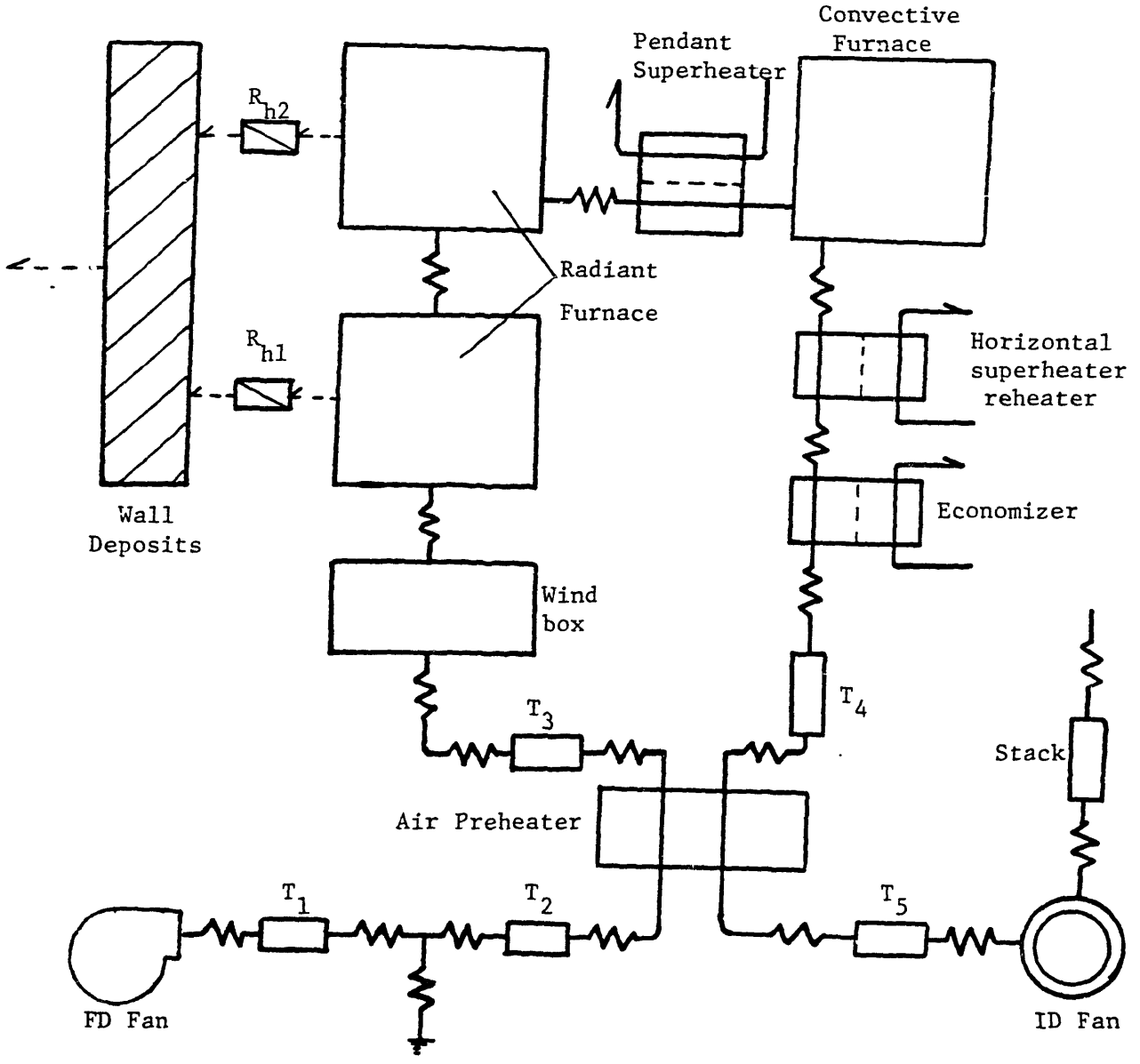

Figure 4-3: Mathematical Model for Greenwood Unit 1

Table 4-2. Estimated Greenwood Unit 1 Plant Parameters

1. Transmission Line Element Parameters

	Length (ft)	Section Area (ft^2)
T_1	50	400
T_2	50	400
T_3	100	320
T_4	200	320
T_5	100	320
T_6	150	320

2. Combustion Furnace Element Parameters

	Volume (ft^3)	Projected Area (ft^2)
F_1	280,000	35,000
F_2	280,000	35,000

3. Plenum Volumes (ft^3)

P_1	120,000
P_2	340,000

Chapter 5
COMPUTER SIMULATION

5.1 Introduction

The simulations of the St. Clair and Greenwood power plants computed the time responses of the pressure, mass flow and temperature at any point in the plant to a main fuel trip. The fuel concentration in the furnace and the heat transfer rate at the boiler, superheater, economizer and air preheater are also computed. The simulation data has been compared with experimental data and used to evaluate the range of the validity of the analysis method. This chapter describes the algorithmic structure of the simulation methods and computer software implementation.

The simulation is based on a plant representation in terms of basic elements. The plant representation for St. Clair Unit 3 and Greenwood Unit 1 are described in Chapter 4. The step-wise numerical simulation represents the furnace combustion dynamics, the pressure and temperature dynamics in the air/gas system and temperature dynamics in tube walls and slag, the acoustic wave propagation through the ducts and the reflection and transmission properties of wave phenomena at junctions. The simulation updates the system parameters at each time step due to the temperature dependent nonlinear fan characteristics, flow resistances and transmission line delay times. The system input is obtained by representing the main fuel trip as a step or a exponential decay of fuel mass flow rate. The system control actions are modeled by

simulating time varying fan inlet guide vane angles or damper openings.

In the present implementation, the plant structure is specified through a set of user written subroutines. This choice was made to enhance program adaptability to a wide range of plant configurations.

5.2 Simulation Structure

The system simulation structure is represented by a diagram shown in Figure 5-1. All the dynamic elements developed in Chapter 2 must be simulated in integral causality as shown in the first block of Figure 5-1. The system disturbance matrix $\underline{D}$ and the reflected variable matrix $\underline{U}$ at transmission lines, the flow matrix $\underline{W}$ and the transport energy matrix $\underline{h}$ are the rate variables to the dynamic elements, the state variable matrices are the mass matrix $\underline{M}$, the internal energy matrix $\underline{U}_o$, the incident matrix $\underline{V}$ at transmission lines and the momentum matrix $\underline{M}_o$. The state variables are the integration and delay results from first block; they determine the system state at any given time of simulation.

In air/gas systems, it is possible and desirable to transform the state variables of all the dynamic elements into a preferred set. The set is chosen either because of possible direct measurement of the state variables or because of convenient simulation procedures. For plenum type of elements, the pressure $\underline{P}$ and the temperature $\underline{T}$ are chosen to be the preferred state variables; for a transmission line, the incident wave variable at both ends $\underline{V}$ and average temperture $\underline{T}$; for an axial fan element, the fluid flow $\underline{W}$ and for a solid thermal element, the temperature $\underline{T}$. The preferred set of state variables replaces the original state variables to represent the system at any given time

during the simulation. It is transferred from original state variables by the operation in the second block in Figure 5-1. Through the junction operation in the third block, it also determine all the rate variables which can be used for the next time step simulation.

A flow chart of the major functional blocks of the simulation is shown in Figure 5-2. The first three blocks of this flow chart involve initialization of the system parameters. The first block is the input of the minimum data needed for the simulation of the plant representations described in Chapter 4. These data include:

1. Type of fuel used (oil or coal fired plant)
2. Number of each type of element, the program will ask for information if a particular type of element is included
3. Line specifications (length, cross-sectional area, temperature, mass flow rate and pressure)
4. Fan specifications (mass flow rate, gas density, RPM and diameter)
5. Plenum and furnace parameters(volume, heat transfer area, temperature and pressure)
6. Heat exchanger input and output temperatures, mass flow rates
7. Fuel specifications (mass flow rate, heat value and composition)

The remainder of the initialization phase involves the computation of additional system parameters including an estimation of ash and slag deposits on furnace walls and the initialization of the wave variable delay buffers.

The simulation proceeds in a step wise manner with a constant time step between iterations. At each time step the following actions described in the subsequent blocks are executed. Block 4 generates the main fuel mass flow rate

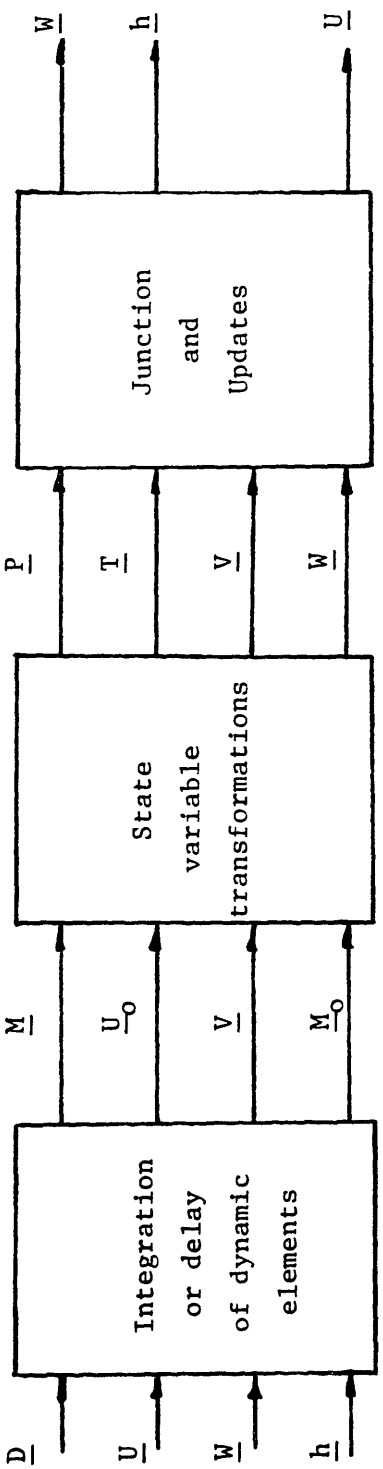

Figure 5-1: The General Simulation Causality

decay as a system disturbance. Block 5 generates the heat transfer rate at all heat transfer resistance elements and the heat exchanger elements. These heat transfer rates are ultilized by Block 10 to compute the new state variables.

Block 6 updates all system parameters which are time varying, such as fan characteristic coefficients and the flow resistances. At Block 7 the algebraic equations of the junctions are solved, generating a set of acoustic wave variables that propagate away from the junction toward the opposite end of the line. At this point in the simulation the pressure at any junction is computed as the sum of the incident and generated wave variables by Block 8.

The generated wave variables are stored in a set of first-in-first-out buffers as indicated in Block 9 to simulate the propagation delay through each duct. These delay buffers are organized to provide linear interpolation between sample points if the required acoustic delay is not an integer number of simulation time steps.

All the dynamic elements such as the combustion furnace, plenum volume, solid thermal and actuator elements (see Appendix C) are solved in Block 10 for the time step, using a fourth-order Runge Kutta integration method to solve the set of simultaneous first-order differential equations. The complete state of the plant is determined at this point and the simulation time is incremented in order to begin the next step.

5.3 Implementation Details

The simulation software package has been written to operate under the program DYSYS (DYnamic SYstem Simulator) described in reference [10]. The program solves time responses of the systems described by a set of linear or nonlinear ordinary differential equations and is capable of solving a mixture of algebraic and differential equations.

To use DYSYS a FORTRAN subroutine EQSIM is written and linked to the main program. The primary numerical integration is performed by a fourth-order Runge Kutta subroutine RKDIF which is called once each time step. RKDIF in turn calls the user supplied EQSIM four times each time step. A flag variable NEWDT in the COMMON block is used to signal EQSIM as to the nature of each call (whether it is the first call of the simulation, a new time step, or an intermediate call).

The plant simulations were written as special versions of EQSIM with reference to a library of junction and element subroutines. The hierarchy of subroutine calls is shown in Figure 5-3. The subroutines are, in general, divided into two groups. The subroutines PLENUM, FURNACE, STHERM, LINE, FANAX belong to the dynamic element subroutine group. They charactrerize the dynamics of the plenum, furnace, transmission line, solid thermal and axial fan elements. These subroutines are called four times each time step by RKDIF. The other subroutines represent the elements or junctions which are static or quasi-static in nature. They are called only once each time step by RKDIF.

The subroutine MFT is used to characterize the main fuel trip as a disturbance to the system.

The subroutine HTRS and HTEX represent the heat transfer characteristics of the heat transfer resistance and heat exchangers. The heat transfer rates are computed by the subroutines from the temperature differences across the heat transfer resistances.

The system parameter updates are performed by RESIST, FANAX and FANCT. RESIST updates a new pressure-flow relation for a resistance element when the temperature at that element has changed. FANCT produces a new centrifugal fan characteristic after each time step accounting for changes in gas density, inlet guide vane angle and fan RPM. FANAX updates axial fan characteristics in the same way as FANCT does for centrifugal fans.

The algebraic solution of the junction equations is performed by the subroutine JUNC, which in turn calls a set of specific junction subroutines that solve the wave equations for each type of junction structure that has been defined.

The subroutine DELAY stores the generated wave variables in the delay buffers and retrives the delayed versions for use as incident variables in the next time step. The subroutine PWTRF is used to combine wave variables to compute the pressure variables at the junctions.

5.4 Simulation of Specific Plant Configurations

The computer model organization described in Figure 5-3 has been implemented in a modular fashion so that it may be easily modified to represent other plant configurations.

The MAIN program and subroutine RKDIF requires no modification as

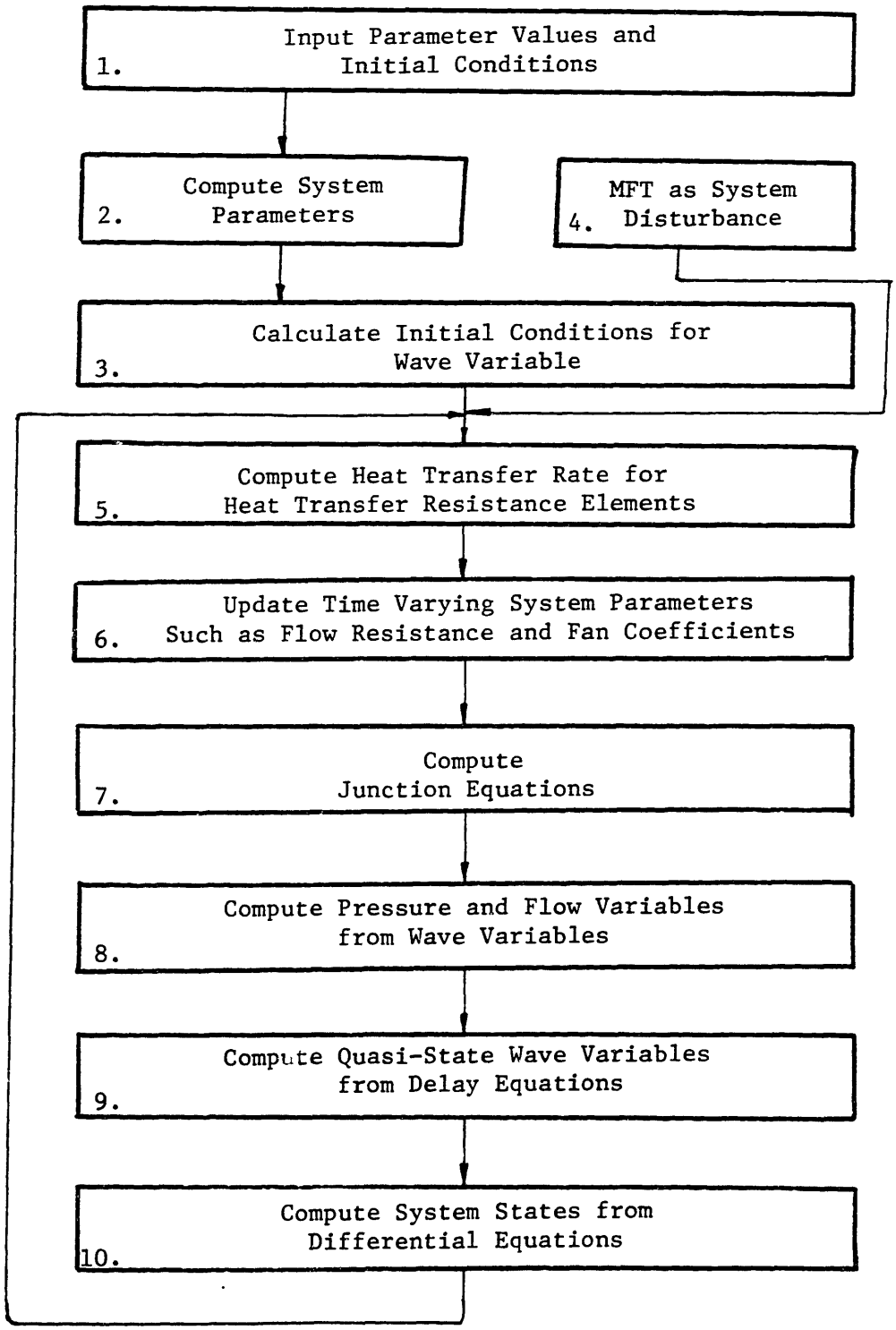

Figure 5-2: Computer Simulation Program Flow

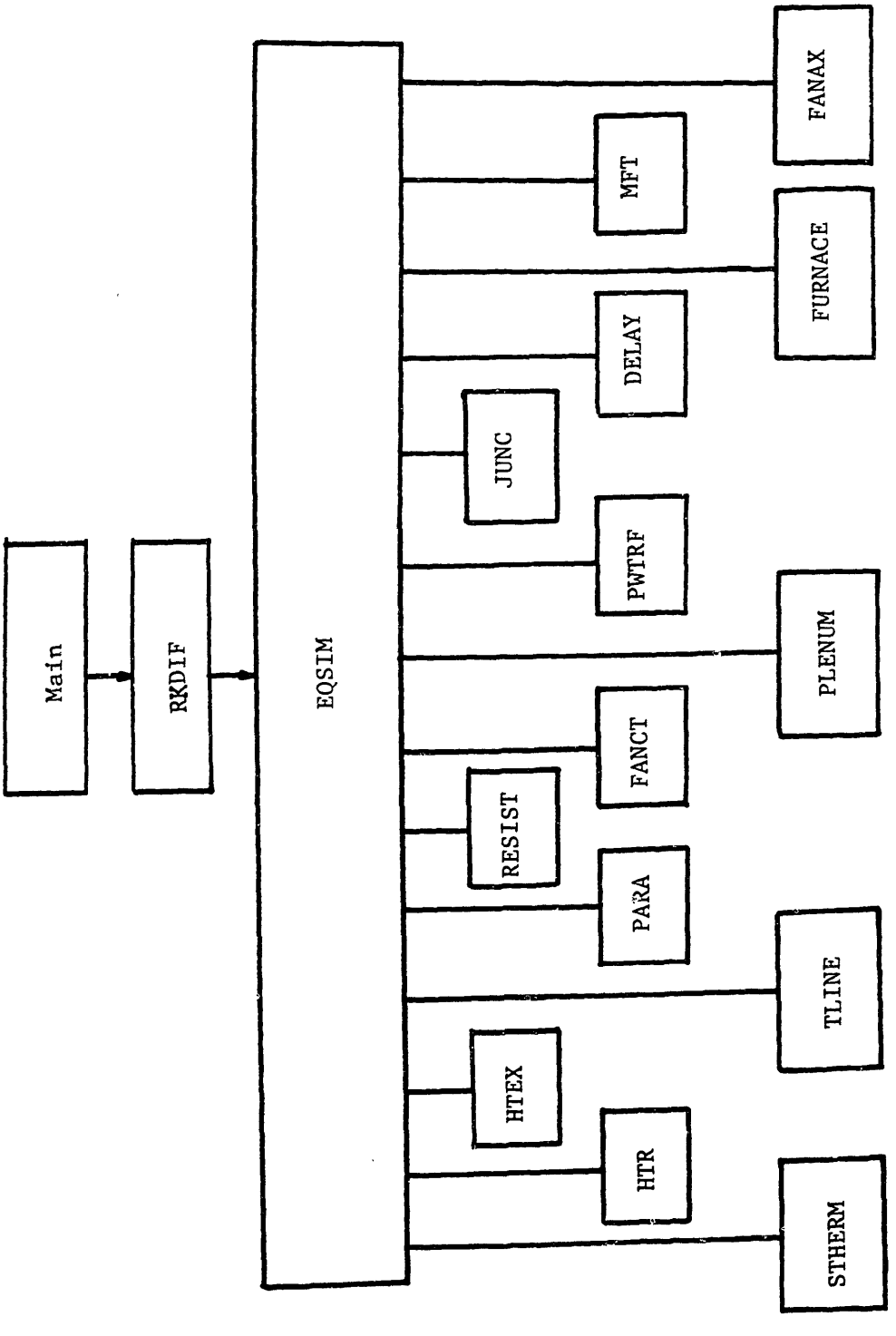

Figure 5-3: Computer Model Organization

long as there are less than 30 system state variables. If more than 30 state variables are present in the model a larger version of DYSYS should be linked; up to 98 state variables can be simulated.

The subroutine corresponding to each basic element is written in generic terms, no modification is needed for different plants. The subroutine JUNC contains the information specifying element interconnections for a specific plant. It has to be prepared for each plant configuration.

The subroutine EQSIM is prepared by the user to represent different plant configurations. The input portion of EQSIM has been written so that the specification of the input parameters indicate the number of transmission lines, furnaces, plenums and other elements. Their associated physical parameters are read in from a data file and no program modification is required for initialization of the other plants.

Chapter 6
COMPARISON OF SIMULATION MODELS WITH EXPERIMENTAL RESULTS

6.1 General Cases

The main fuel trip tests conducted at the St. Clair and Greenwood plants provide data to evaluate the mathematical models formulated in Chapter 4. For main fuel trip disturbances to both systems, pressure versus time traces at several locations in the system have been computed and compared with the measured data to evaluate the model capability. The sensitivity of system response to parameters, such as ash deposit, has also been studied.

6.2 St. Clair Plant

6.2.1 Test Description

Units 1 through 4 at the St. Clair Power Plant were scheduled for retrofitting with appropriate gas handing equipment for firing low sulfur Decker coal. The Engineering Research Department at Detroit Edison Company conducted a set of main fuel trip tests on Unit 3 prior to the retrofit and collected the data for calibration of their mathematical model and design of the new system as described in reference [14].

The time histories of the gas and air pressures at 13 points were measured by pressure transducers after the MFT. The transducer locations are shown as circles on the cross sectional view of the Unit, Figure 6-1. The trip was initiated from a steady state partial load of 132 MW. The other steady state data recorded before the trip included:

- Gas flow rate : 1180800 lbm/hr
- Main steam flow rate : 994000 lbm/hr
- Coal flow rate : 90000 lbm/hr
- Drum pressure : 1900 Psig
- Main steam temperature : 1000 ^{o}F
- Reheat steam temperature : 975 ^{o}F
- Coal heat value : 10950 Btu/lbm
- Coal moisture percentage : 12.2
- Ash percentage : 11.0

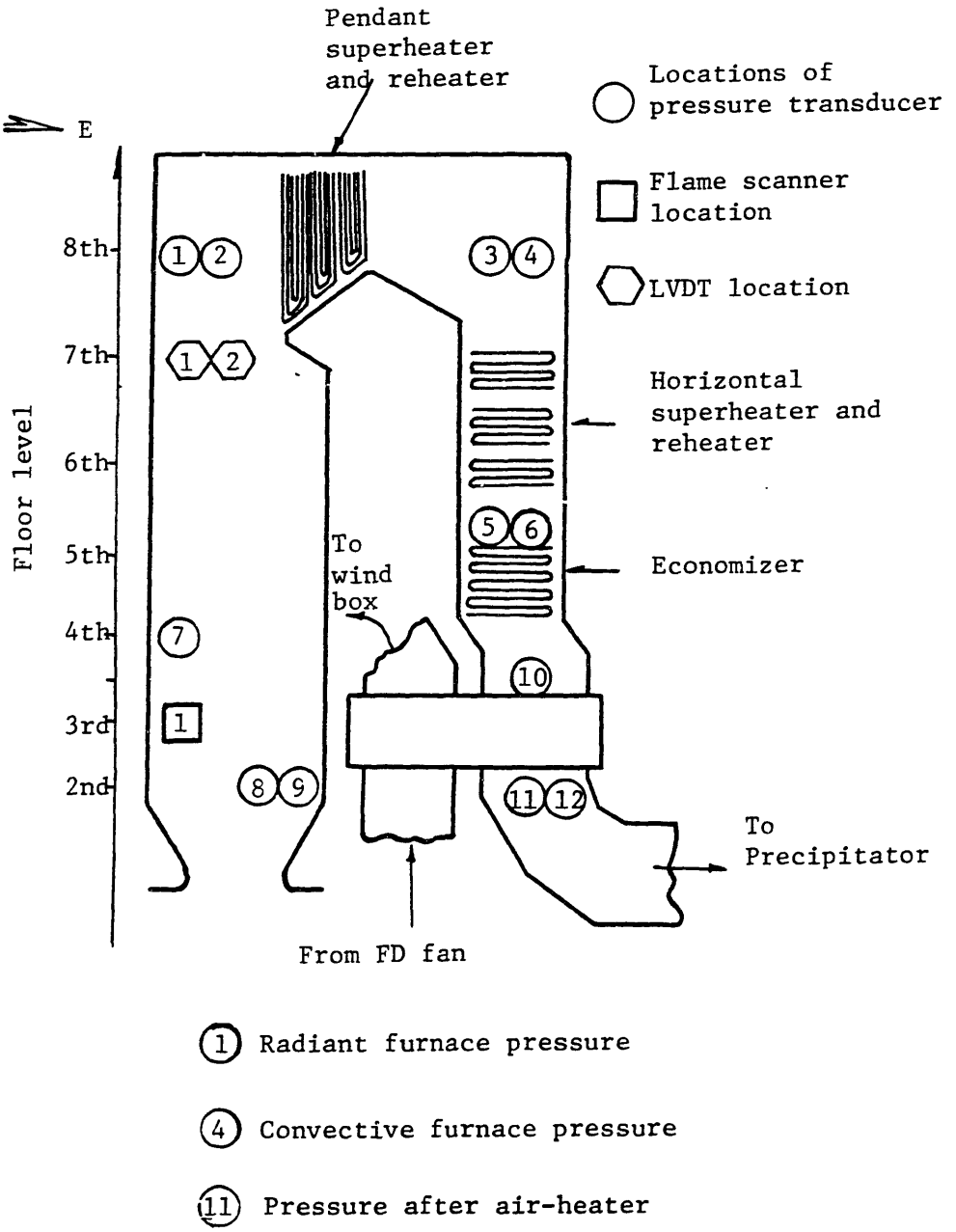

Figure 6-1: Instrumentation locations at St. Clair Unit 3 Ref. [14]

Table 6-I: Summary of Transient Pressure Data, Unit 3
St. Clair Power Plant Ref. [14]

Transducer Location*	Steady State (at time = 0) Pressure, in. H_2O	Peak Transient Pressure, in. H_2O	Time to Peak sec
1 - Radiant Side, 8th Floor, Southwest Corner	+2.5	-4.3	5.7
2 - Radiant Side, 8th Floor Northwest Corner	+2.5	-3.8	5.7
3 - Convective Side, 8th Floor Southeast Corner	+0.5	-6.0	5.8
4 - Convective Side, 8th Floor Northeast Corner	0	-6.0	5.8
5 - Convective Section, 5th Floor, Southeast Corner	-3.0	-7.3	5.7
6 - Convective Section 5th Floor, Northeast Corner	-2.9	-8.0	5.7
7 - Radiant Side, 4th Floor Windbox	+3.5	-1.1	5.6
8 - Radiant Side, 2nd Floor East Wall, South Door	0	-2.8	5.7
9 - Radiant Side, 2nd Floor East Wall, North Door	0	-5.5	5.7
10 - South Duct Upstream of Air Heater, 3½ Floor	-6.0	-10.7	6.0
11 - South Duct Downstream of Air Heater, 2nd Floor	-9.0	-11.0	6.0
12 - North Duct Downstream of Air Heater, 2nd Floor	-7.5	-12.0	5.8
13 - South Duct, FD Discharge 2nd Floor	+10.0	+3.5*	9.0

*Numbers correspond to circled numbers shown in Figure 6-1.

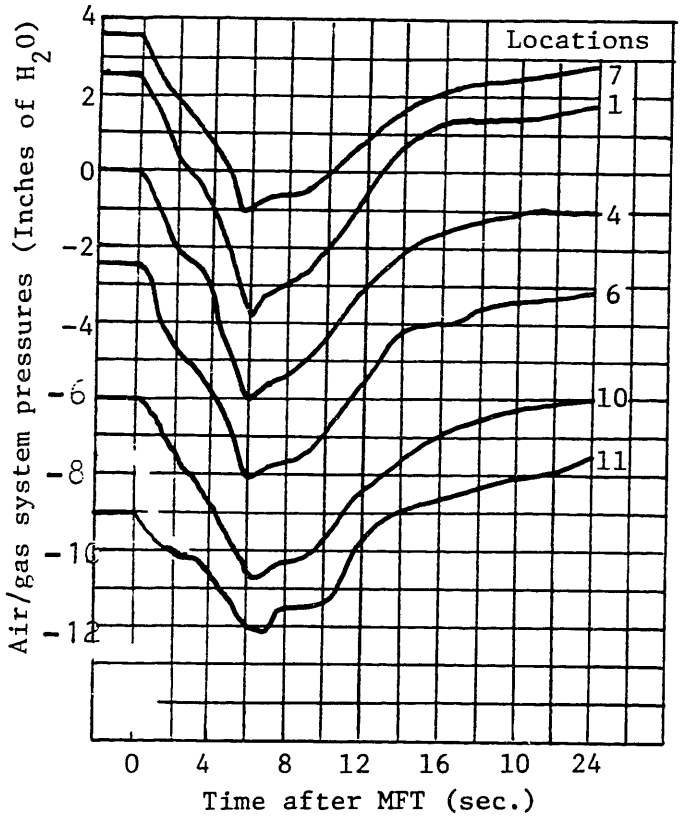

Figure 6-2. Pressure Throughout the Unit. Ref. [14]

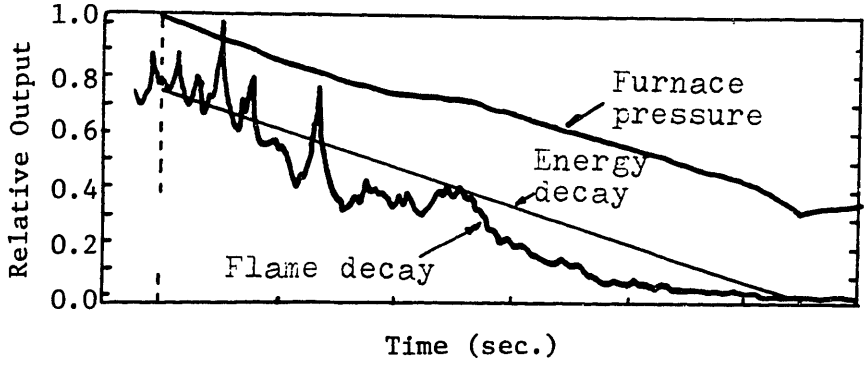

Figure 6-3. Flame Luminosity and Furnace Pressure vs. Time. Ref. [30]

- Sulfur percentage : 2.1

Table 6-I summarizes the values of the initial steady-state and the peak pressures during the MFT transient, and the time to the peak. A complete transient history of seven representative pressures is plotted in Figure 6-2. All the furnace pressure traces have the same general shape. The negative pressure excursion characteristics are reproduced throughout the system.

Another important test result is the furnace flame decay pattern. The flame luminosity was monitored through a photo diode detector as described in reference [30]. The location of the detector was at the burner level shown as a square in Figure 6-2. The output of this measurement is presented in Figure 6-3. The information given in Figure 6-3 can be used to indicate the energy decay in the furnace following a MFT.

6.2.2 Comparison of Model Simulation and Test Data

Since furnace ash deposits and energy stored in these deposits strongly affect the maximum pressure excursion in an implosion, an initial steady state ash deposit estimation has been conducted for the St. Clair Plant following to the procedure outlined in Chapter 3. Using the plant data provided in Chapter 4 and this chapter, the ash deposit estimation results are summarized as follows:

1. Total furnace heat transfer and energy rate are computed by the estimation model as:

$$Q = 129{,}000 \text{ Btu/sec.}$$

$$E_c = 273{,}750 \text{ Btu/sec.}$$

E_w = 6,253 Btu/sec.

2. Average heat transfer rate in the furnace compartments are computed according to an assumed heat absorption distribution:

q_1 = 32,968 Btu/hr ft^2

q_2 = 21,978 Btu/hr ft^2

3. The ash melting critical temperature T_{cv} can be computed using the ash chemical composition data. The data used for this case are for a typical U.S. eastern coal:

SiO_2 = 37.64	Al_2O_2 = 20.11
TiO_2 = 0.81	Fe_2O_3 = 29.28
CaO = 4.25	MgO = 1.25
Na_2O = 0.80	K_2O = 1.60

Using above data, the ash melting critical temperature T_{cv} is computed as 2490 °R according to the equations and figures defined in Appendix B.

4. A layer of solid ash deposit is assumed, the ash deposit surface temperatures are then calculated as:

T_{s1} = 2163 °R

T_{s2} = 1960 °R

The surface temperature at both furnace compartments are lower than the critical temperature T_{cv} defined in Appendix B. The solid ash deposit assumption is confirmed.

5. Estimate the ash deposit thickness from the conduction heat transfer model:

$l = 0.22$ inch

Although there is only one layer of deposit as assumed and confirmed, the temperature decrease aross the ash deposit is more than 700 °R. Two solid thermal elements of equal thickness are used to represent the dynamic characteristics of this ash deposit layer.

The transient response of the fuel supply shut-off is considered as follows. The mass fuel rate after the trip signal is approximated by a exponential decay. The effective time constant of the decay depends on the time constant of the coal handling and supply units and the distance between the burner and these units. The mathematical expression for the fuel trip disturbance is:

$$W_f(t) = W_{fs}\, e^{-t/\tau} \tag{6.1}$$

where: W_{fs} = steady state fuel flow rate

τ = effective time constant for fuel trip decay

The computed pressure responses at the radiant furnace, convective furnace and precipitator resulting from the fuel trip are compared with experimental test data in Figures 6-4, 6-5 and 6-6. The simulation pressures follow the test results accurately throughout the system over the complete transient range indicating that the residue time distribution of the air/gas system is well represented by the lumped and distributed system elements. The maximum negative pressure excursion at each point is also very well predicted. The deviations of the simulation result from the experimental data at the maximum pressure excursion points are less than $\pm 5\%$ of the the total pressure excursion values. No deviation is more than 15% of maximum pressure excursion during the entire time span of the simulation as indicated in

Figures 6-4, 6-5 and 6-6.

The simulation of energy generated by the combustion process in the furnace is plotted against the flame luminosity after a MFT, in Figure 6-7. Both of the variables are in non-dimensional form and are of the same general shape and decay time, indicating that the combustion furnace element has predicted very well the combustion transient after a MFT. An energy decay with that general shape can be used in a simplified model when detailed representation of combustion dynamics is not required in the model. This plot also shows that the energy decay time corresponds to the maximum negative pressure excursion time. This characteristic leads to possible control measures to slow the fuel shut off rate which can delay the maximum pressure excursion.

Time histories of temperature and fuel concentration in the furnace are plotted in Figures 6-8, and 6-9. At the initial stage after the fuel is shutoff, the chemical reaction of combustion continues at a very fast rate so that the unburnt fuel in the furnace decreases rapidly. The rapid decrease in fuel concentration in the first few seconds shown in Figure 6-9 demonstrates the phenomena. As the fuel decreases in the furnace, the combustion energy generated decreases, the temperature of the gas, in turn, drops. The decrease in temperature has an exponential affect on the combustion rate. When the temperature drops to a lower level and the combustion rate decreases, the reduction of the amount of fuel in the furnace is essentially due to removal by the draft system. The flat portion of the concentration curve in Figure 6-9 reflects the change of operating conditions.

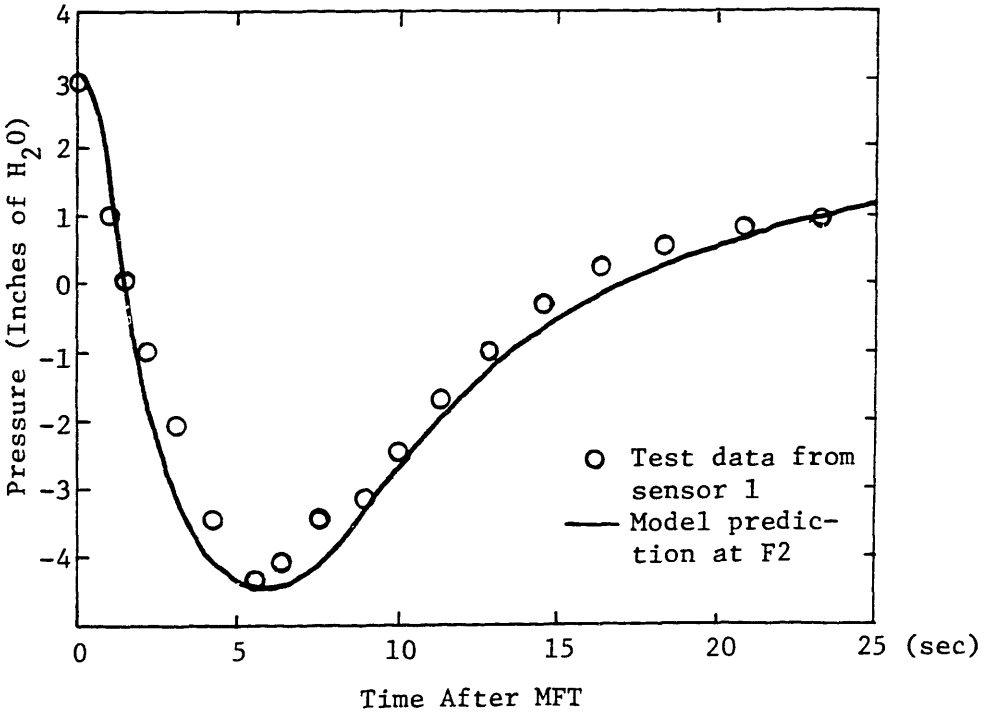

Figure 6-4: Pressure Comparison at Radiant Furnace

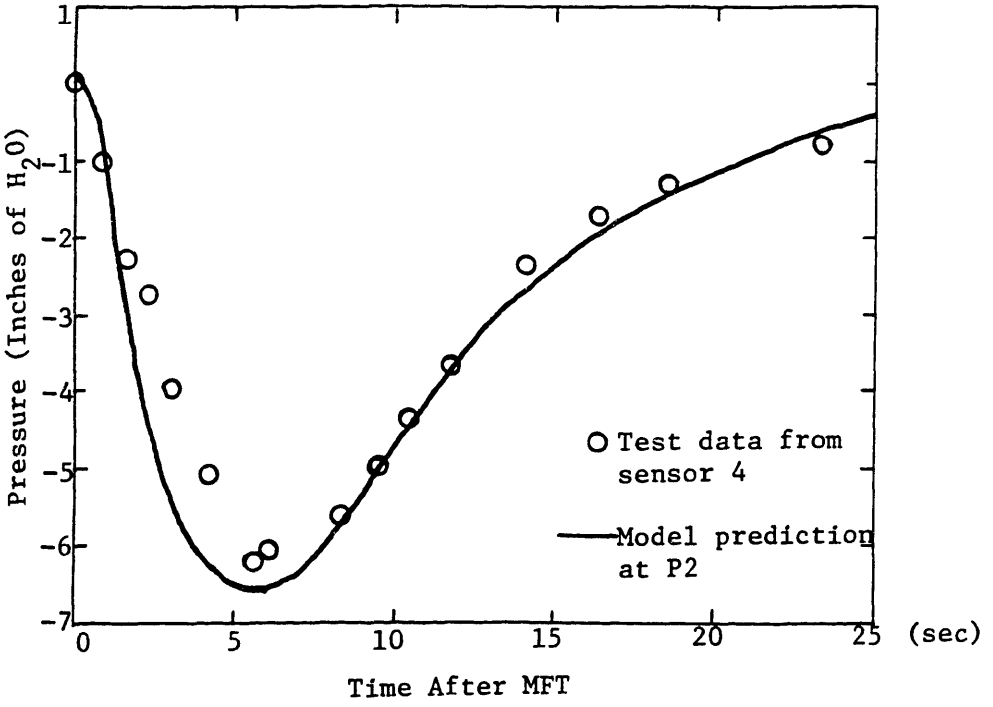

Figure 6-5: Pressure Comparison at Convective Furnace

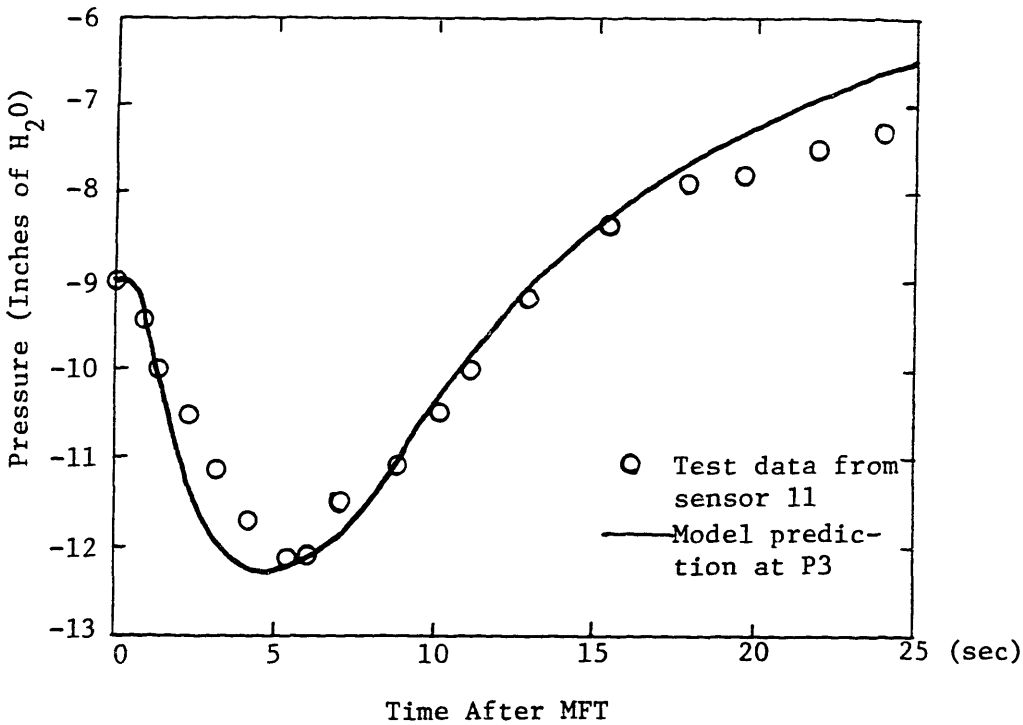

Figure 6-6: Pressure Comparison at Precipitator

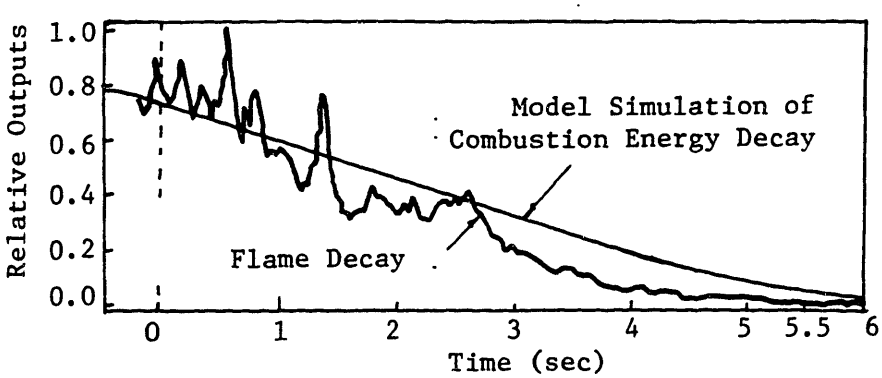

Figure 6-7: Flame Luminosity Compared with Combustion Energy.

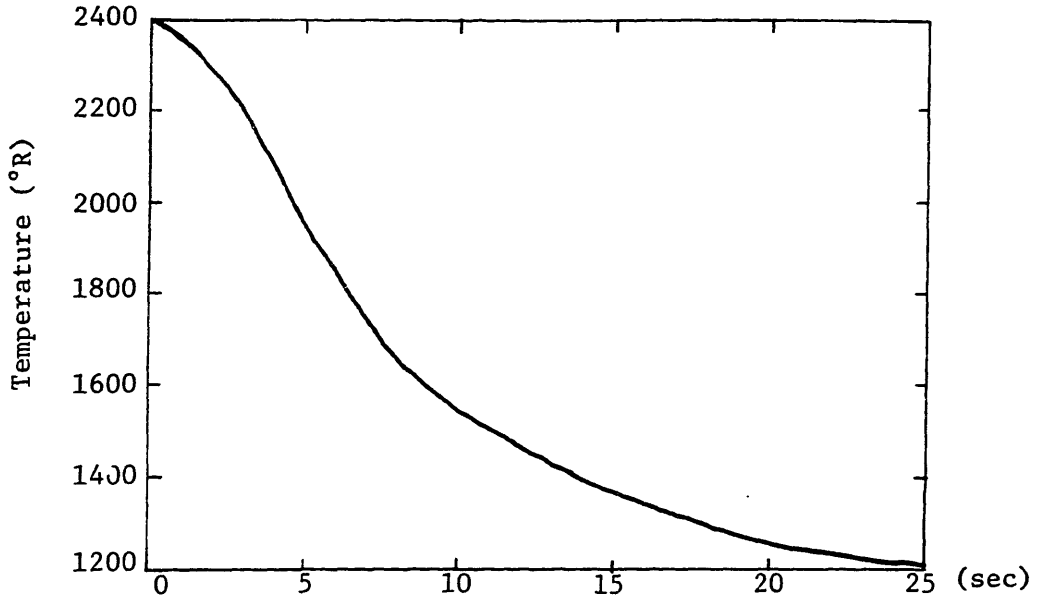

Figure 6-8: Temperature in Radiant Furance

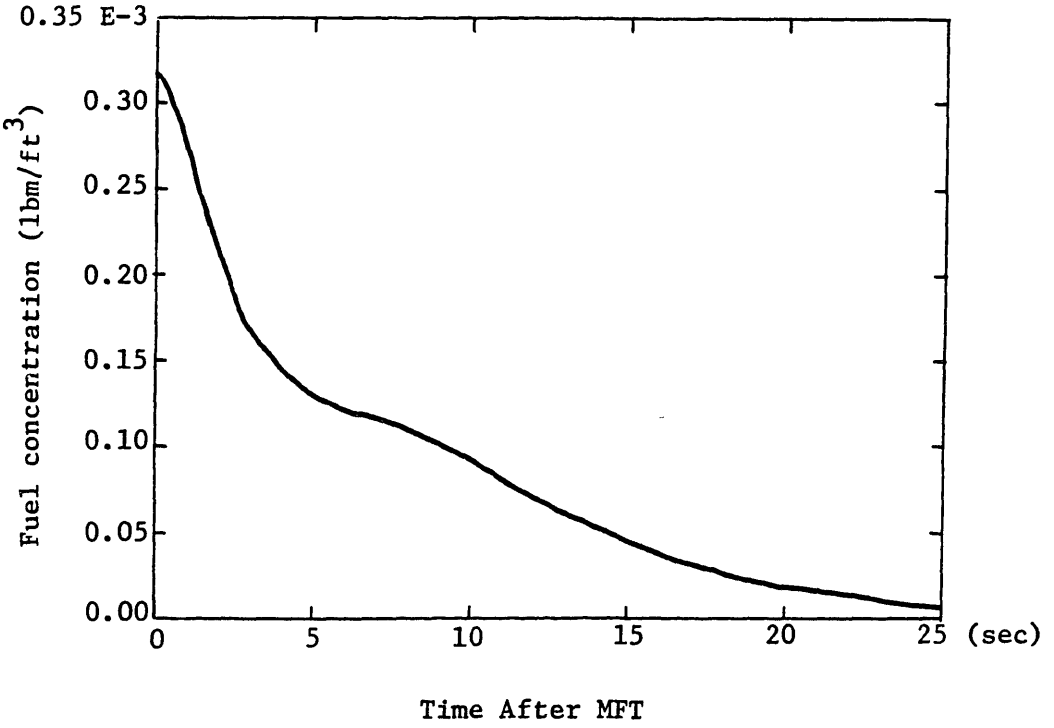

Figure 6-9: Fuel Concentration in Radiant Furnace

6.3 Greenwood Plant

6.3.1 Test Description

Greenwood Unit 1 is an 800 MW oil fired unit. Main fuel trip tests at different load levels have been conducted on the unit as described in reference [55].

Figure 6-10 is a schematic representation of the cross section of Greenwood Unit 1. The small circle represents the location where the pressure was recorded during the tests. Three particular tests were selected at load levels of 50%, 66% and 100% to compare with the model simulations. The initial steady state conditions are summarized in Table 6-II.

6.3.2 Comparison Of Model Simulation And Test Data

The maximum pressure excursions in the radiant furnace were computed with the dynamic simulation model after a main fuel trip. The fuel mass flow for this oil fired plant is modeled as a step from its steady state condition to zero. Three simulations were made at initial loads of 50%, 66% and 100%. The comparison of the simulations with corresponding test data are shown in Figure 6-11. The maximum negative furnace pressure excursion increases with the plant load. The simulation predicates about 25% larger maximum pressure excursion than the experimental data at all three load levels. One of the reasons for the inaccuracy is due to the incomplete information on the axial fan characteristic, especially in stall region, since the maximum pressure excursion is a function of ID fan operating conditions. If the ID fan is tripped following the MFT, the pressure excursion may be decreased because of

reduced ID fan suction. Axial ID fan stall leads to a decreased flow which reduces the furnace pressure excursion. A smaller initial blade angle, which causes ID fan stall at a smaller fan head, further reduces the furnace pressure excursion. Figure 6-12 shows a furnace pressure vs. time plot for which the axial ID fan stalls after MFT. The quasi-steady fan operating point locus is shown in Figure 6-13.

Plots of temperature and the combustion energy decay after MFT are shown in Figure 6-14 and Figure 6-15 respectively. The combustion energy decay time is less than 2 seconds in this oil-fired plant while the combustion energy decay is 5.5 seconds for the coal-fired St. Clair plant as shown in Figure 6-7.

6.4 Summary

The comparison of the simulation model and experimental data has shown that the pressure transients resulting from a main fuel trip may be predicted accurately by the analysis. For the coal-fired St. Clair plant, deviations of the simulation result from the experimental data at the maximum pressure excursion points are less than $\pm 5\%$ of the the total pressure excursion values. No deviation is more than 15% of maximum pressure excursion during the entire time span of the simulation. For the oil-fired Greenwood plant, the deviation is about 25% of the maximum pressure excursion due to the incomplete information.

The simulation results have shown that the furnace pressure excursion after MFT depends on several initial conditions, such as fan operating points, unit load percentage and furnace ash and slag deposits. These quantities should

Table 6-II: Steady State Gas Condition at Greenwood Unit 1

Percent of load		47.5%	67%	100%
FD Fan Air Flow Rate		890	1200	1550
ID Fan Gas Flow Rate		670	890	1170
Fuel Input Flow Rate		55	72	102
Gas State at Radiant	T	1800-	1900	1960
Furnace Outlet	P	0.	0.	0.
Gas State of Convective	T	1412	1600	1850
Furnace Outlet	P	-1.5	-2	-2
Gas State at Primary	T	905	1056	1290
Super Heater Outlet	P	-3	-4	-5
Gas State at	T	610	706	872
Economizer Inlet	P	-5	-6	-7.5
Gas State at	T	520	565	600
Economizer	P	-5.5	-6.5	-8.5

Units: Pressure in inches of H_2O

Temperature in °F

Mass Flow Rate in lbm/sec

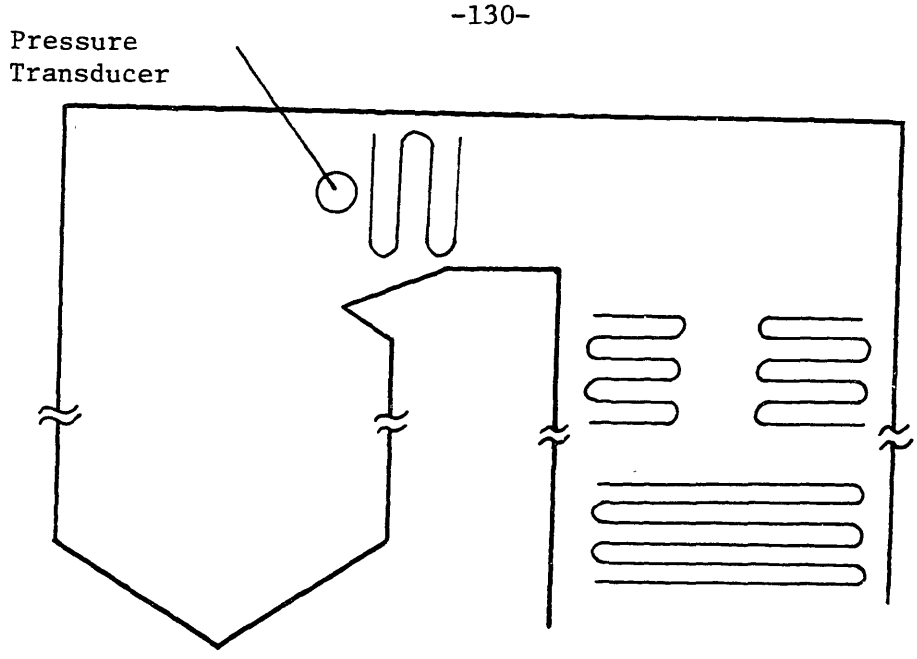

Figure 6-10: Measurement Location on Greenwood Unit 1

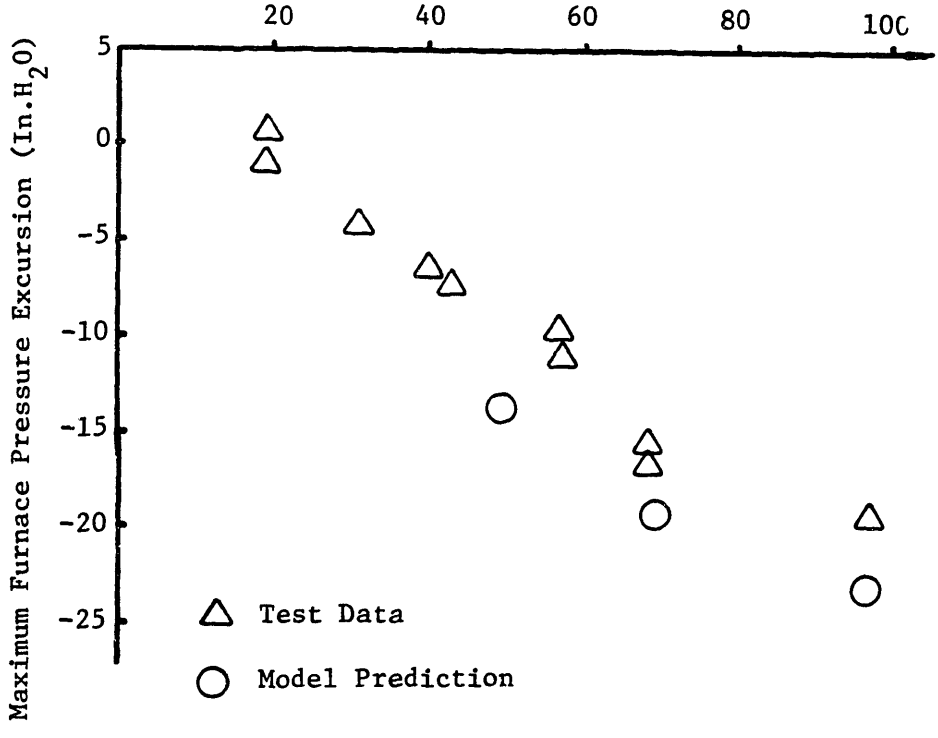

Figure 6-11: Pressure Comparison at Transducer Location

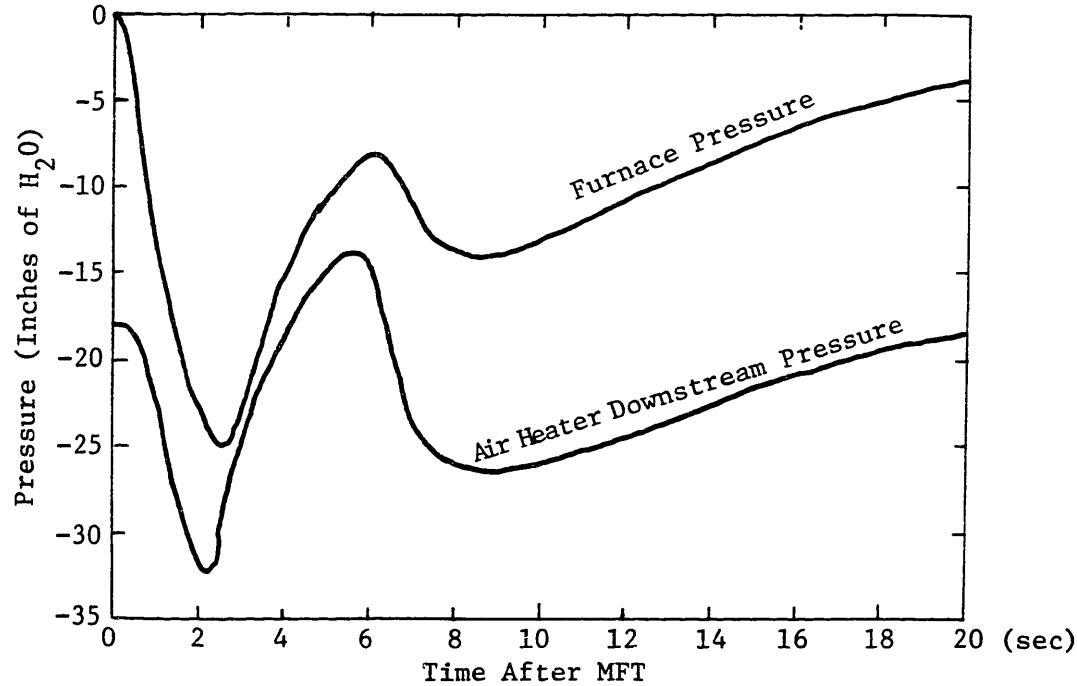

Figure 6-12: Pressure vs. Time after MFT (100% load)

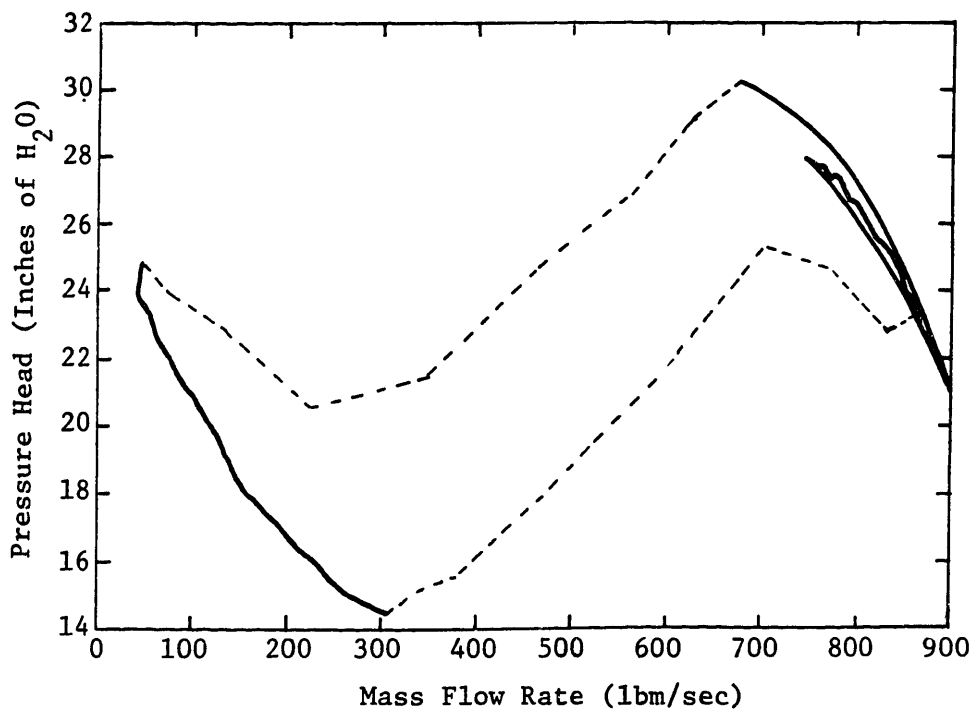

Figure 6-13: Axial ID Fan Operating Locus in Implosion Transient

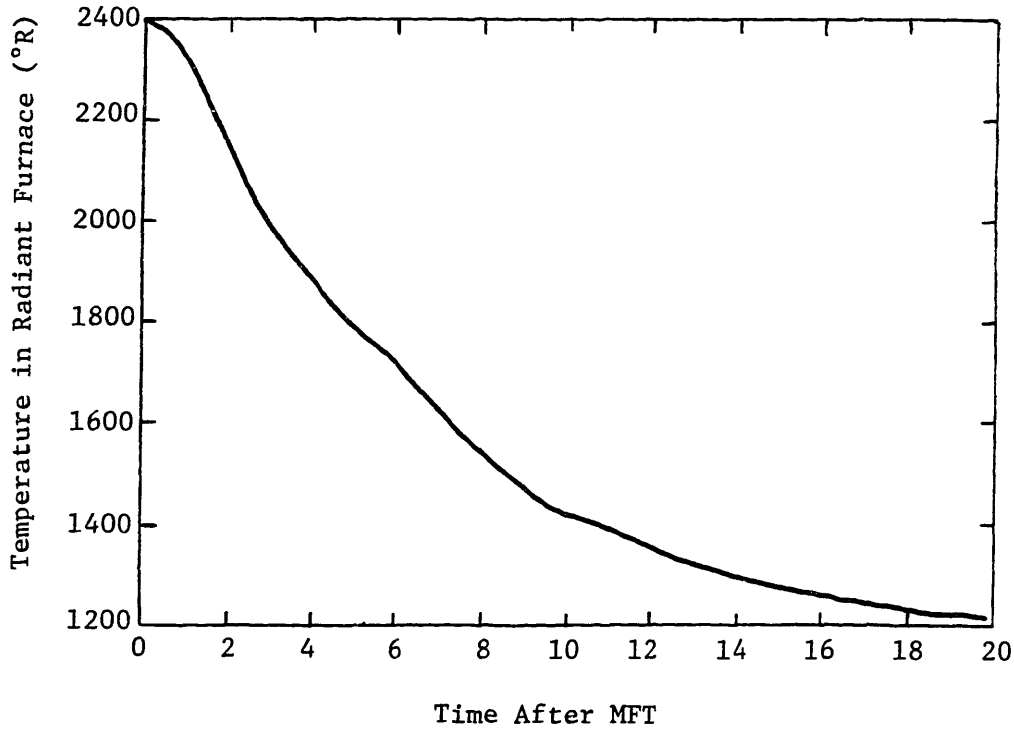

Figure 6-14: Temperature after MFT (100% Load)

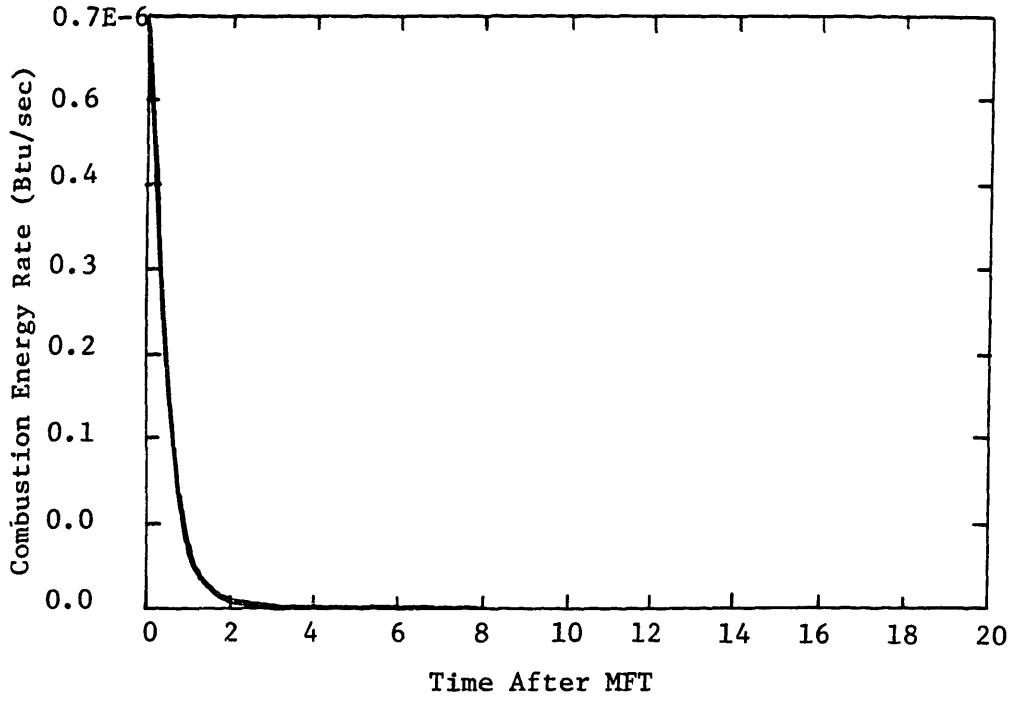

Figure 6-15: Combustion Energy Decay after MFT

be carefully measured or estimated prior to the dynamic simulation. The sensitivity analysis of some these parameters is performed in Chapter 7.

In general the oil-fired unit has a faster energy decay time than the coal-fired unit since the oil combustion rate is faster than that of the coal and the time needed to shut off the coal mass flow is also longer than that for oil.

Chapter 7
MODEL SIMPLIFICATION

7.1 Introduction

The system models developed in Figure 3-2 and 3-3 are relatively detailed models. These types of detailed models are neccessary when the system dynamic behavior dependency on individual plant components is required. However, it may also be advantageous to use simple models to represent the essential global characteristics of the system. When a model is simplified, it is important to compare it with the detailed model under selected conditions. If the two models have similar results under a specific condition, a simplified model could be used for further analysis under the specified condition. Simplified model accuracy is limited to a specified range of applications which must be determined using either detailed model data or experimental data.

7.2 Development of Simplified Models

If only the furnace pressure excursion after a MFT is of interest, a model may be simplified to the one shown in Figure 7-1. A single plenum volume element represents the entire furnace volume. The temperature and pressure are averaged over the entire volume space and represented by single values. Two transmission line elements are included to represent the gas inertance and compressibility along the ducts. One single heat exchanger is used to provide the neccessary temperature drop across the superheater and economizer. The

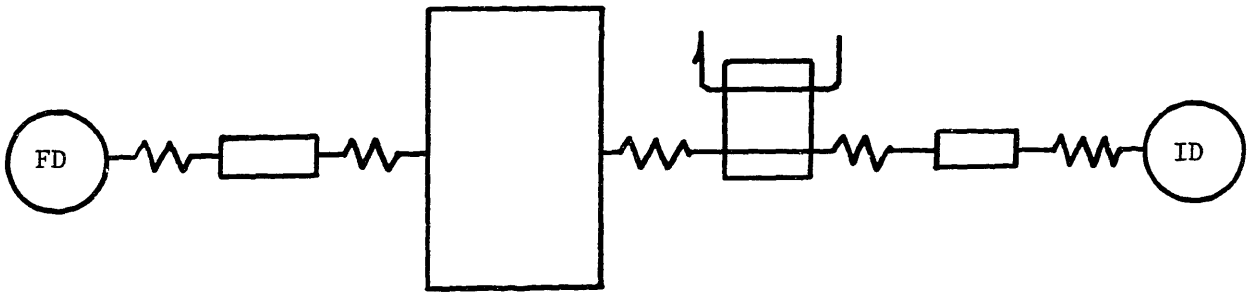

Figure 7-1: Non-linear Simple Model

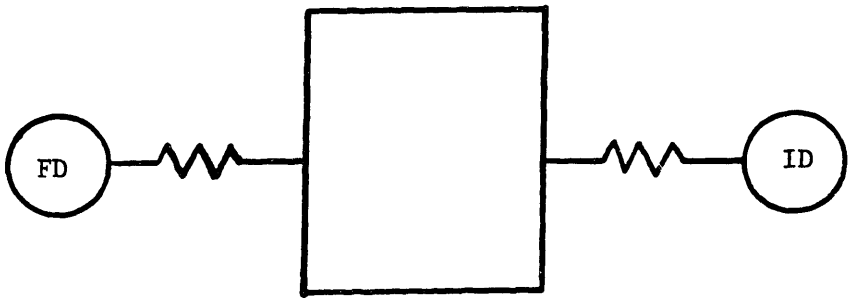

Figure 7-2: Linearized Simple Model

FD and ID fan along with lumped resistances represent the correct system pressure states.

A further simplification can be made to this model to eliminate the transmission line elements as shown in Figure 7-2. Elimination cf the transmission line excludes the gas inertance and compliance effects from the system. This exclusion is valid only when the air/gas flow does not have rapid changes. A property of this model is that it may be linearized at an initial condition. The equations which represent elements in this system are summarized as:

For the furnace plenum:

$$dM/dt = W_i - W_o \tag{7.1}$$

$$dP/dt = RQ/c_vV + \rho T_iRW_i/V - \rho W_oP/M \tag{7.2}$$

For the fan elements and resistance elements at the initial state:

$$\Delta P = B(\alpha) + Y(\alpha)W - S(\alpha)W^2 \tag{7.3}$$

$$\Delta P = RW \tag{7.4}$$

The system state equations are written as:

$$dM/dt = f_1(\ P,\ M,\ Q,\ \alpha_1,\alpha_2) \tag{7.5}$$

$$dP/dt = f_2(\ P,\ M,\ Q,\ \alpha_1,\alpha_2) \tag{7.6}$$

The linearized state equations using incremental furnace mass and pressure change as state variables are derived as:

$$d(\Delta M)/dt = f_{11}\Delta P + f_{12}\Delta M + f_{13}\Delta Q + f_{14}\Delta\alpha_1 + f_{15}\Delta\alpha_2 \tag{7.7}$$

$$d(\Delta P)/dt = f_{21}\Delta P + f_{22}\Delta M + f_{23}\Delta Q + f_{24}\Delta\alpha_1 + f_{25}\Delta\alpha_2 \quad (7.8)$$

The f_{ij} coefficients in the linearized state equations are the partial derivatives of the function f_i with respect to its jth variable evaluated at the initial condition. They are summarized as:

$$f_{11} = \partial f_1/\partial P = 1/\sqrt{(Y_2-R_2)^2 + 4S_2B_2} - 1/\sqrt{(Y_1-R_1)^2 + 4S_1B_1} \quad (7.9)$$

$$f_{12} = \partial f_1/\partial M = 0 \quad (7.10)$$

$$f_{13} = \partial f_1/\partial Q = 0 \quad (7.11)$$

$$f_{14} = \partial f_1/\partial\alpha_1 = \partial W_1/\partial\alpha_1 \quad (7.12)$$

$$f_{15} = \partial f_1/\partial\alpha_2 = -\partial W_2/\partial\alpha_2 \quad (7.13)$$

$$f_{21} = \partial f_2/\partial P = -\rho W_2/M \quad (7.14)$$

$$- \rho T_i TR/V\sqrt{(Y_1-R_1)^2 + 4S_1B_1} - \rho P_a/M\sqrt{(Y_2-R_2)^2 + 4S_2B_2}$$

$$f_{22} = \partial f_2/\partial M = \rho W_2 P_a/M^2 \quad (7.15)$$

$$f_{23} = \partial f_2/\partial Q = R/c_v V \quad (7.16)$$

$$f_{24} = \partial f_2/\partial\alpha_1 = \rho T_i R/V\partial W_1/\partial\alpha_1 \quad (7.17)$$

$$f_{25} = \partial f_2/\partial\alpha_2 = -\rho P/M\partial W_2/\partial\alpha_2 \quad (7.18)$$

The parameters used in above equations are summarized as:

P = furnace plenum pressure

M = mass accumulation in the furnace plenum

Q = energy rate into the furnace plenum

V = volume of the furnace plenum

T_i = furnace inlet air temperature

W_1 = mass flow rate through the FD fan

W_2 = mass flow rate through the ID fan

c_v = specific heat value of the gas

ρ = 1.4

R = gas constant

R_1 = linear flow resistance from FD fan to furnace

R_2 = linear flow resistance from furnace to ID fan

B_1, Y_1, S_1 = FD fan characteristic coefficients

B_2, Y_2, S_2 = ID fan characteristic coefficients

α_1 = FD fan inlet guide vane angle

α_2 = ID fan inlet guide vane angle

The partial derivative of $\partial W/\partial \alpha$ may be obtained by graphical methods from the fan characteristic curves. When the fan inlet guide vane control is not active, these partial derivatives are zero.

This set of linear system equations allows the use of well developed linear control theory to design the closed loop control system. Because of the nonlinear nature of the air/gas system, this model must be used with caution. A verification by the detailed model or experiments is usually neccessary.

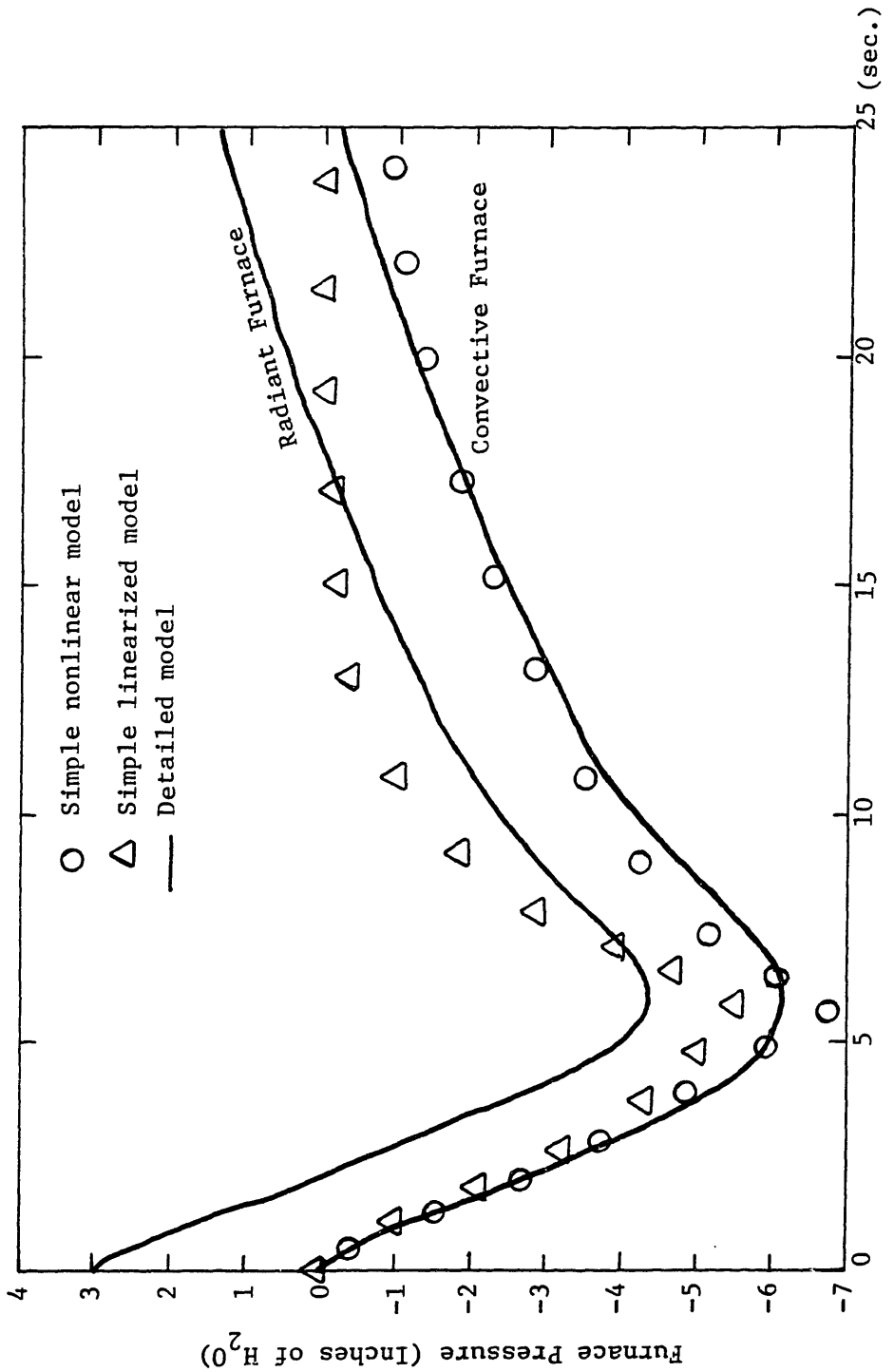

Figure 7-3: Model Comparison by St. Clair Unit 3

7.3 Model Comparison

Computer simulations were conducted of the St. Clair Unit 3 main fuel trip test using both simplified models. The fuel trip disturbance was modeled as an energy decay approximated from the luminosity decay shown in Figure 5-3. The furnace pressures of the simulations are plotted for comparison with those of the detailed model in Figure 7-3. Both models predict a maximum pressure excursion value which is only 10% off that predicted by the detailed model. The linearized model has a significant deviation 6 seconds after the MFT, since the state of the plant at this time is far from the initial conditions upon which it was linearized.

The comparison has shown that the simple models represent the most important system characteristics, such as maximum pressure excursion and the time at which this excursion occurs. Their application, in preliminary study, is recommended. However, these models are "over-simplified" models for any real plant. One example which shows their limitation is to determine the response to fan control action after a MFT as shown in Figures 7-4 and 7-5. When Figure 7-4 shows the pressure respones when the control actuator time constant is 2 seconds, there is no significant difference in pressure response between a detailed model and a model without transmission line elements. When the control actuator time constant is 0.5 seconds as shown in Figure 7-5, the response difference between these two models is apparent. The simplified model does not predict the pressure oscillation in the system for a given draft control action. The simplified models also do not include the effects of either the actual combustion decay or the heat exchange between metal, ash or slag and the combustion gas and are not useful for studies

evaluating these effects.

Two modifications of the detailed model have been simulated to study the parameter sensitivities of the detaied model. In the first case, the ash deposits on the furnace wall tubes are assumed to be equal to zero. The simulation predicates a 50% increae in maximum pressure excursion. The reason for this over-predication is explained in previous chapters. In the second case, the temperatures downstream of the furnace are assumed constant after the main fuel trip, the simulation predicates a 15% decrease in maximum pressure excursion. The under-predication is due to the higher assumed downstream temperature which introduces a over value the downstream system resistance during the simulation. Simulations on both cases are shown in Figure 7-6 along with the detailed model.

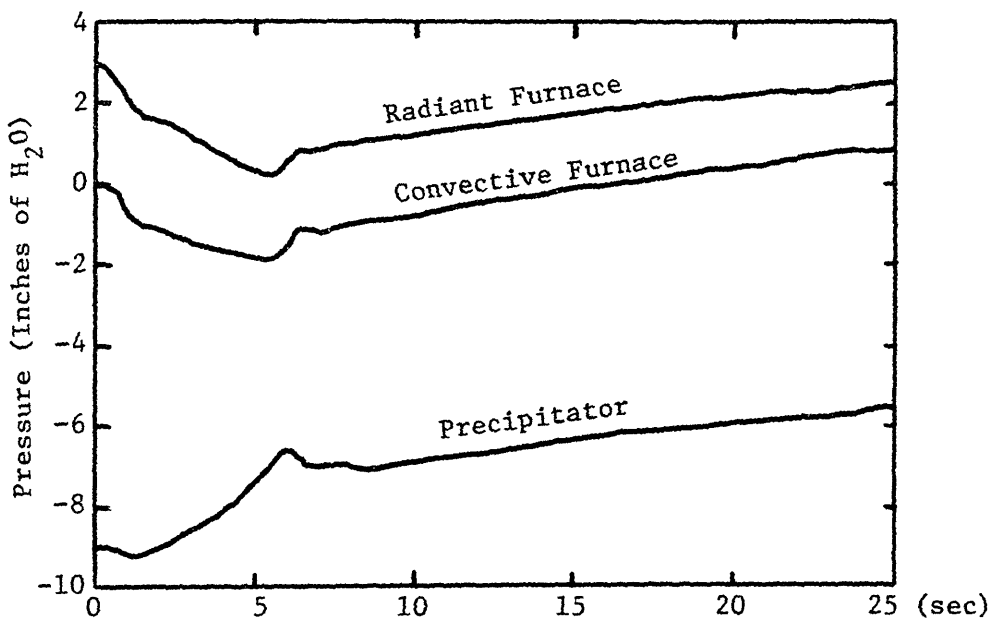

Model Includes Transmission Line Elements

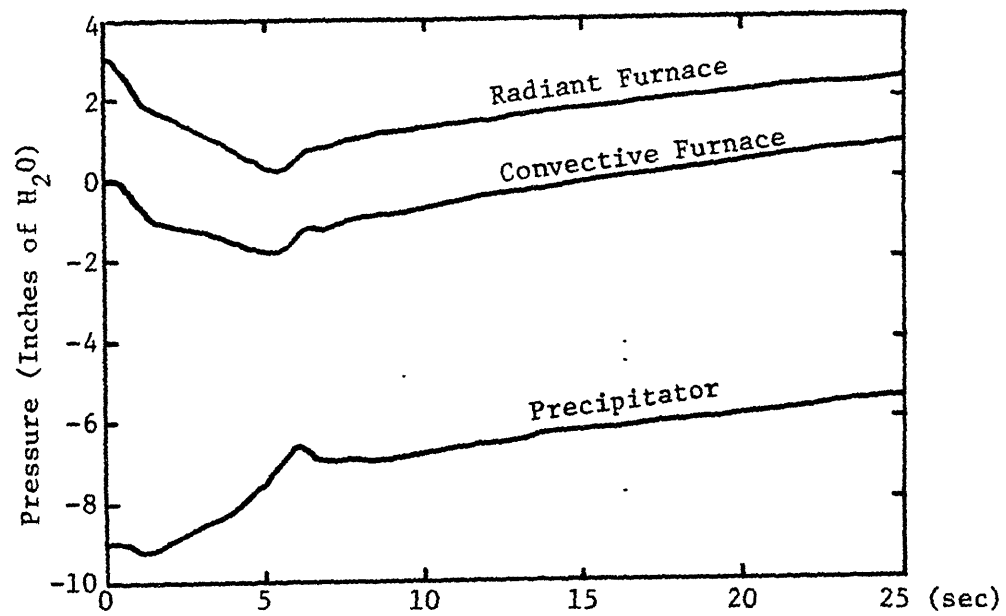

Model without Transmission Line Elements

Figure 7-4: Slow Fan Control Action Case

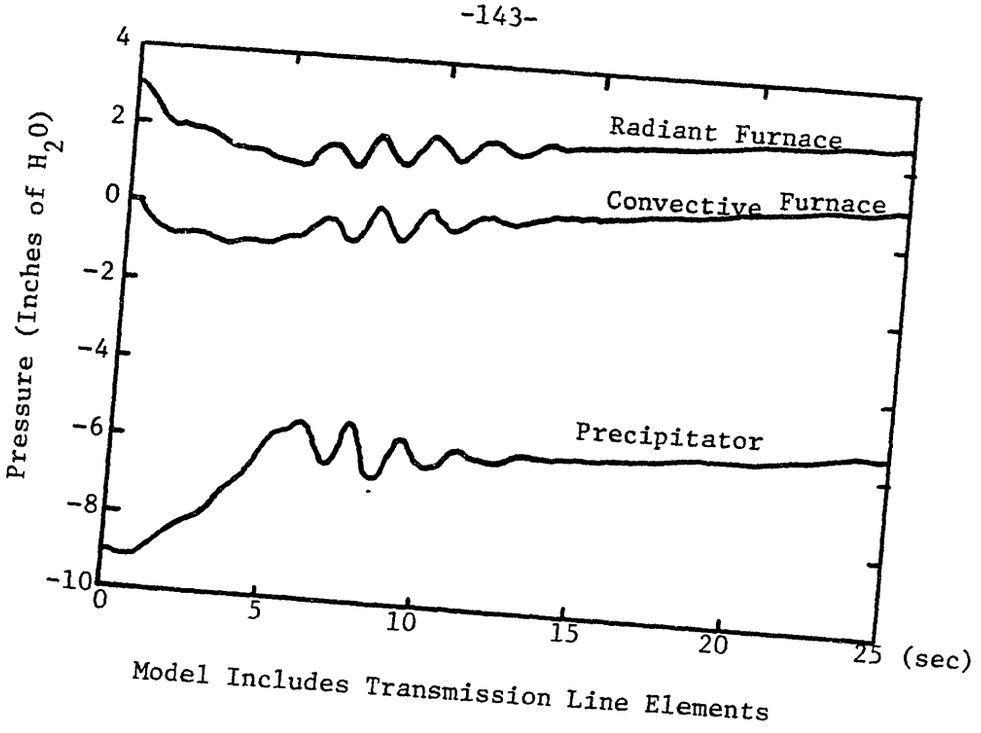

Model Includes Transmission Line Elements

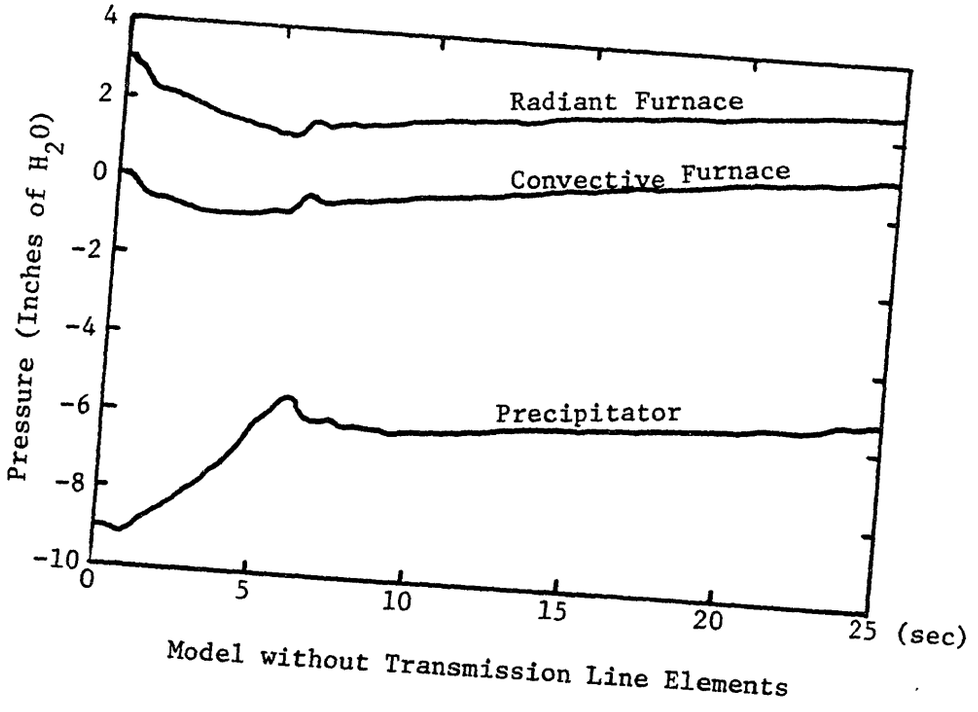

Model without Transmission Line Elements

Figure 7-5: Fast Fan Control Action Case

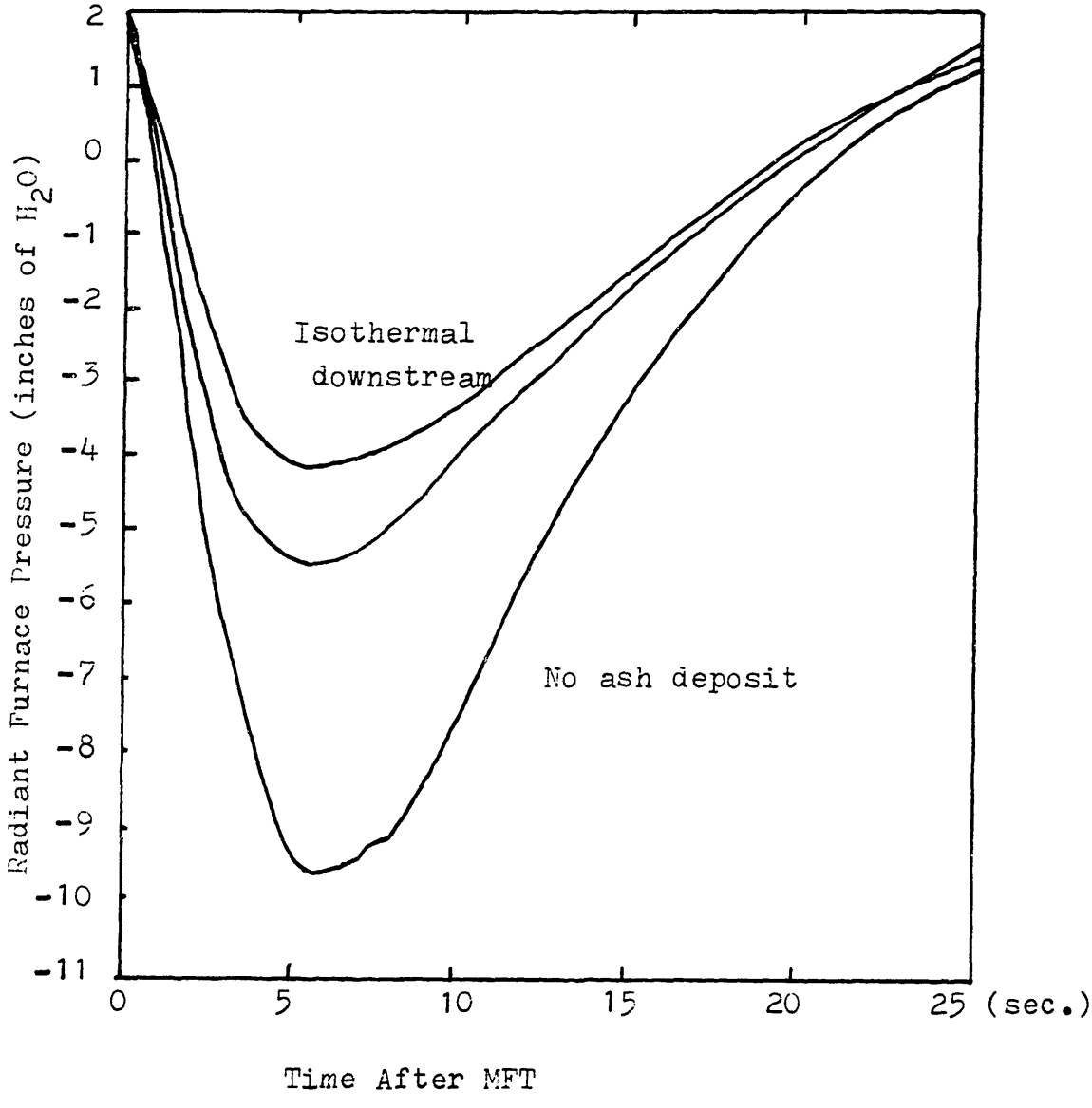

FIGURE 7-6: MODEL PARAMETER SENSITIVITY SIMULATION

Chapter 8
CONTROL OF FURNACE IMPLOSION

8.1 Introduction

There have been a number of implosions in utility boilers where sufficient force developed to exceed the furnace structural strength. The cost of implosion incidents from loss of generation and structural damage can be significant. Probably the most conservative and expensive long term solution for furnace implosion prevention is to strengthen the boiler structure to withstand the maximum possible negative pressure in the transient. However, recent draft requirements such as the addition of stack gas scrubbers may require boiler structural design to withstand negative pressure as low as -50 inches of water. Thus, evaluation of control systems to prevent implosion is of interest.

Several methods for controlling implosions have been proposed and are described in the following sections, also, a general control scheme to meet the Standards for Prevention of Furnace Implosions determined by National Fire Protection Association (NFPA) has been described in reference [42]. Since almost all reported implosions have occured either prior to main fuel lightoff or following a fuel trip, a control system must accomodate a sudden main fuel trip condition. The negative draft pressure excursion after a MFT may be limited by increasing the net gas flow into the draft system as soon as possible after a MFT. The control system described in reference [42] attempts

to increase the net flow into furnace to reduce the pressure excursion. This control system has been combined with the St. Clair plant model to illustrate the use of the simulation techniques to evaluate implosion control systems.

8.2 Fan Characteristic Modification

After a MFT the furnace pressure drops and the pressure across the FD fan decreases resulting in an increase in airflow, at the same time the pressure across the ID fan increases resulting in a flue gas flow decrease. The furnace pressure is therefore partially self-correcting due to the normal, negatively sloped, fan characteristic. The flatter the fan curve, the stronger is this self-correcting control. At the Greenwood plant as described in Chapter 6, six holes, each twelve square feet, were cut in the FD fan duct to bypass part the flow to atmosphere. This, in fact from system point of view, provided a new and flatter fan characteristic as shown in Figure 8-1. With these holes not only the FD duct but also the entire draft system has more protection from an implosion.

The ID fan head is an important parameter in implosion. On the basis of reported incidents and field tests, the maximum negative furnace pressure is not likely to exceed the low gas flow maximium head capacity of the ID fan. A major objective of the final design is to limit draft equipment maximum head capacity to that required for satisfactory operation. Euchner in reference [13] has defined a limiting ID fan control scheme that keeps the fan operating point out of the shaded area in Figure 8-2. Special consideration is given to selection of the fan and the duct arrangement to limit the negative head developed before the ID fan at low flue gas flow rates. This consideration leads

to the bypass ID fan control system configuration described later in this chapter.

An axial ID fan may stall when the furnace pressure drops after a MFT. The stall condition leads to an immiediate flow reduction which minimizes the drop in furnace pressure. The Greenwood plant simulation results show however that oscillations may be present throughout the draft system.

Although the fan characteristics have strong affects on the furnace pressure dynamics, the passive measures taken to change these characteristics may not be sufficient to control the furnace pressure to a satisfactory level after a MFT.

8.3 General Control Scheme

A general control scheme has been recommended by the National Fire Protection Association in reference [42] to meet the standards for prevention of a furnace implosion. The general control scheme has been studied using the St. Clair plant model.

The schematic representation of this control system is shown in Figure 8-3. There are two stages in this control system, the controllers and the actuators. The system contains two control loops - a feedforward loop taking a MFT signal as the input and a feedback loop taking the deviation of the measured furnace pressure from its set point as an input. Within the feedback loop, there are two controller branches. The PI controller is designed with a relatively small gain. Its primary function is to keep the furnace pressure at the set point and provide sufficient air for combustion at steady state. The large gain P controller is designed for implosion protection. A negative pressure

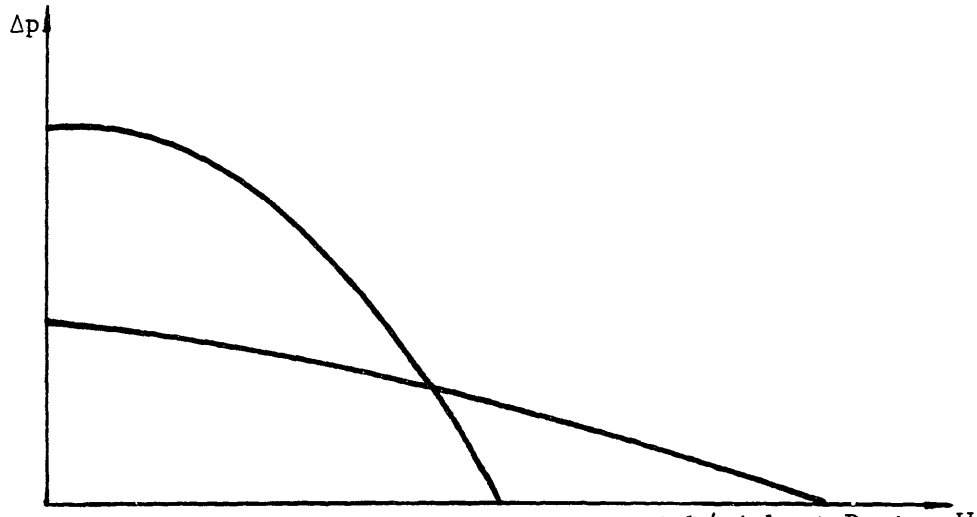

Figure 8-1: FD Fan Characteristics with/without Duct Holes

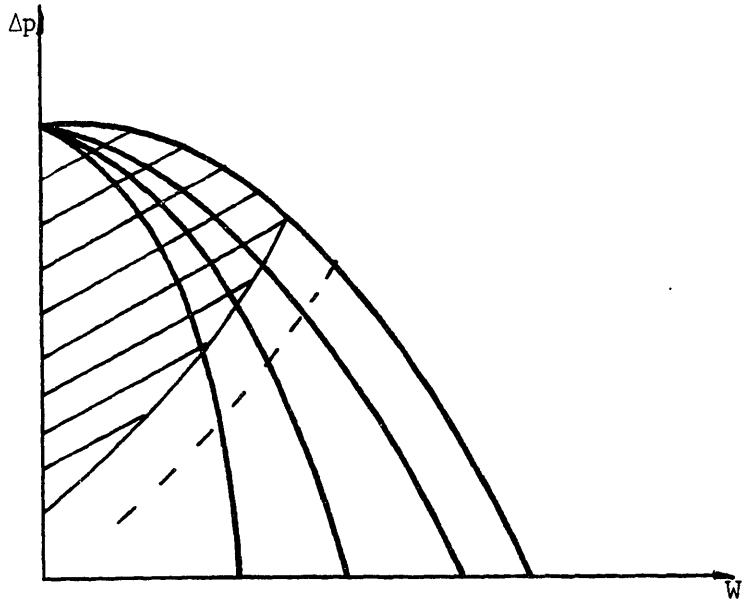

Figure 8-2: ID Fan Limiting Control Scheme

limit is set for the P controller. When the measured furnace pressure is higher than the limit, the output of the P controller is zero. When a large furnace pressure excursion occurs, the measured furnace pressure drops below the limit and the P controller produces a feedback signal proportional to the pressure deviation. Since the gain of the P controller is much larger than than steady state PI controller, a much stronger control action is taken when the furnace pressure drops below the predefined limit.

The simulation results of St. Clair plant model have shown that the feedback control alone may be too slow for furnace implosion control after a MFT. The feedforward loop is designed to use a MFT signal directly to move the control devices even before the negative furnace excursion occurs. If the furnace pressure excursion phenomena have been well documented by field tests and model simulation, a predesigned function may be used for the forward control signal generation as shown in Figure 8-4. Immediately after a MFT a step is generated by the feedforward controller for fast control action. This step lasts until the maximum negative pressure has passed, then a ramp down to zero in the next 15 seconds occurs to allow for a smooth transition to steady state.

The control command to drive the physical control device actuators is the sum of all computed signals from the three controllers designated as Y in Figure 8-3.

The control system elements have been developed in reference [51], their formulation and representations are summarized in Appendix

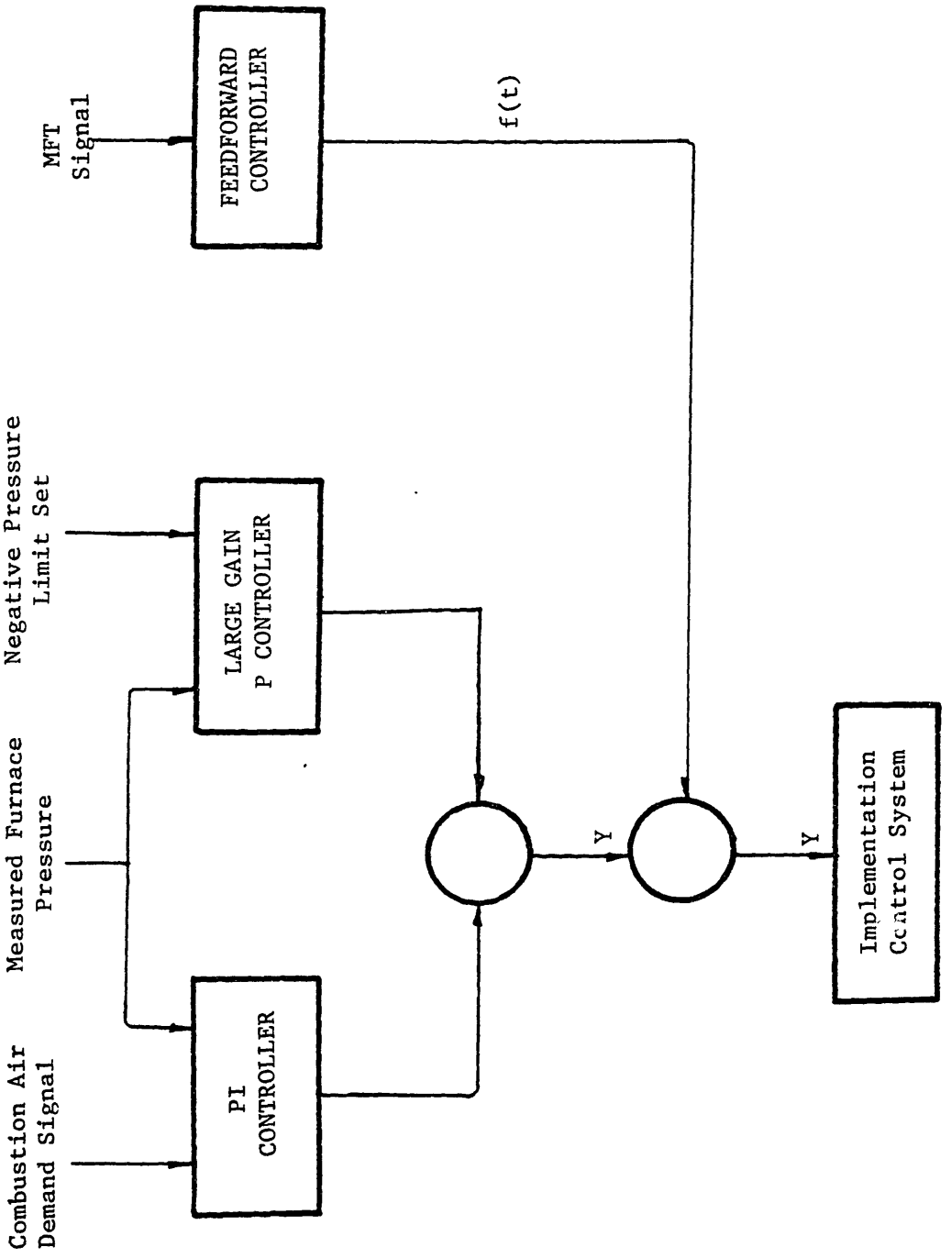

Figure 8-3: General Control Scheme

8.4 Implementation Control Systems

The implementation control devices and systems illustrated in this study include mechanical damper control, inlet guide vane control on both FD and ID fans and a bypass control system across the ID fan.

8.4.1 Mechanical Damper Control

During a negative furnace pressure excursion it is necessary to reduce the flow out of the furnace as quickly as possible. This can be accomplished by closing a mechanical damper at the inlet of the ID fan.

An actuator is used to drive the mechanical damper. The actuator accepts a control command signal from the controller and moves the damper. The actuator element is developed to represent the actuator dynamics as in equation (2-48):

$$\alpha_d(S) = \frac{K_d}{\tau_d S + 1} Y(S) \tag{8.1}$$

where:

α_d = damper angle

K_d = damper actuator gain

τ_d = damper actuator time constant

Y = control command signal

The flow through the damper is reduced as the damper α_d decreases determined by equation (2-39):

$$\Delta P = D_f(W, \alpha_d) \tag{8.2}$$

8.4.2 Fan Inlet Guide Vane (IGV) Control

Another effective way of reducing the furnace negative pressure excursion is to close the ID fan IGV and open the FD fan IGV after a MFT. The flow changes resulting from the changes of IGVs are illustrated by the fan characteristic curves in Figure 8-5. If the inlet guide vane changes $\Delta\alpha$ and the pressure across the fan does not change, the fan operating point moves horizontally, causing the flow change ΔW.

The numerical value of fan flow rates as a function of the IGV are determined by the fan characteristic relations:

$$\Delta P_{FD} = f_{FD}(W_{FD}, \alpha_{FD}) \tag{8.3}$$

$$\Delta P_{ID} = f_{ID}(W_{ID}, \alpha_{ID}) \tag{8.4}$$

The actuator elements are used to represent dynamics of the actuators which drive the FD and ID fan IGVs:

$$\alpha_{FD}(S) = \frac{K_{FD}}{\tau_{FD}S + 1} Y(S) \tag{8.5}$$

$$\alpha_{ID}(S) = \frac{K_{ID}}{\tau_{ID}S + 1} Y(S) \tag{8.6}$$

8.4.3 ID Fan Bypass Control System

An ID fan bypass control system for implosion control has been described in reference [35] as shown in Figure 8-6. Small and fast acting dampers are installed in parallel with the ID fans. When these dampers are modulated open, they provide an additional flow path for the fans. The flow through the fan itself is in the forward direction while the flow in the bypass path is in the backward direction. The flow at points A and B in Figure 8-6 are equal

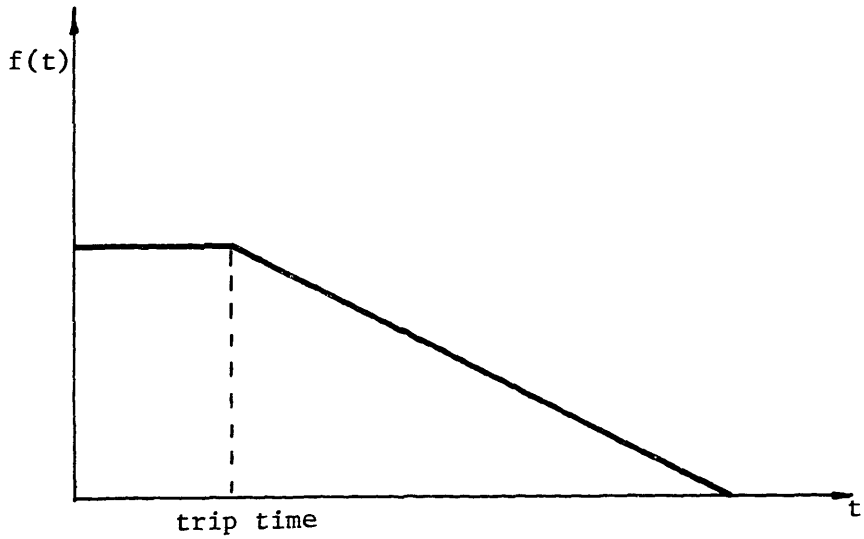

Figure 8-4: Feedforward Controller Generating Function

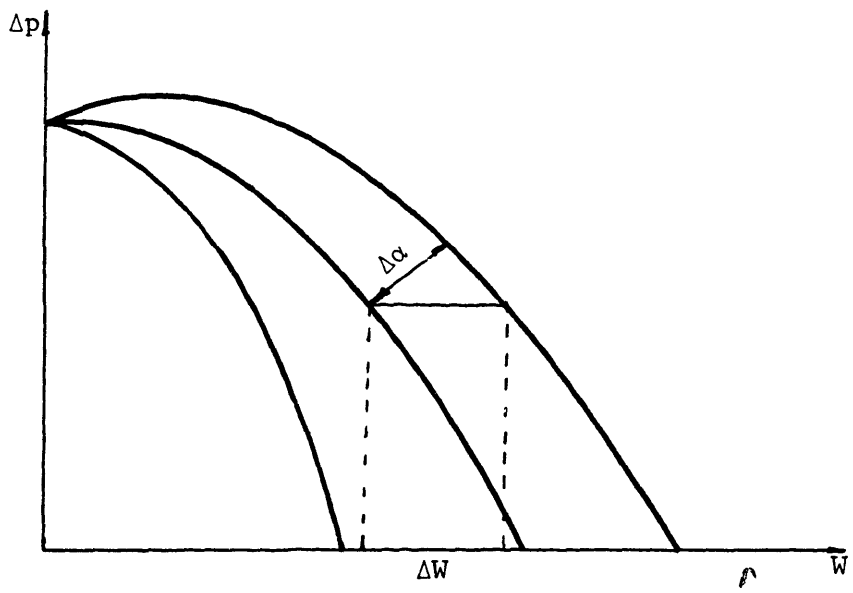

Figure 8-5: Flow Reduction under IGV Control

by the continuity principle. The pressure rise from A to B is determined by the bypass damper position as well as the fan characteristics. The objective of the bypass control system is to decrease the net flow at points A and B while decreasing the pressure rise from A to B. This objective can not be accomplished without a bypass path due to the downward slope of the fan characteristics.

The mathematical model of this bypass system is represented by a fan element and a mechanical damper element in parallel as shown in Figure 8-7.

When the furnace negative pressure occurs, the control command signal from the controller opens the bypass damper. The backward flow through the bypass damper increases at a faster rate than the flow through the fan. The sum of these two flows at A and B are reduced even though the flow through the ID fan may have increased.

The major advantage in using the ID fan bypass control system is that the bypass damper is much smaller and faster acting than the damper installed in the main ducts. After a MFT the flow of the flue gas from the furnace can be reduced faster because of this fast damper action. This in turn provides a more effective implosion control.

8.4.4 Steam Discharge Implosion Control Scheme

All the previous implosion control techniques attempt to reduce the furnace pressure excursion by increasing the net gas flow into the boiler furnace. However, there are certain limitations on these schemes. First, the increase in the incoming flow into the furnace is limited by the FD fan capacity; secondly, the reduction of outgoing flow is limited because of a large

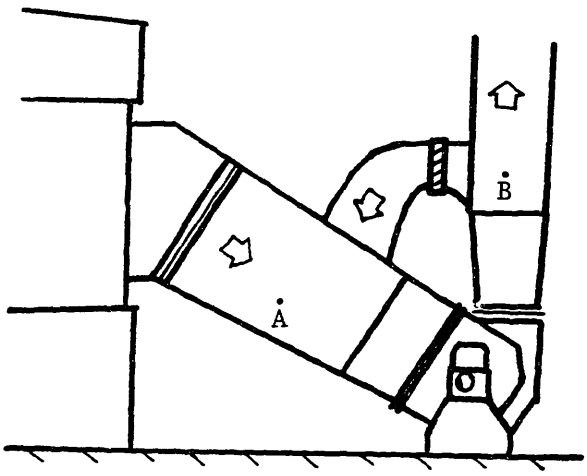

Figure 8-6: The ID Fan Bypass Control System Ref. [35]

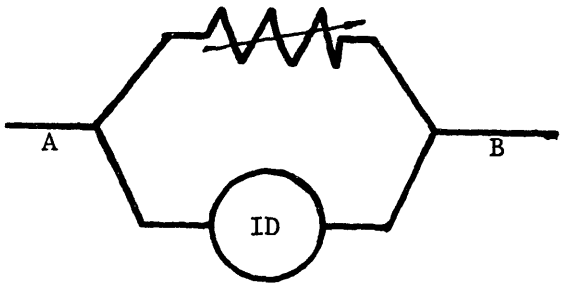

Figure 8-7: Bypass Control System Model

negative pressure excursion that occurs in the stack. There is a need for more mass in the air/gas system to fill the vacuum in the furnace created by a fuel trip. Discharge of the available steam into the furnace in an implosion situation can provide both mass and energy to keep the furnace pressure from dropping.

After a main fuel trip, the common practice is to discharge the system steam into the condenser and stack. Greater utilization may be served by discharging the steam into the boiler furnace to limit the negative pressure excursion.

A preliminary study has been carried out to evaluate the idea. The schematic representation of the steam discharge system is shown in Figure 8-8. Since the pressure of the superheated steam is much higher than the pressure in the air/gas system, the discharge steam flow is supercritical. The general flow discharge equation is formulated as:

$$W_s = A_s\sqrt{(2gkP) \;/\; v(k-1)[r^{2/k} - r^{(k+1)/\gamma}]^{1/2}} \qquad (8.7)$$

For superheated steam k = 1.3, the critical pressure ratio r = 0.5457, then the steam flow becomes:

$$W_s = (1135)(144)/(3600)\; A\; \sqrt{P/v} \quad \text{lbm/sec.} \qquad (8.8)$$

where:

P = steam pressure, psi

v = specific volume, ft^3/lbm

A_s = discharge valve open area, ft^2

The temperatures throughout the air/gas system are assumed higher than 300 °F before and after the steam is discharged into the air/gas systems. There should be no condensation of the discharged steam, the ideal gas law is still valid for the mixture of gas and steam in air/gas system models.

The preliminary study has demonstrated the potential use of discharge steam for furnace implosion control purpose. However, for fuel trips which occur in start-up situations, the availability of steam depends on the existance of an auxiliary boiler. For large scale units, such auxiliary boilers do exist, they may not exist for many smaller units.

8.5 Control System Evaluation By Plant Model

The control schemes and the control devices described in this chapter have been incorporated into the St. Clair plant model. Four control system configurations have been evaluated. The first system is to control the IGV on both fans without a bypass system. The second system is to control the ID fan bypass loop dampers while keeping all the fan IGVs fixed. The third system is to control bypass dampers and fan IGVs at the same time. The fourth is a preliminary study on steam discharge scheme. For all cases the measured signal is the average pressure at the radiant furnace. The objective of the simulations has been to demonstrate the effectiveness of the implosion control scheme and compare the possible implementations. For each particular control system, the values of feedback gain and feedforward function are determined to minimize the furnace negative pressure drop without causing either large stack pressure excursions or system pressure oscillations.

The transient response after a MFT of the St. Clair plant model was

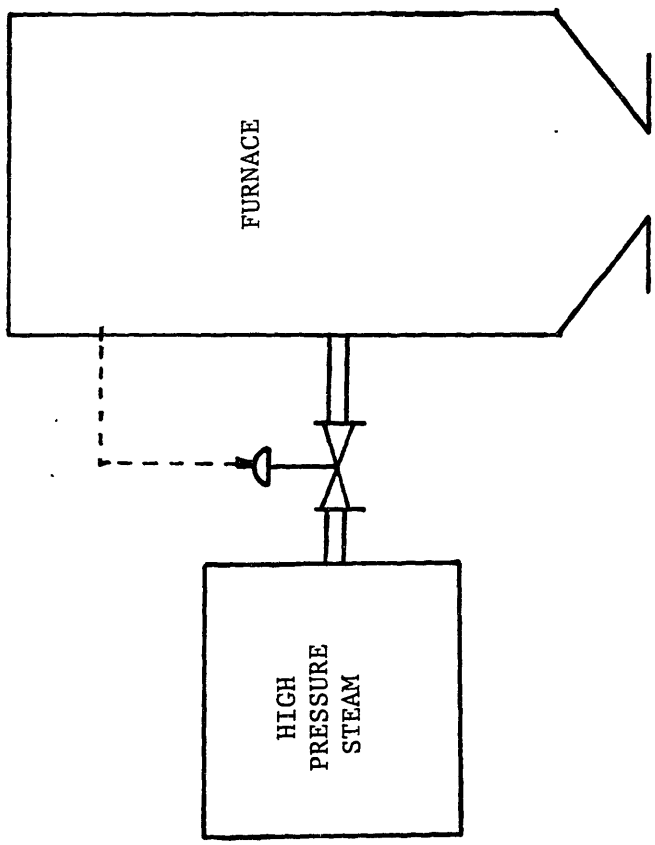

Figure 8-8: Steam Discharge Implosion Control Scheme

simulated when the fan IGV control system was active. The control system parameters are summarized as:

- The feedforward step gain = 25 Deg. of IGV angle
- The pressure feedback gain = 20 Deg. of IGV angle/In. of H_2O
- The IGV actuator time contants for both fans = 1.0 sec.

The simulation result in Figure 8-9 has shown that the furnace pressure excursion is improved to 30% of its uncontrol level. For a particular actuator time constant, the furnace pressure excursion improves when feedforward and feedback gains are increased to optimum values. However, further increase in the gains do not result in further improvements. Since the FD fan IGV is already fully open and ID fan IGV is already fully closed within a few seconds under large control gains. Figure 8-10 has shown that the maximum furnace pressure excursions are the same when control gains are doubled from the above design values.

The IGV control system produces a smooth system response throughout the implosion transient after a MFT. The stack pressure change under this control system is less than one inch of water as shown in Figure 8-11.

The furnace pressure excursion improvement by a ID fan bypass control system is illustrated in Figure 8-12. The control system parameters are summarized as:

- The feedforward step gain = 50 Deg. of angle
- The pressure feedback gain = 15 Deg. of angle/In. of H_2O
- The damper actuator time constant = 1 sec.

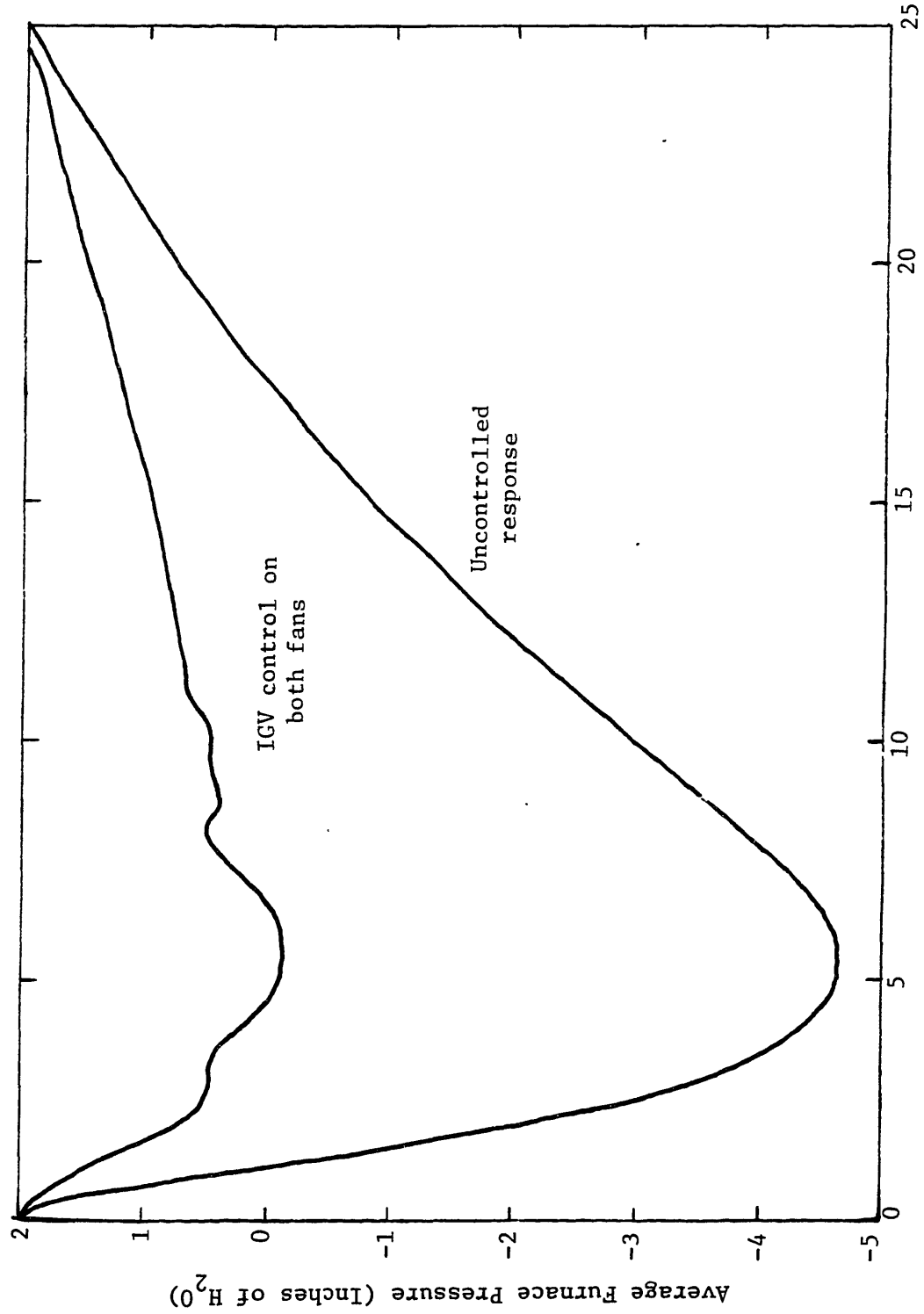

Figure 8-4: Effect of IGV Control on Both Fans

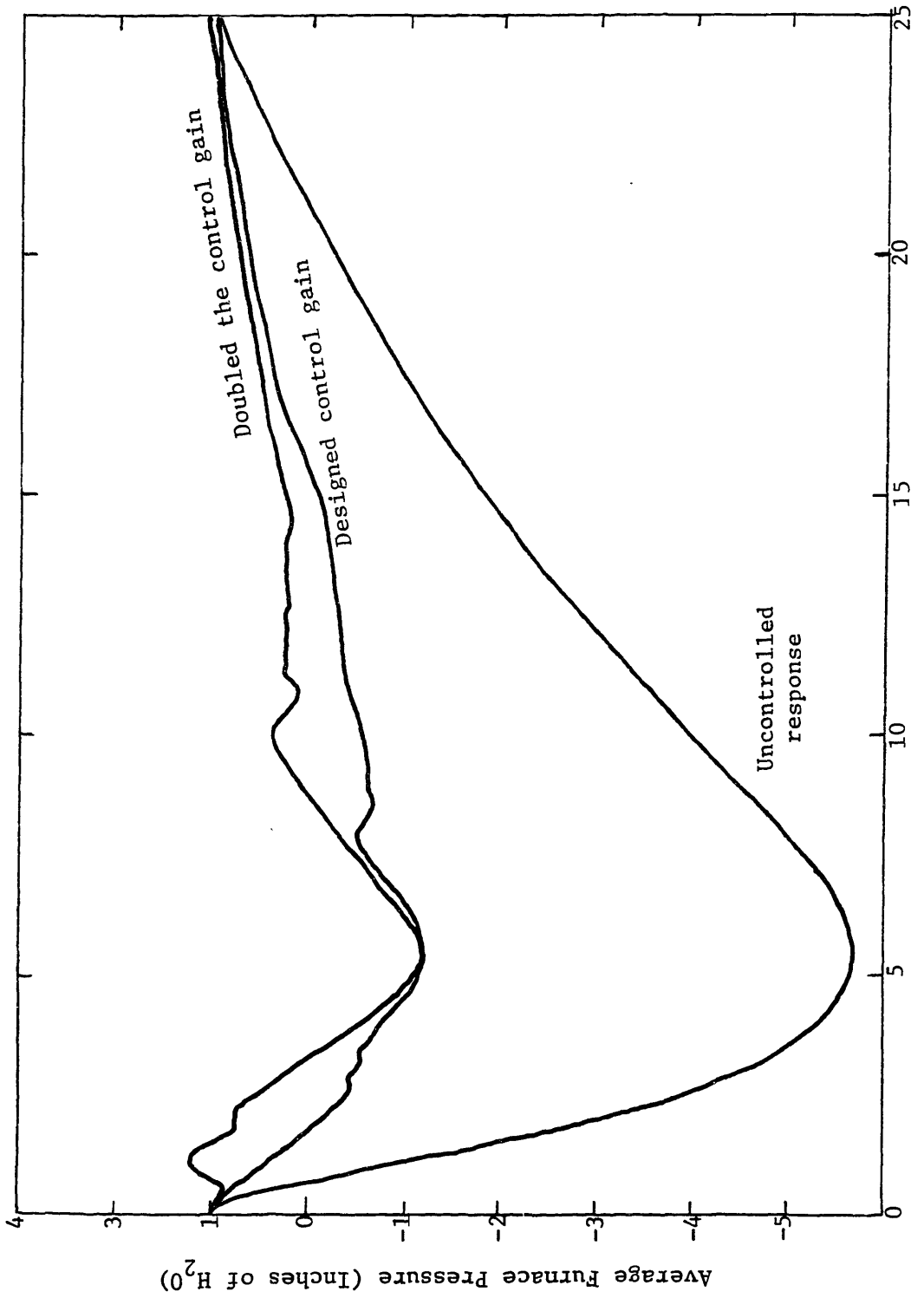

Figure 8-10: Limits of Fan IGV Controls

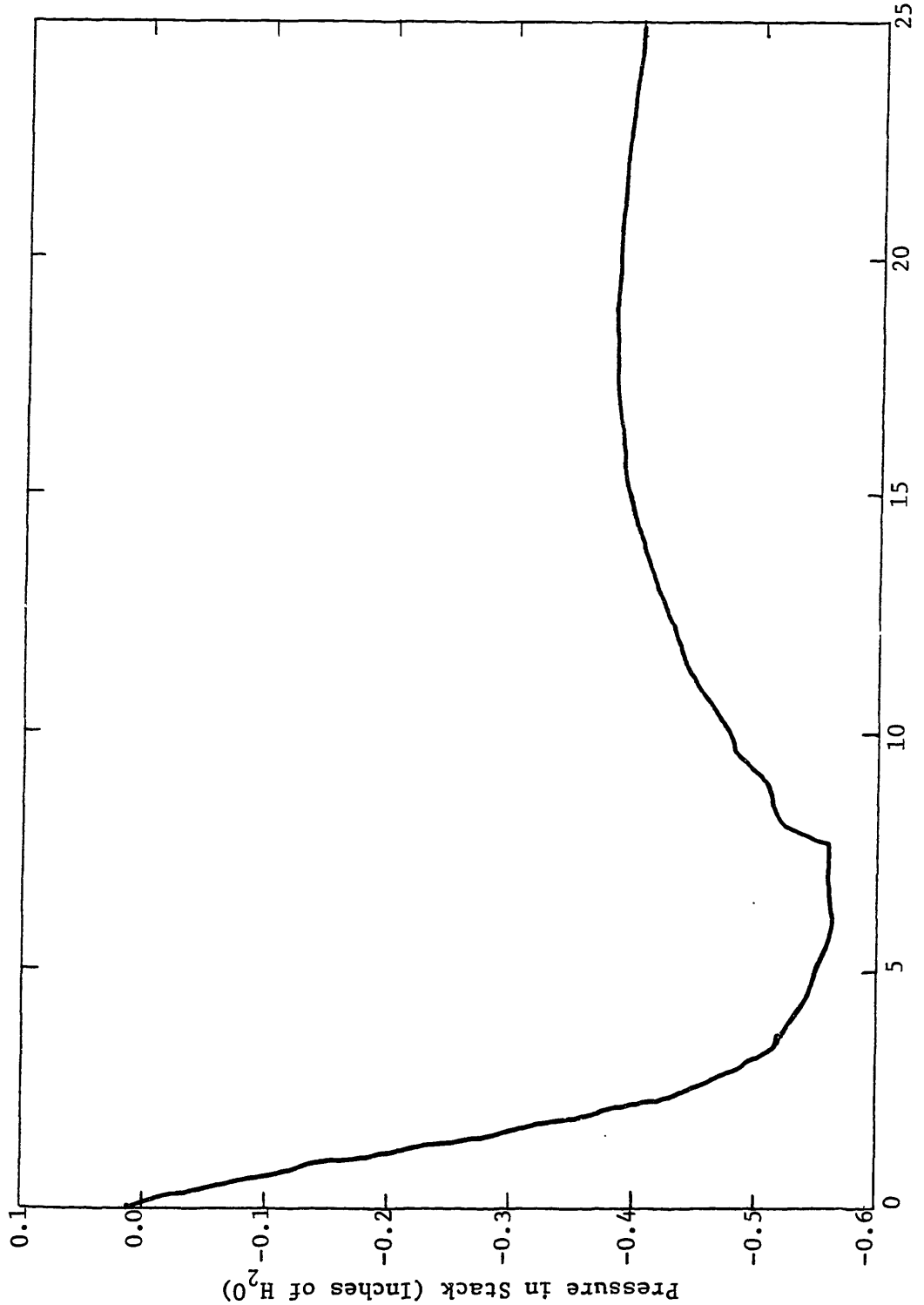

Figure 8-11: Pressure Drop in Stack under IGV Controls

The bypass control action is to open the bypass damper, its ability to reduce the furnace outlet flow is stronger than the fan IGVs. However the ID bypass control system controls only furnace outlet flow, while the IGV control system controls the inlet air as well. The bypass control has to reduce outlet flow faster than the IGV control system using higher control gains to acheive similar furnace pressure improvements. The control gains are limited for two reasons. First, very high gain may result in pressure and flow oscillation in the air/gas system. Second, a large stack pressure drop, shown in Figure 8-13, may also result from high bypass control gains.

A third system consisting of both a bypass and a fan IGV control system has been simulated with the St. Clair model. The furnace pressure transient improvement under this control system is plotted in Figure 8-14. The improvement in stack pressure transient is also shown in Figure 8-15.

These results are summarized in Figure 8-16 which compares the furnace pressure transient response using the various air/gas draft control systems.

The steam discharge control has also been simulated using the St. Clair Plant model. When the furnace pressure dropped 1 inch of water from its steady state value during simulation, a 6 sq.in. release valve started opening according the pressure control signal. The superheated steam started to discharge into boiler furnace. Only 10% of the working steam was used to achieve a fairly effective reduction in pressure excursion to 35% of the uncontrol level as shown in Figure 8-17.

8.6 Summary

The simulation study on the St. Clair plant model has shown that the implosion control systems reduce the furnace pressure excursion significantly during or following a main fuel trip condition. The effectiveness of the control depends on the control system configuration and design parameters. In general, it is necessary to have both feedback and feedforward controls to ensure a fast control action after the main fuel trip. The higher control gains and faster response control dampers result in a smaller furnace pressure excursion after a main fuel trip, however their values are limited by the negative pressure excursion in the stack introduced by the draft control actions. The steam discharge scheme is potentially fast and effective for furnace implosion, its usefulness depends on the availability of steam and has not been tested.

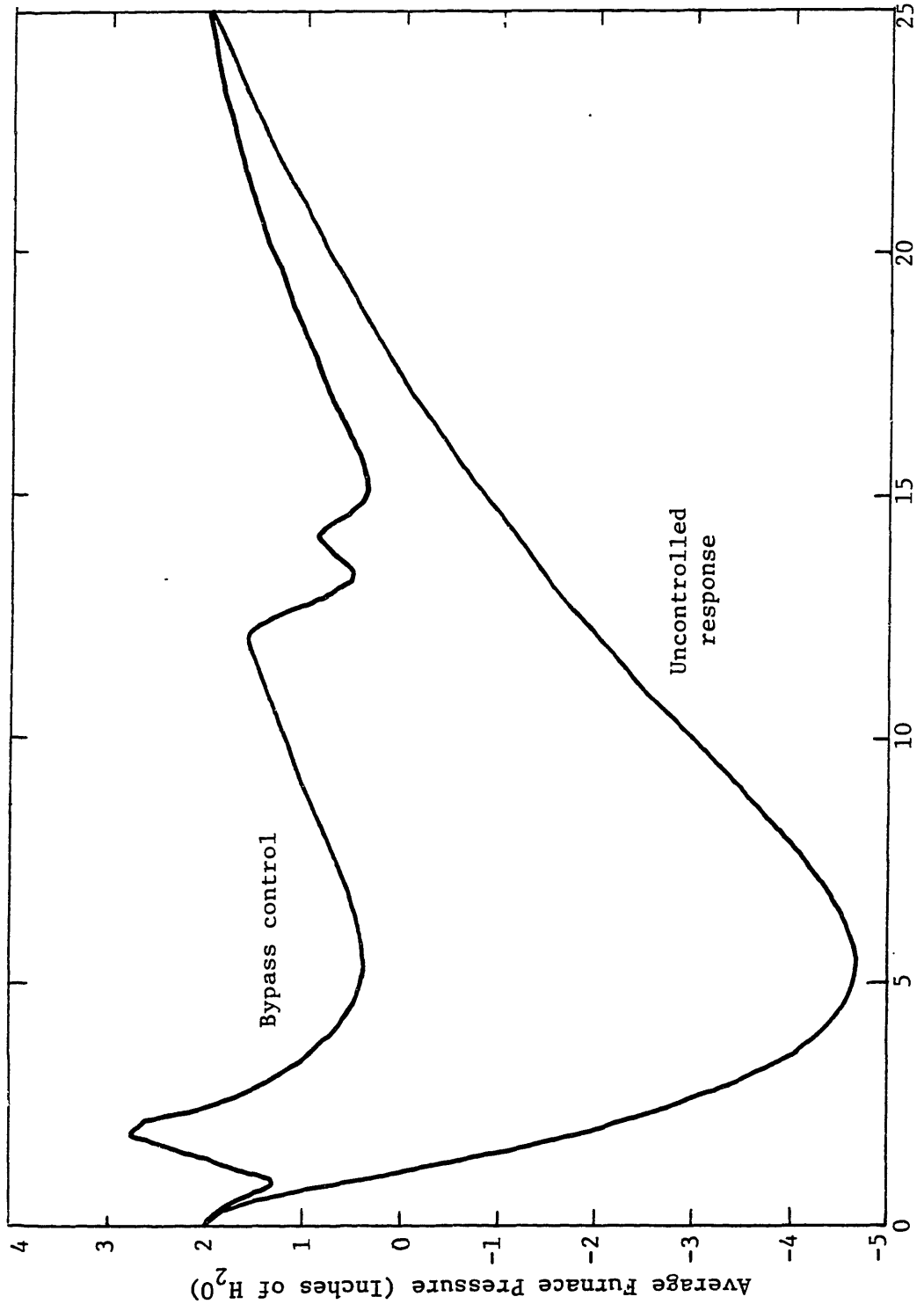

Figure 8-12: Effect of ID Fan Bypass Control

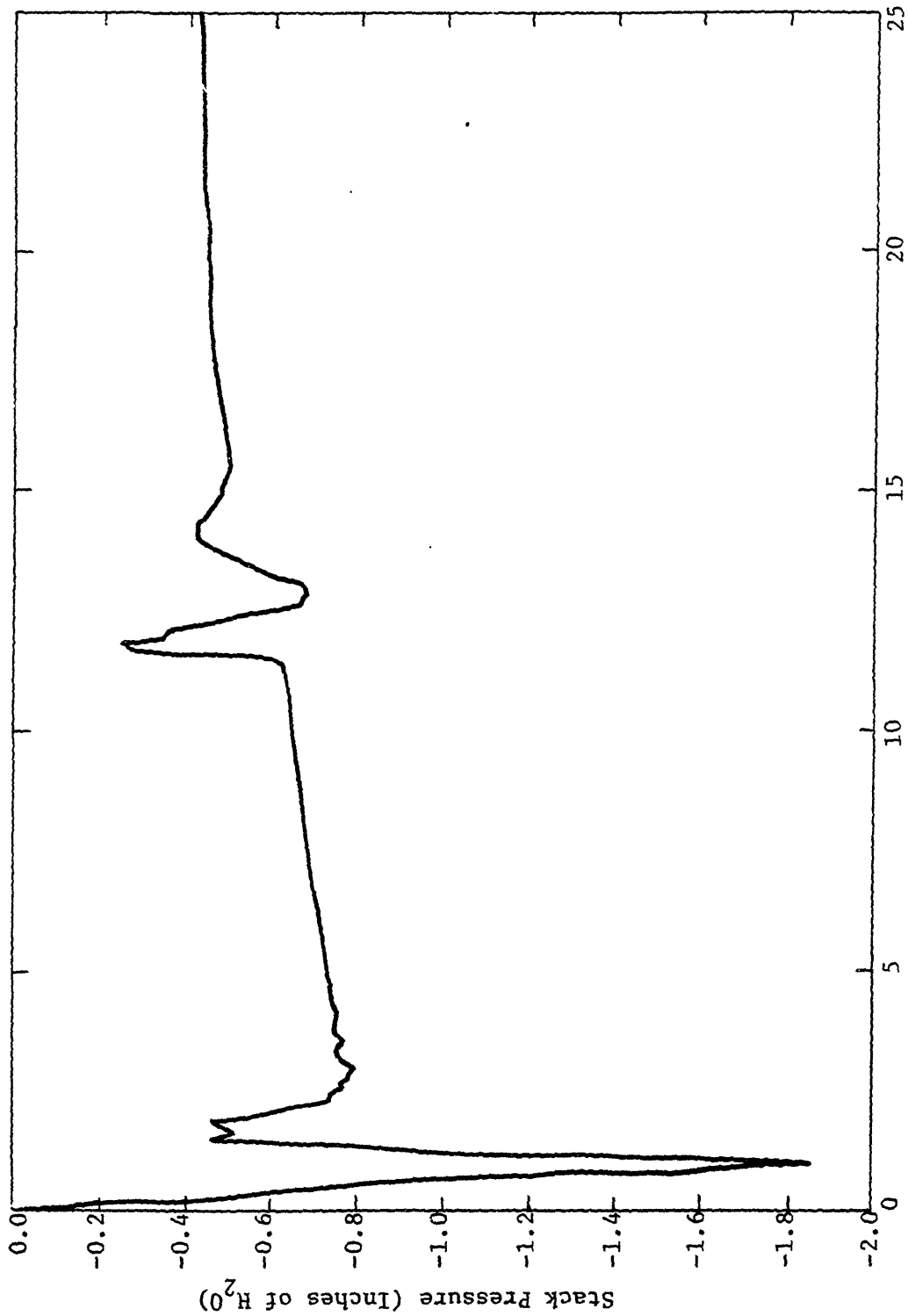

Figure 8-13: Pressure Drop in Stack under ID Fan Bypass Control

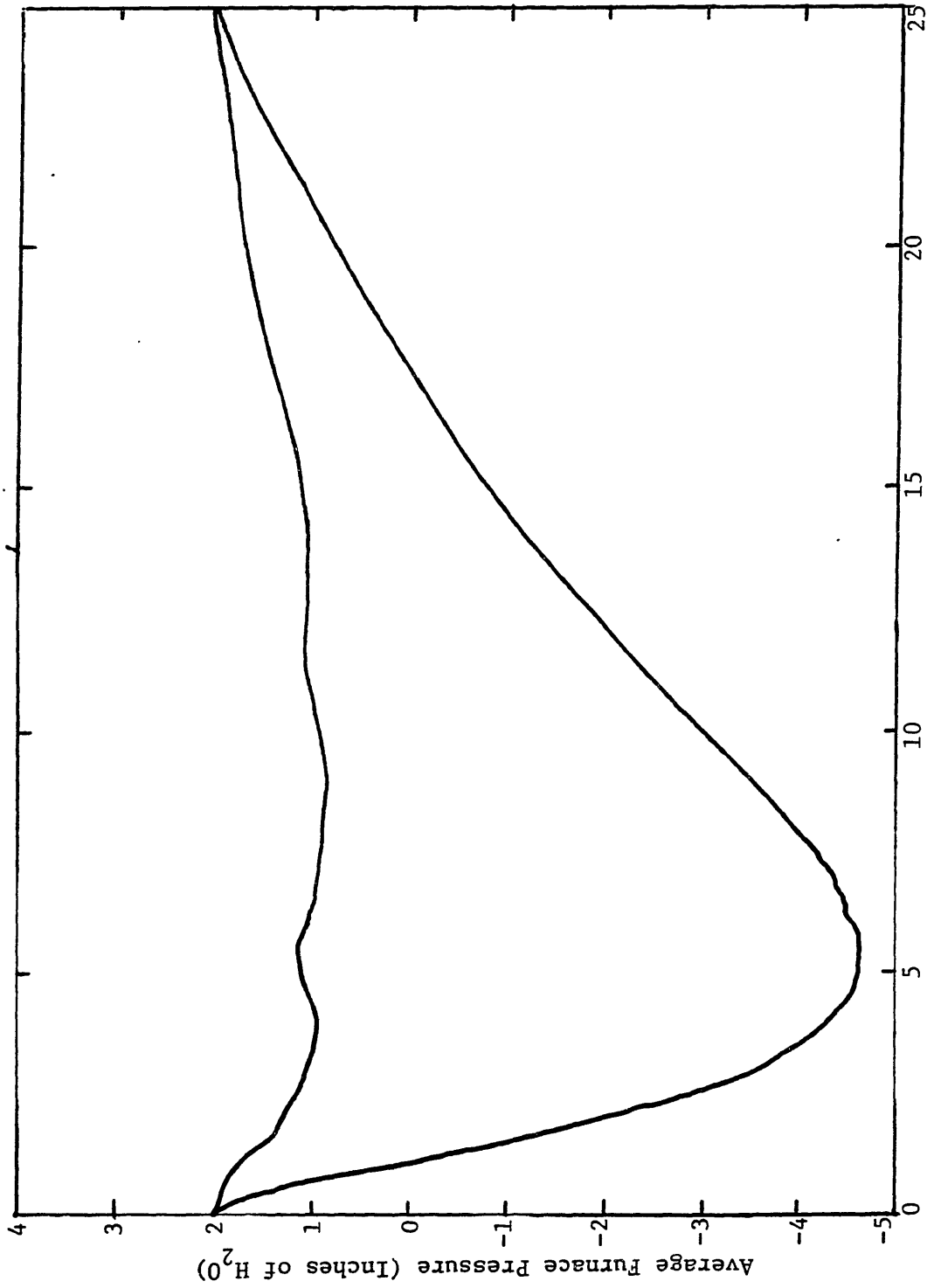

Figure 8-14: Effect of Both Bypass and IGV Controls

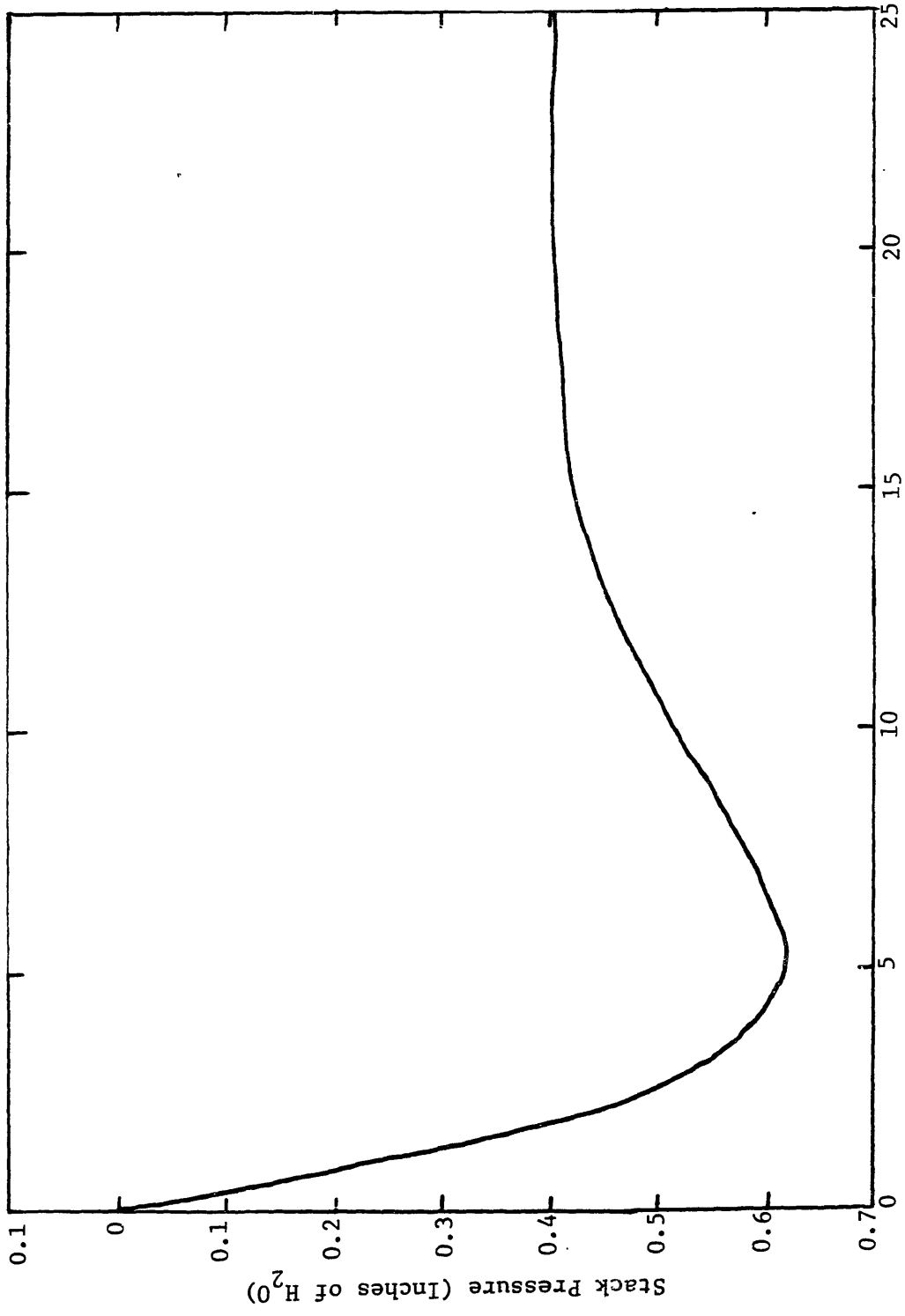

Figure 8-15: Stack Pressure under Both Bypass and IGV Controls

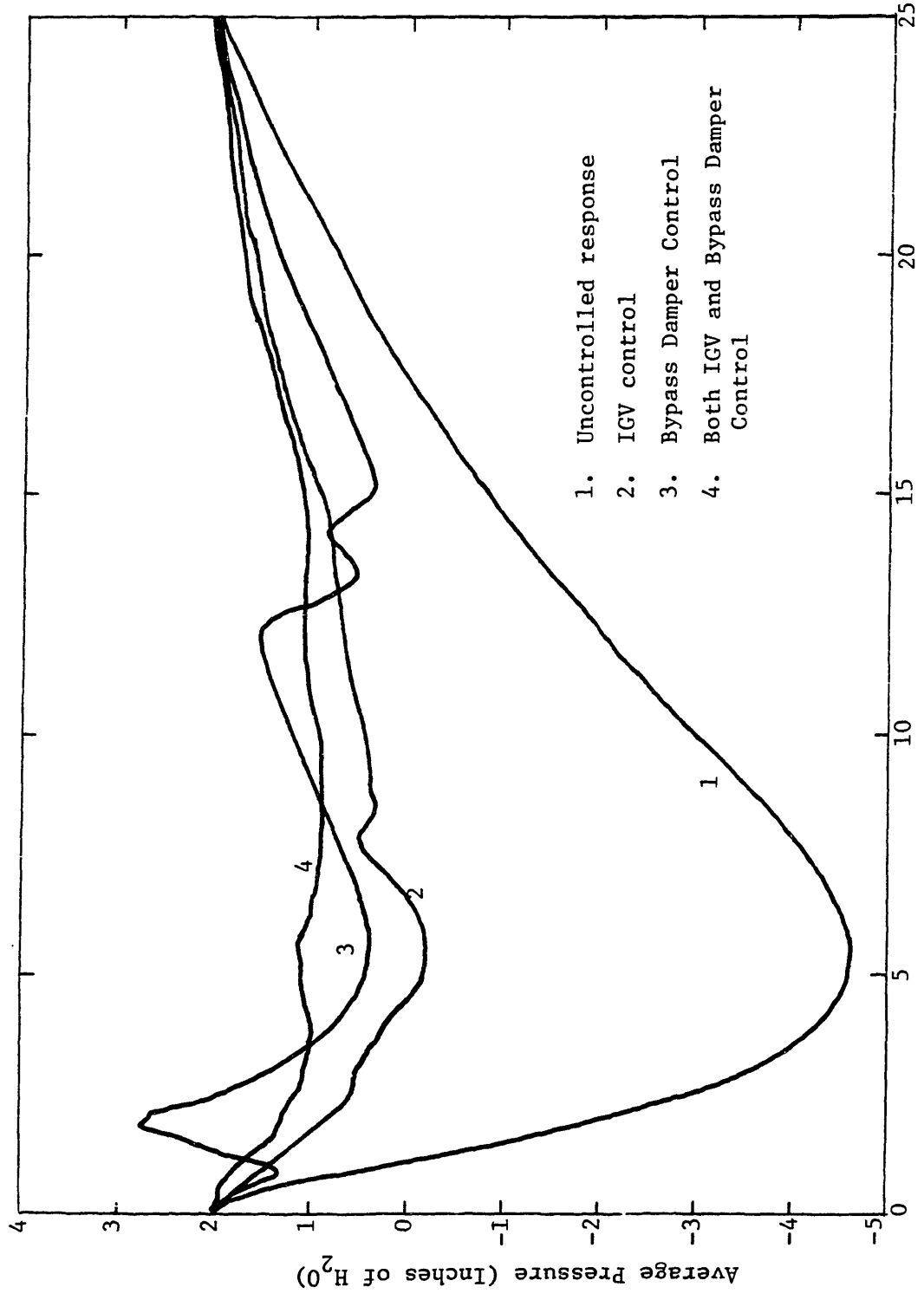

Figure 8-16: Comparison of Different Draft Control Systems

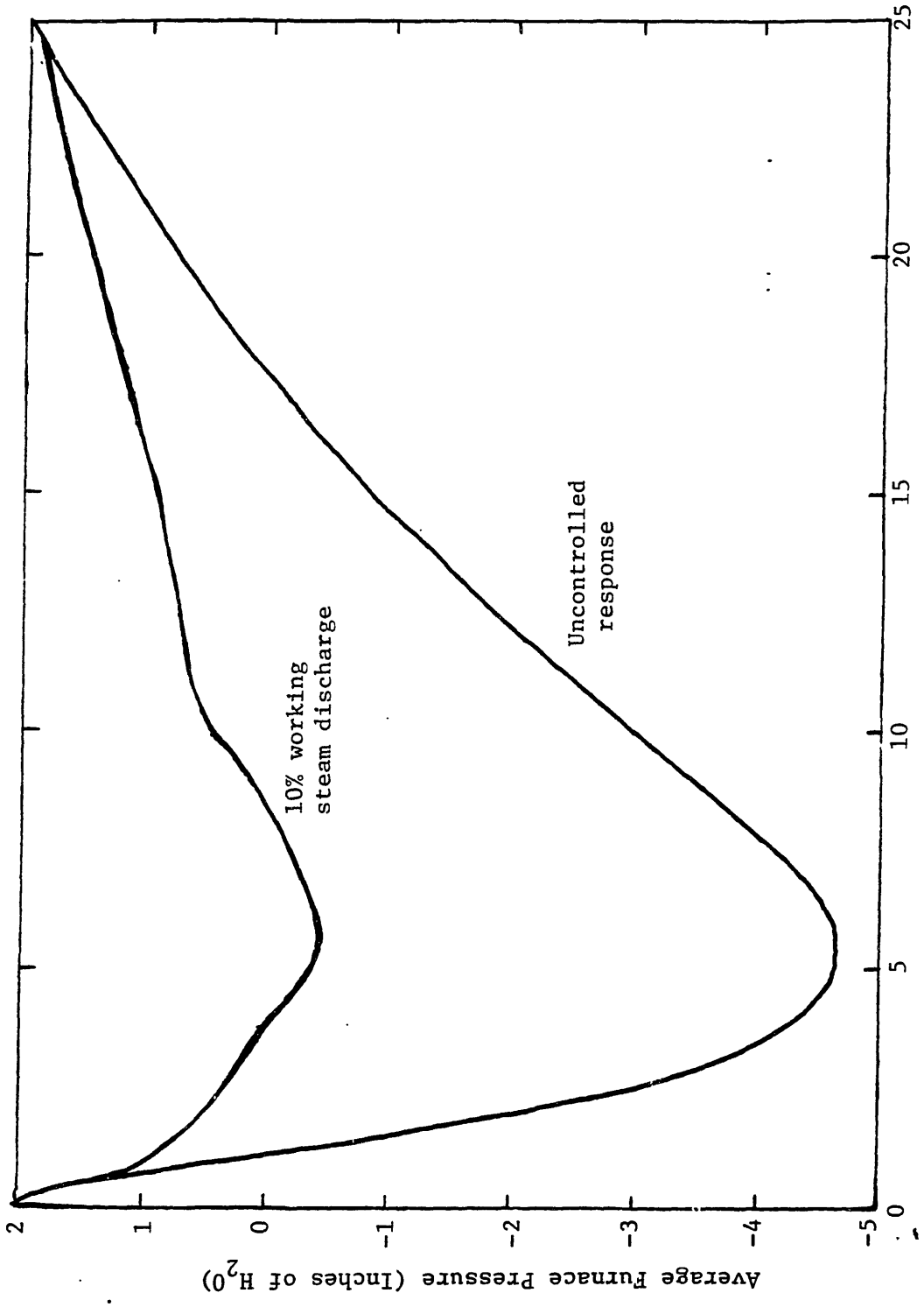

Figure 8-17: Steam Discharge for Furnace Implosion Control

Chapter 9
CONCLUSIONS AND RECOMMENDATIONS FOR FURTHER RESEARCH

9.1 Conclusions

The basic components of fossil fuel power plant air/gas systems have been mathematically modeled as a set of generic elements in this research. This set of generic elements can be connected by generalized junction structures to represent a variety of plant configurations. The elements are developed from the conversation laws of mass, momentum and energy, and are coupled together in an active manner by a well defined system structure. The response of pressure, flow, temperature, and heat transfer rate at any point in the system can be determined by the computer simulation subject to a wide range of fluid, mechanical and thermal disturbances. Such a formulation and simulation of the air/gas model is particularly useful for studies of air/gas pressure dynamics coupled with thermal transients in the same time frame, such as boiler furnace implosions.

To validate the mathematical model and illustrate the use of the computer code, basic system models for the Detroit Edison coal fired St. Clair Unit 3 and the oil fired Greenwood Unit 1 plants have been developed. Main fuel trip simulations have been conducted for both plants. The simulation predictions of the furnace pressure excursion for the two plants are in close

agreement with the data from the field implosion tests in terms of magnitude and time delay after a MFT. The applicability of the model for both predicting the furnace pressure excursion and designing an implosion control system has been demonstrated.

In the coal fired plant, the coal-ash deposit on the waterwall tubes has been identified as an important factor in determining the maximum pressure excursion after the main fuel trip. This is due to the fact that the ash deposit may have larger heat capacity than the combustion gas inside the furnace. After the fuel trip, the furnace gas temperature may drop below the ash deposit temperature causing heat transfer from the ash deposit to the flue gas inside the furnace. An analytical model has been developed to represent the ash deposit and a formal procedure has also been outlined to estimate the steady state heat transfer rate and the amount of deposition.

The system models used for the St. Clair and Greenwood plants are detailed, nonlinear models. For preliminary design studies, one simplified simulation model and its linearized version have been developed. If only furnace pressure is of interest and the control action is slow, the use of simplified methods for implosion studies is acceptable.

The detailed mathematical model has been used to evaluate various implosion control system designs. A set of damper and fan inlet guide vane positions can be modeled as control actions. Different draft control system implementations and actuator designs have been investigated using the computer model. These simulation results have shown that well designed draft control systems can limit pressure excursion in the furnace to an acceptable level. The limitations of these systems are the control actuator speed and the maximum negative pressure excursion in the stack during the control actions.

9.2 Recommendation For Further Research

Although the generic elements have been programmed in modular forms to represent different plant configurations, the user has to write a computer code to connect them together according to the junction structures. The difficulties associated with writing this code will be a major obstacle for wide usage of the mathematical model. Development of a general purpose user-friendly computer code which can construct system equations from user provided simple information would be very useful. A preliminary study has shown that the generic elements and junctions are adequate for a general purpose thermofluid network formulation. The code may take a format similar to DUCSYS with another degree of complexity. With such a computer code, the system modeling procedure would be greatly simplified, and the application of computer simulation techniques for power plant air/gas system dynamic analysis will become more widely used. The potential application scope for such a general purpose computer program may go beyond power plant air/gas systems.

The pulsation and implosion transient problems are interrelated in some situations. A large pressure variation resulting from pulsation may cause a trip and possibly initiate an implosion. On the other hand, a large furnace pressure excursion, and the control actions associted with it, may cause fans to work in their stall regions introducing oscillation and possibly instability. Using presently available model capability, such problems can be investigated in detail.

A steam discharge implosion control system has been proposed to overcome the draft control limitations. Preliminary study has shown that the

steam discharge control system can be potentially effective. A further investigation on steam availability and design feasibility is merited.

The effectiveness of proposed implosion control systems were never verified experimentally. A set of laboratory facilities for simulating power plant dynamics has been constructed at M.I.T., and some laboratory based evaluations on the control systems described in the thesis would be valuable.

The air/gas system model developed in this thesis has the capability to simulate the interface dynamics between the gas side and the water/steam side of the plant. To incorporate the model with some steam/water models would provide the capability to study an overall plant control system which responds to the system requests from both sides of the power generation unit in a wide time frame.

Appendix A
FLUID TRANSMISSION LINE

The equation for one dimensional, longitudinal wave propagation in a rigid walled duct of length L, with constant cross section area A may be derived with the aid of Figure A-1. In the derivation it is assumed that the line is lossless and that the average flow velocity is small compared to the velocity of sound in the fluid.

The application of continuity and momentum equations to the elemental control volume of Figure A-1 is the basis for the dynamic analysis of the transmission line. The continuity equation provides the following relationship for control volume:

$$\rho vA - (\rho vA + \frac{\partial(\rho vA)}{\partial x}dx) = \frac{\partial}{\partial t}(\rho A dx) \qquad (A.1)$$

where:

v = velocity of flow

P = static pressure

ρ = fluid density

x = distance along line

t = time

or in a form:

$$\rho\frac{\partial v}{\partial x} + v\frac{\partial \rho}{\partial x} = -\frac{\partial \rho}{\partial t} \qquad (A.2)$$

By applying the equation of state for a compressible fluid,

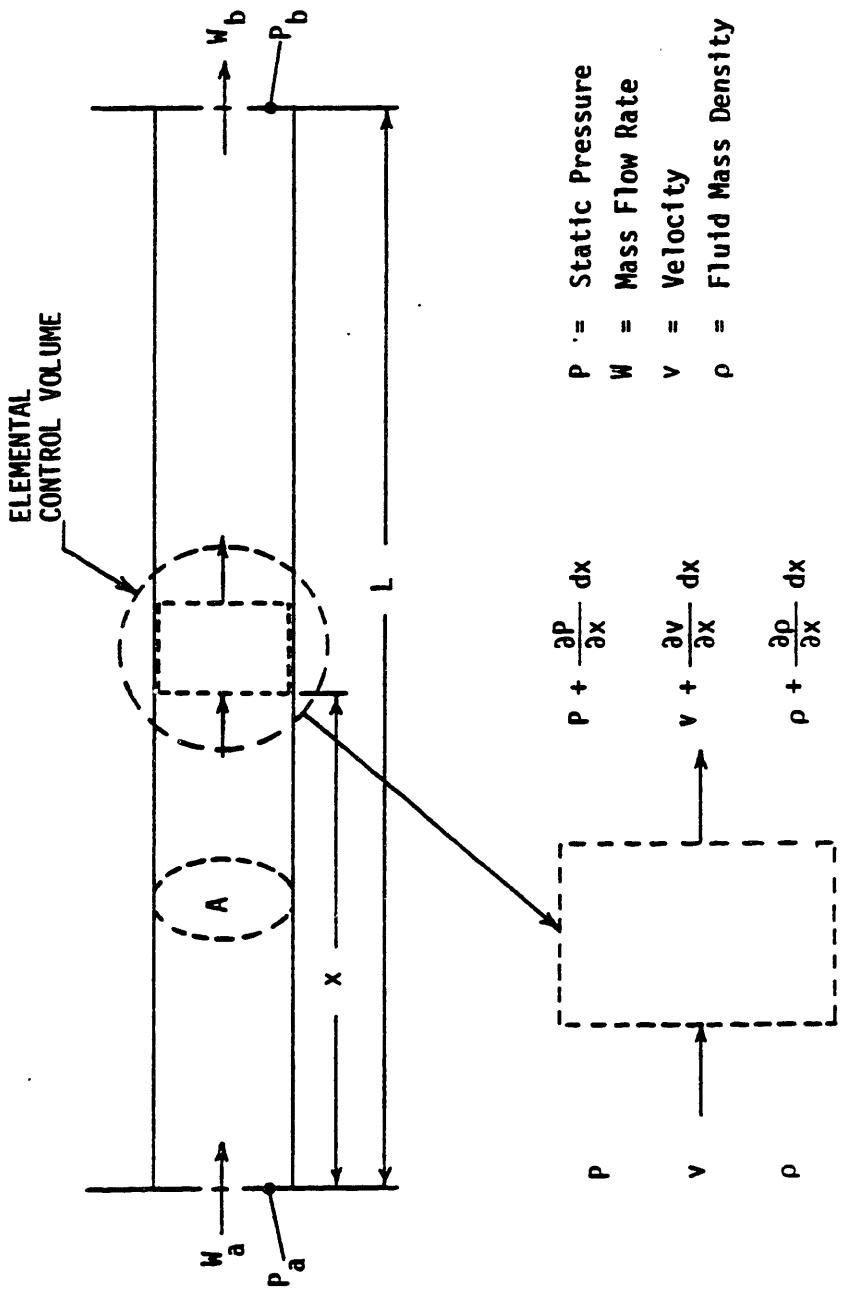

Figure A-1. Fluid Transmission Line Sktech Ref. [21]

$$d\rho = \frac{\rho}{\beta} dP \tag{A.3}$$

where β is fluid bulk modulus, the equation (A.2) then becomes:

$$\rho \frac{\partial v}{\partial x} + v \frac{\partial \rho}{\partial x} = - \frac{\rho}{\beta} \frac{\partial P}{\partial t} \tag{A.4}$$

The velocity of the sound in fluid is defined as:

$$C_o = \sqrt{\beta/\rho} = \sqrt{RT} \tag{A.5}$$

Applying the momentum equation to the control volume and neglecting the second order terms yields the equation:

$$(\rho \frac{\partial v}{\partial x} + v \frac{\partial \rho}{\partial t}) A dx - 2Av\rho \frac{\partial v}{\partial x} dx - Av^2 \frac{\partial P}{\partial x} dx \tag{A.6}$$

$$= -A \frac{\partial P}{\partial x} dx$$

By introducing the variable

$$v^* = \int \frac{dP}{\rho C_o} \tag{A.7}$$

The continuity and momentum equations can be written as [57]:

$$\frac{\partial (v + v^*)}{\partial t} + (v + C_o) \frac{\partial (v + v^*)}{\partial x} = 0 \tag{A.8}$$

$$\frac{\partial (v - v^*)}{\partial t} + (v - C_o) \frac{\partial (v - v^*)}{\partial x} = 0 \tag{A.9}$$

Ezekiel and Paynter [46] had used these two equations to solve the tranmission line with the convective terms. If using the assumption that the fluid velocity is much smaller than the acoustic velocity, $v << C_o$, equation

(A.4) becomes:

$$\rho \frac{\partial v}{\partial x} = -\frac{\rho}{\beta} \frac{\partial P}{\partial t} \tag{A.10}$$

Using equation (A.2) and the assumption that $v << C_o$, the equation (A.6) becomes:

$$-\frac{\partial P}{\partial x} = \rho \frac{\partial v}{\partial t} \tag{A.11}$$

If equation (A.11) is differentiated with respect to x and equation (A.10) is differetiated with respect to t, then the equations can be combined to form the classical wave equation:

$$\frac{\partial^2 P}{\partial x^2} = \frac{\rho}{\partial t^2} \frac{\partial^2 P}{\partial t^2} \tag{A.12}$$

and similarly the wave equation in terms of mass flow can be derived with a substitution:

$$W = \rho A v \tag{A.13}$$

and the dynamic mass flow wave equation becomes:

$$\frac{\partial^2 W}{\partial x^2} = \frac{\rho}{\partial t^2} \frac{\partial^2 W}{\partial t^2} \tag{A.14}$$

A spacial solution to the wave equations is obtained by using the Laplace transform on time. The Laplace transfomation of equations (A.12) and (A.14) is:

$$C_o^2 \frac{\partial^2 P(x,S)}{\partial x^2} = S^2 P(x,S) \tag{A.15}$$

$$C_o^2 \frac{\partial^2 W(x,S)}{\partial x^2} = S^2 W(x,S) \tag{A.16}$$

where:

C_o = velocity of sound in fluid

S = Laplace operator

The boundary conditions of P and W can be defined at x=0 as P(0,S) and W(0,S), additional boundary conditions can be derived by applying the Laplace transform to equations (A.10) and (A.11):

$$\frac{\partial W(0,S)}{\partial x} = -\frac{A\rho}{\beta} SP(0,S) \tag{A.17}$$

$$\frac{\partial P(0,S)}{\partial x} = -\frac{1}{A} SW(0,S) \tag{A.18}$$

The solutions of equations (A.15) and (A.16) become:

$$P(x,S) = (\cosh\gamma Sx)P(0,S) - Z_c(\sinh\gamma Sx)W(0,S) \tag{A.19}$$

$$W(x,S) = (\cosh\gamma Sx)W(0,S) - \frac{1}{Z_c}(\sinh\gamma Sx)P(0,S) \tag{A.20}$$

where Z_c is defined as the characteristic impedance by:

$$Z_c = \frac{C_o}{A} \tag{A.21}$$

Note that the hyperbolic trigonometric function can be expressed in exponential forms:

$$\sinh(u) = (e^u - e^{-u})/2 \tag{A.22}$$

$$\cosh(u) = (e^u + e^{-u})/2 \tag{A.23}$$

also note that that inverse Laplace transformation of a exponential function can be a delay operation in the time domain:

$$L^{-1}[e^{\gamma Sx}f(S)] = f(\ t+\gamma x\ ) \tag{A.24}$$

$$L^{-1}[e^{-\gamma Sx}f(S)] = f(\ t-\gamma x\ ) \tag{A.25}$$

This two mathematical properties in the solutions of the wave equations (A.19) and (A.20) give the time domain solutions a very convenient form if pressure and flow are represented by an alternative set of variables called wave scattering variables. The pressure waves in the line are partitioned into waves which travel in the flow direction, represented by U, and waves which travel opposite to the flow direction, represented by V. The pressure and flow at upstream and downstream ends of the line can be defined in terms of the wave scattering variables and the characteristic impedance Z_c:

$$PU = UU + VU \tag{A.26}$$

$$WU = (UU - VU)/Z_c \tag{A.27}$$

$$PD = UD + VD \tag{A.28}$$

$$WD = (UD - VD)/Z_c \tag{A.29}$$

Using the scattering wave variables, the solutions to the wave equations (A.12) and (A.14) are expressed in a form of pure delay.

$$UD(t) = UU(t-T_D) \tag{A.30}$$

$$VU(t) = VD(t-T_D) \tag{A.31}$$

The wave propagation delay is:

$$T_D = L/C_o \tag{A.32}$$

The time delay, T_D, represents the time required for a pressure wave to travel the length of the line. Equation (A.30) shows that for the wave which travels downstream the downstream value of UD at time $\bar{t}$ is equal to the upstream value UU at time $(t - T_D)$ where the time difference is the time required for the wave to travel the length of the line. Similarly, for the upstream traveling wave, the upstream value of VU at time t is equal to the downstream value of VD at time $(t - T_D)$.

Appendix B
COAL-ASH DEPOSIT ESTIMATION

B.1 Coal-Ash Fusibility Property and Deposit Structure

Ash fusibility has long been recognized as a tool for measuring the performance of coals related to slagging and deposit buildup. It is still perhaps the most basic means for predicting coal-ash performance. Other parameters are primarily used to explain or amplify ash-fusibility temperatures. In general, high fusion temperatures result in low slagging potential in dry-bottom furnaces while low fusion temperatures are considered mandatory for wet-bottom furnaces.

Many experimental methods have been developed for measuring the fusion temperature of coal-ash. The one used in this research is ASTM Standards D 1857, Fusibility of Coal-Ash. The test is based on gradual thermal deformation of a pyramid-shaped ash sample, 3/4 inch in high and 1/4 inch in equilateral trianglar base width. Mounted on a refractory substrate, the sample is heated at a prescribed rate in a gas or electric furnace. A controlled atmosphere (reducing or oxidizing, depending upon the test to be performed) is maintained inside the furnace. During the heating process, changes in the shape of pyramid are observed such as shown in Figure B-1, and the following four characteristic deformation temperatures are recorded.

1. Initial Deformation Temperature (IT): The temperature at which the tip of the ash pyramid begins to show any evidence of deformation. Shrinkage of the corn is ignored if the tip remains in

sharp.

2. Softening Temperature (ST), H = W: The temperature at which the ash sample has fused into a spherical shape in which the height is equal to the width at the base. The H = W softening temperature in a reducing atmosphere frequently is referred as the "fusion temperature".

3. Hemispherical Temperature (HT), H = W/2: The temperature at which the ash sample has fused into a hemispherical shape where the height is equal to 1/2 the width of the base.

4. Fluid Temperature (FT): The temperature at which the ash sample has fused down into a nearly flat layer with a maximum height of 1/16 inch.

The temperature fusibility of a coal-ash gives insight to the type of deposit formation to expect on a furnace tube surface. When the ash arrives at a heat-absorbing surface at a temperature near its softening temperature, the resulting deposit is likely to be porous in structure. If such a deposit is permitted to build up in a zone of high gas temperature, its surface can reach the melting point and then run down the furnace.

If the ash particles arrive at the heat-absorbing surface at temperature below the softening temperature, they will not form a bonded structure, but instead, will settle out as dust.

Molten to semimolten coal-ash slag deposit usually will not form on clean waterwall tubes since, upon approaching the relatively cooler tube surface, the slag particles become less adhesive because of rapid cooling in the adjaent wall area. Accordingly, coal-ash deposit is generally considered to be a two stage process. A primary layer of deposit first form on the waterwall tube surface. The resulting rise in the surrounding surface temperatures subsequently allows the adherence of a rigid plastic secondary deposit. Figure B-2 shows a cross

section of a typical waterwall slag deposit. The transition from primary to secondary layer, and the determination of molten or solid state of the secondary layer are all depend on the slag deposit fusion characteristics.

Barrett [2] has shown that fusion behavior of coal ashes is quite similar to that of a corresponding oxide mixture. Barrett concluded that if coal-ashes are findly grounded, intimately mixed, and brought to the same standard state before the fusion tests are made, then (1) the fusion temperature depends on the composition and not on the manner in which the composition is obtained; (2) the softening temperature is closely related to the equilibrium phase diagram of the corresponding oxide components which make up the ashes.

Based on these results, most ashes fusibility temperature calculations are made using the ash chemical compositions. One of the calculation methods is described in reference [8] to estimate the softening temperature in a reducing atmosphere of ash from U.S. eastern coal. The method assumes ASTM Standard experimental condition. The procedure is as follows:

1. Calculate S, A and T, which are defined as:

$$S = SiO_2 + TiO_2 + P_2O_5 \tag{B.1}$$

$$A = Al_2O_3 \tag{B.2}$$

$$T = CaO + 0.7MgO + 2.25Na_2O + 1.5K_2O \tag{B.3}$$

2. Obtain the percents S, A and T, which are expressed as:

$$\%S = \frac{S}{S+A+T} \times 100 \tag{B.4}$$

$$\%A = \frac{A}{S+A+T} \times 100 \tag{B.5}$$

$$\%T = \frac{T}{S+A+T} \times 100 \tag{B.6}$$

3. From Figure B-3, estimate the softing temperature of the coal-ash free of iron oxide, using the above designated percentage.

4. Define I = Fe_2O_3 and calculate the percent I, which is expressed as:

$$\%I = \frac{I}{S+A+T+I} \times 100 \tag{B.7}$$

5. From Figure B-4, estimate the lowering of the softening temperature due to the presence of Fe_2O_3. This will give the softening temperature of the ash.

Estep, et al. [12], has develop a procedure to estimate the hemispherical temperature under the ASTM Standard. The hemispherical temperature can facilitate the calculation of the critical temperature T_{cv} in the slag in Figure B-2. The critical temperature is defined as the temperature above which slag becomes completely molten. It is demonstrated that the critical temperature of the U.S. eastern coals at about 20% ferric percentage can be estimated from the following equation in terms of the hemispherical temperature HT:

$$T_{cv}(^{\circ}F) = HT + 200 \tag{B.8}$$

The transition from a primary to a secondary deposit has also been shown to be a function of a temperature. The temperature at which the secondary deposit begins to form has been referred to as the initial slagging temperature T_{is}. Alekhnovich,et al. [1], has proposed estimating the initial slagging temperature by the following procedure, using consituents on a weight-

fraction (not percentage) basis:

1. Calculate K:

$$K = (Na_2O+K_2O)^2 + 0.048(CaO+Fe_2O_3)^2 \quad (B.9)$$

2. Estimate T_{is}:

$$T_{is} = 1025 + 3.57(18\text{-}K) \quad (B.10)$$

The flow temperature is used to estimate the limit of thickness of the slag deposit. It is defined as the temperature at which slag has sufficient fluidity to allow free flow without difficulty. In general, the slag surface temperature in Figure B-2 can not exceed the flow temperature, since no accumulation of slag is expected beyond this point. Normally the flow temperature correspond to a slag viscosity of approximately 80 poise. Hoy,et al. [26], has defined the temperature-viscosity relation according to the following procedure:

1. Calculate the silica percentage

$$SP = \frac{100 \times SiO_2}{SiO_2+Equiv.Fe_2O_3+CaO+MgO} \quad (B.11)$$

2. Relate the slag viscosity to its temperature from the following equation

$$Log_{10}\eta = 4.468(SP/100)^2 + 1.265(10^4/T) - 7.44 \quad (B.12)$$

where η is slag viscosity (poise) and T is temperature (^oK). For coal-ash slag of known chemical composition, the flow temperature can be calculated by letting $\eta = 80$ poise and obtaining the corresponding temperature value.

Another temperature defined in the ash deposit model in Figure B-2 is

the freezing temperature T_{fr} where the movement of the slag is completely terminated. An estimation of freezing temperature T_{fr} is proposed by Reid and Cohen [49].

B.2 Coal-Ash Deposit Model

The structure of typical coal-ash deposit has been demonstrated in Figure B-2. A simplified analytical model can be established by dividing the coal-ash deposit into two layers -- the primary and the secondary. Each layer can be modeled as a pure thermal element as shown in Figure B-5. The radiant heat transfer resistance element developed in Chapter 2 can be used to model the heat transfer from the combustion gas to the surface of the ash deposit while the conduction heat transfer resistance element can be used to model the heat transfer through the primary and secondary deposit layers.

$$c_s M_s dT/dt = Q_i - Q_o \tag{B.13}$$

where c_s is the specific heat, and T is the temperature of the slag; Q_i and Q_o are the heat transfer into and out of the slag model element; M_s is the mass of the slag element, the densities of various forms of coal-ash slag deposits were averaged from several investigations and are listed in Table B-I. The volume of the coal-ash deposit shall be estimated using the procedure developed in Chapter 3.

Figure B-6 shows the thermal conductivities of ash deposits as functions of temperature. Seperate curves are given for the secondary and primary layer, because the thermal conductivity differs with the physical structure of the deposit. The given conductivities are averaged values of composite data

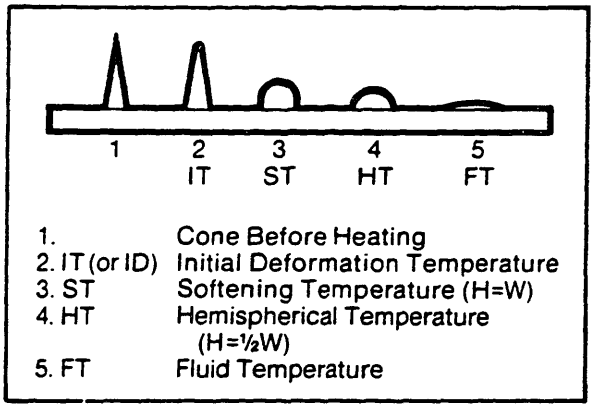

Figure B-1: Critical Temperatures in ASTM Standards D 1857 Ref. [8]

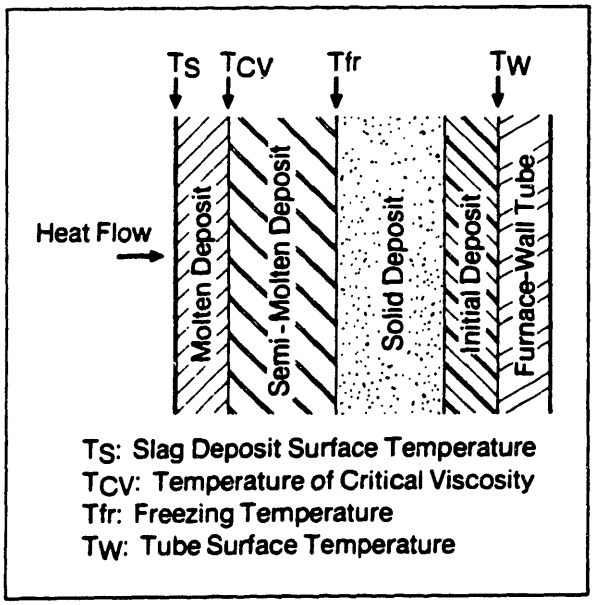

Figure B-2: Typical Coal-Ash Deposit Structure Ref. [8]

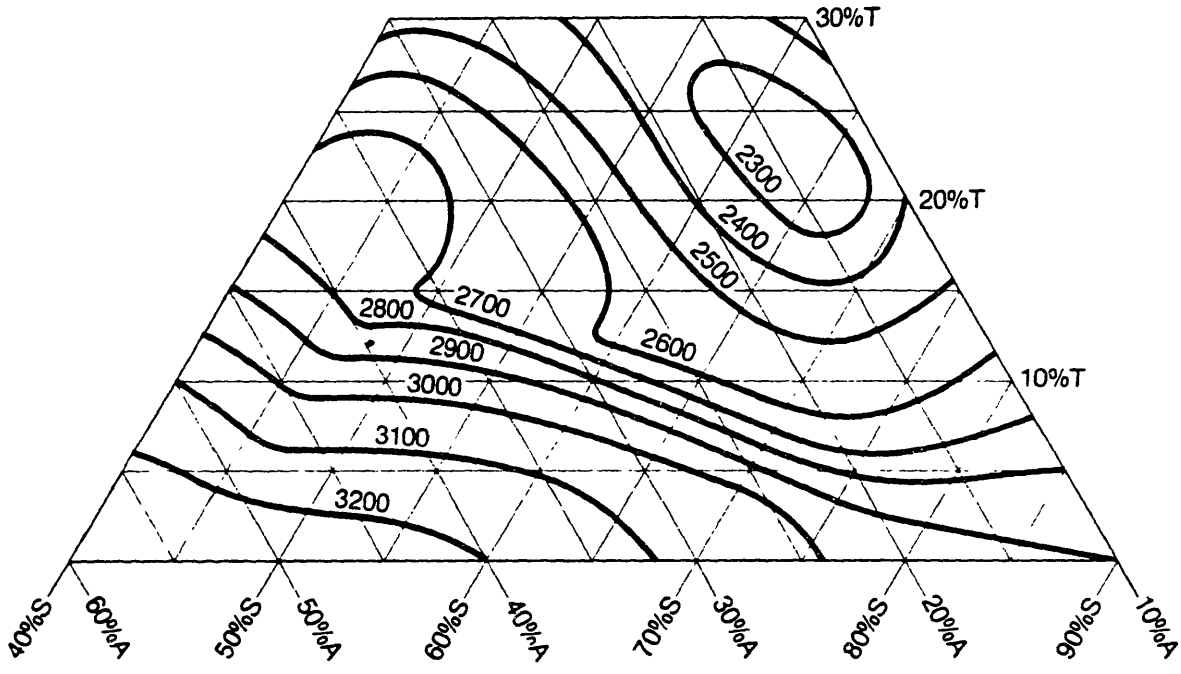

Figure B-3: Softening Temperature of Coal-Ash Free of Iron Oxide Ref. [8]

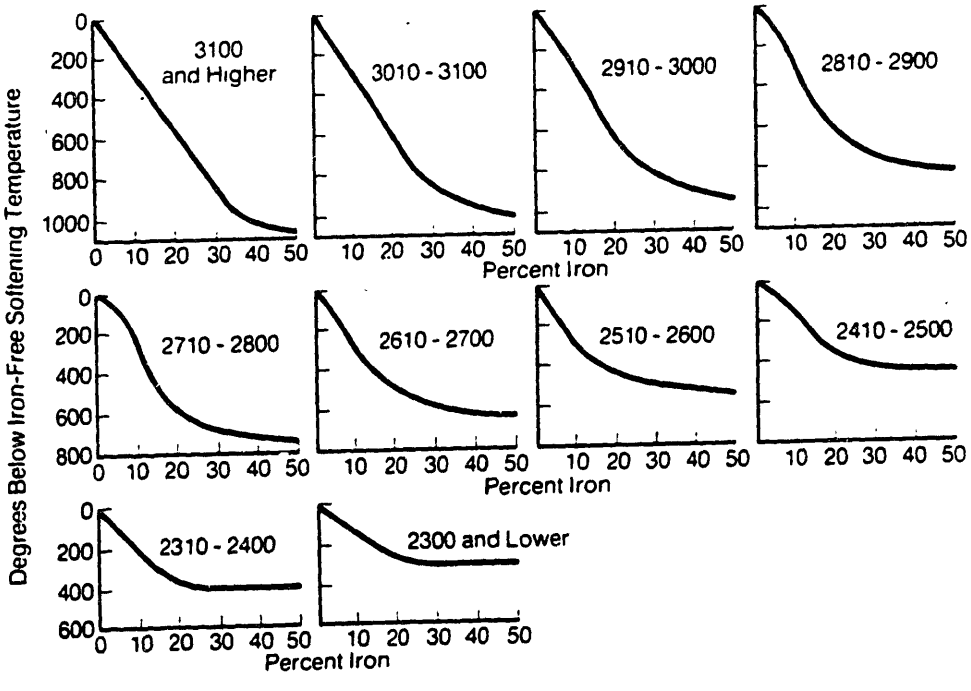

Figure B-4: Lowering of Softening Temperature from Iron Oxide Ref. [8]

obtained from Australian, Soviet and U.S. investigations [8].

Voskoboinikov [8] derived the following empirical equations for estimating the specific heat c_s of the slags. For the temperature range of 20 °C to 1350 °C

$$c_s = 0.169 + 0.201\times10^{-3}T - 0.277\times10^{-6}T^2 + 0.139\times10^{-9}T^3 + 0.17\times10^{-4}T(1\text{-}CaO/\mathcal{E}) \quad (B.14)$$

For the temperature range of 1350 °C to 1600 °C

$$c_s = 0.15\times10^{-2}T - 0.478\times10^{-6}T^2 - 0.876 + 0.016(1\text{-}CaO/\mathcal{E}) \quad (B.15)$$

where: c_s = specific heat (cal/gm. °C)

T = temperature (°C)

$\mathcal{E} = SiO_2 + Al_2O_3 + FeO + MgO + MnO$

Foerster and Weston [16] showed that their experimentally measured values for liquid and solid slags agreed well with the calculated values for Voskoboinikov's equation. The experimental values were slightly higher than the calculated values.

The radiative heat-transfer properties of the ash deposit are important in determining the heat transfer in the radiant furnace. The absorptivity of the ash deposits plays an important role in determining the heat absorbed by the deposit-laden waterwall tubes, while the emissivity of ash deposits determines how much heat will be reradiated by the tubes. The emissivity and absorptivity of ash deposits are a function of the wavelengths of the absorbed and emitted radiation, the surface temperature of the deposit, and the physical

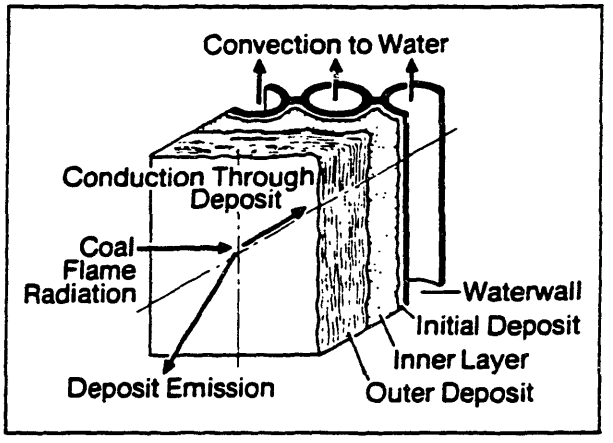

Figure B-5: Coal-Ash Deposit Heat Transfer Model Ref. [8]

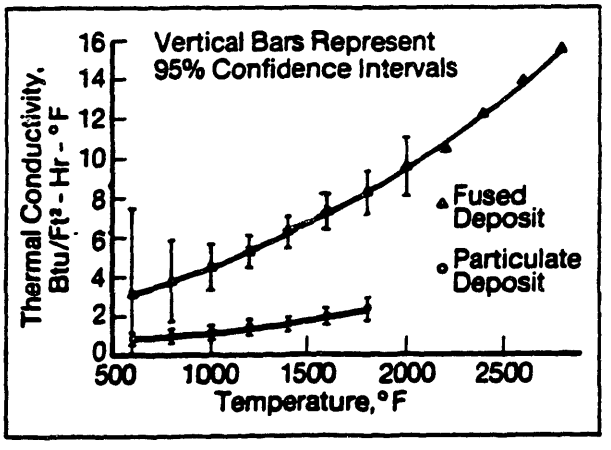

Figure B-6: Thermal Conductivity of Coal-Ash Deposits Ref. [8]

state of the deposit and the properties of the coal from which the deposits originated. The experimental determination of the emissivity and the absorptivity of coal-ash deposits involves a fair amount of procedural and instrumentational complexity. Goetz, et al. [18], has developed a laboratory technique employing spectral spans, and a computational procedure, to determine the overall emissivity and the absroptivity of ash deposits. Table B-II summarizes the results. Here the deposits are categorized by physical state of the deposit as well as the parent coal source. The surface emissivity is also temperature dependent. Figure B-7 plots the surface emissivity of the coal-ash deposit as a function of temperature. Seperate curve are given for the fused layer and the primary deposits emissivity differs with the deposit structure. Such emissivities are the average values of composite data from Australian, Soviet and U.S. investigations [8].

DENSITY OF VARIOUS COAL-ASH SLAG DEPOSITS

Deposit Form	Density (lb/ft^3)
Liquid Slag	150-180
Dense Solid Slag	140-170
Solid Ash	120-160
Loose, Powder Ash	15-35
Fine, Ground Slag	60-90

TABLE B-I Density of Various Coal-Ash Deposits Ref. [8]

A SUMMARY OF EMISSIVITIES AND ABSORPTIVITIES OF ASH DEPOSITS

Physical state	Parent Coal Region	Emissivity	Absorptivity
Initial deposit	Eastern U.S.	0.75-0.76	0.71-0.76
Initial deposit	Western U.S.	0.37-0.56	0.52-0.61
Inner layer	Eastern U.S.	0.79-0.93	0.67-0.84
Inner layer	Western U.S.	0.68	0.62
Outer deposit	Western U.S.	0.66-0.87	0.62-0.82
Molten inner layer	Western U.S.	0.90	0.91

TABLE B-II: Emissivities and Absorptivities of Coal-Ash Deposit Ref. [8]

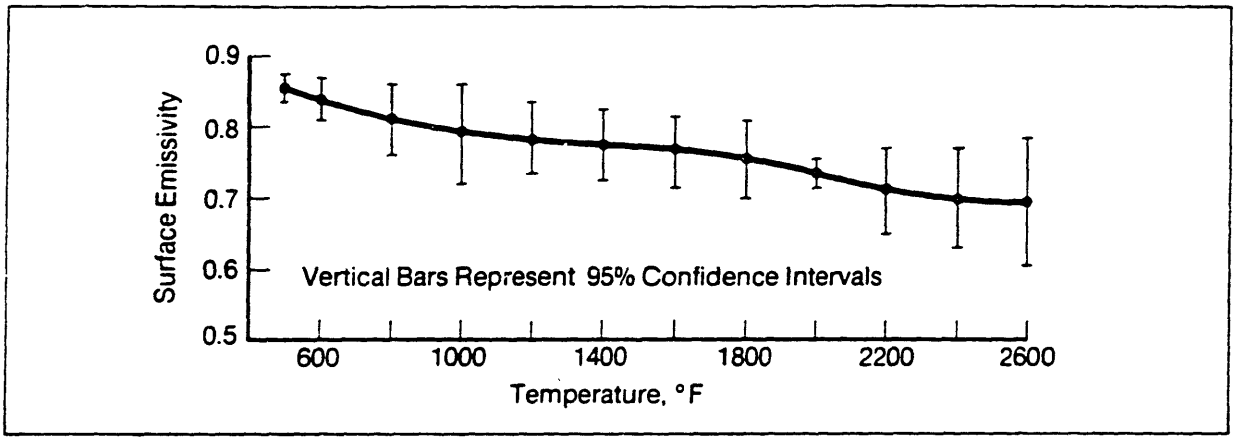

1 Surface emissivity of fused coal-ash deposits

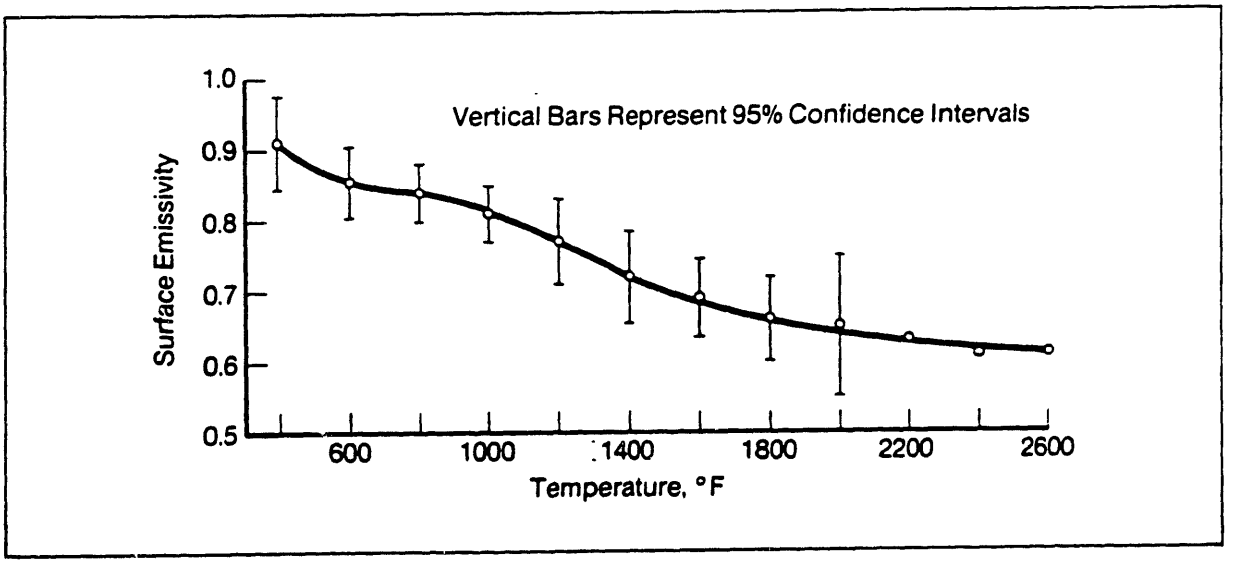

2 Surface emissivity of particulate coal-ash deposits

Figure B-7: Surface Emissivity of Coal-Ash Deposits Ref. [8]

Appendix C
CONTROL ELEMENTS

The gain, summer and integrator blocks are the fundamental blocks of linear control systems. From these three building blocks, virtually any linear control system can be synthesized. The gain and integrator blocks are single-input single-output devices, while the summer is a multi-input single-out device. Certain combinations of the basic blocks are commonly used in control systems. The proportional plus integral control block has two gains associated with it and is most often used as a controller. The symbolic representations of these blocks are shown in Figure C-1.

In the simulation of dynamic systems, the introduction of control elements creates interfacing problems between the control system and the controlled system. Two elements are created to serve as interfaces, the sensor and the driver. These two elements are not elements per se, because they do not have any equations of state which describe their behavior. They are merely links between two information systems. Figure C-2 shows a conceptual diagram and the symbols for these two elements. In a simulation, the sensor will output a control signal equivalent to the value of variable it is sensing. Similarly, a driver will take a signal at its input and deliver it to a system parameter (such as a system resistance).

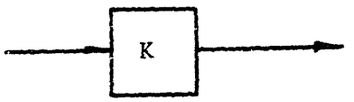

Gain

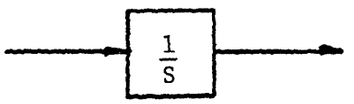

Integrator

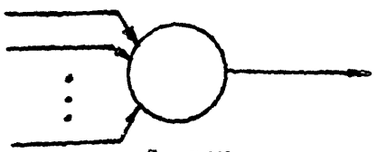

Summer

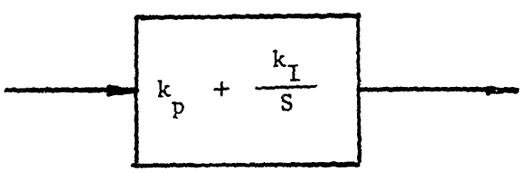

P-I Controller

Figure C-1: Control Element Representation

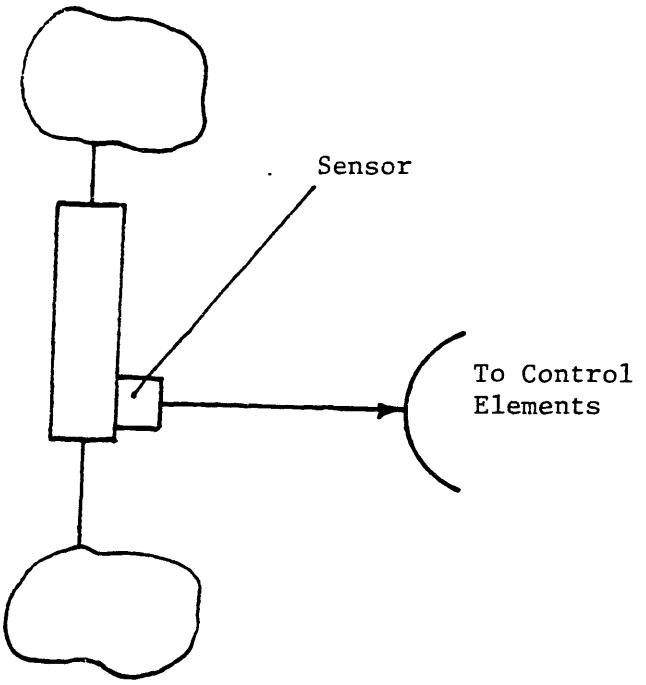

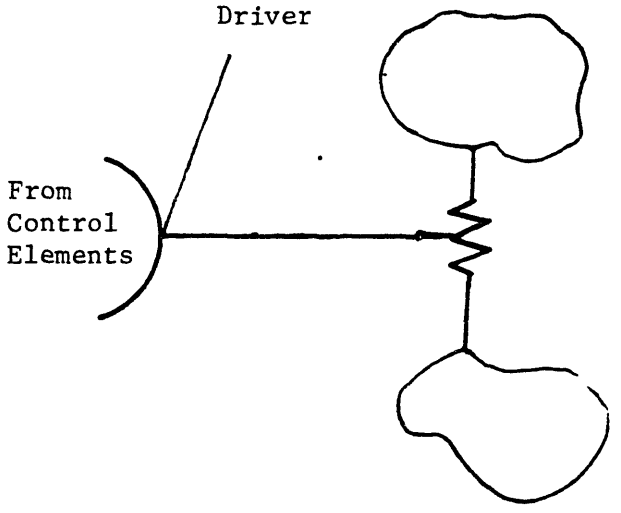

Figure C-2: The Sensor and Driver Representation

References

[1] Alekhnovich,A.N., Bogomolov,V.V., Novitskii,N.V. and Ivanova,N.I.
A Study of the Slagging Properties of Kuzneck Coal Ash.
In *Soviet Power Engineering* , . Electricheskie Stantsii, 1977.

[2] Barrett,E.P.
The Fusion, Flow, and Clinkering of Coal Ash: A Survey of the Chemical Background.
In Lowry,H.H. (editor), *Chemistry of Coal Ultilization*, chapter 15. John Wiley and Sons, New York, 1945.

[3] Bragg,S.L.
Application Of Reaction Rate Theory To Combustion Chamber Analysis.
Technical Report Technical Report 16170, C.F., Aeronautical Research Council, 1953.

[4] Bragg,S.L. and Holliday,J.B.
The Influence of Altitude Operating Conditions On Combustion Chamber Design.
In *In Proceedings Of Combustion Colloquium.* Butterworth, 1955.

[5] Brown,F.T.
The Transient Response Of Fluid Line.
Journal Of Basic Engineeering, Trans. ASME 84:547, Dec., 1962.

[6] Brown,F.T., Margolis,D.L. and Shah,R.P.
Small-Amplitude Frequency Behavior Of Fluid Line With Turbulent Flow.
Technical Report 69-FE-11, ASME, 1969.

[7] Babcock and Wilcox.
Steam/Its Generation and use.
Babcock and Wilcox, New York, 1978.

[8] Singer,J.G.
COMBUSTION: Fossil Power Systems.
Combustion Engineering, Inc., 1981.

[9] Dolezal,R.
Large Boiler Furnace.
Elsevier Publishing Company, Amsterdam, 1967.

[10] Joint Computer Facility.
Dysys-Users Manual.
Technical Report 2nd Edition, Massachusetts Institute of Technology, 1980.

[11] Essenhigh,R.H.
Introduction To Stirred Reactor Theory To Design Of Combustion Chamber.
In Palmer,H.B. and Beer,J.M. (editor), *Combustion Technology*, . Academic Press, 1974.

[12] Estep,T.G., Seltz,H. and Osborn,W.J.
Determination of the Effect of Oxides of Sodium, Calcium, and Magnesium on the Ash Fusion Temperatuture by Use of the Synthetic Coal Ash.
In *Mining and Metallurgical Advisory Boards, Bulletin 74*, . Carnegie Institute of Technology, 1937.

[13] P.Euchner and J.Undrill.
Furnace Implosions - An Analysis and Proposed Protective Systems.
American Power Conference , 1975.

[14] F.Faubert.
Main Fuel Trip Test On Unit 3 At St. Clair Power Plant.
Technical Report 76C84, The Detroit Edison Company, 1976.

[15] F.Faubert.
Main Fuel Trip Test On Unit 3 At River Rouge Power Plant.
Technical Report 76D90, The Detroit Edison Company, 1977.

[16] Foerster,E.F. and Weston Jr,P.L.
Heat Content of Some Blast-Furnace and Synthetic Slags.
Technical Report 6886, U.S. Bureau of Mines, 1967.

[17] Franks,R.
Modeling and Simulation in Chemical Engineering.
Wiley-Interscience, 1972.

[18] Goetz,G.J. et al.
Development of a Method for Determining Emissivities and Absorptives of Coal-Ash Deposits.
Technical Report ASME paper 78-WA/FU-6, American Society of Mechanical Engineers, 1978.

[19] Goldscheid,F.R. and Wormley,D.N.
Frequency Response Of Blower/Duct/Plenum Air Cushion System.
Journal Of Hydronautics , 1977.

[20] F.Goldschmied, D.Wormley and D.Rowell.
Air/Gas System Dynamics of Fossial Fuel Power Plants Volume 1: Phase 1 Overview.
Technical Report CS-1444, EPRI, 1980.

[21] F.Goldschmied, D.Wormley and D.Rowell.
Air/Gas System Dynamics of Fossial Fuel Power Plants Volume 2: Mathematical System Analysis.
Technical Report CS-1444, EPRI, 1980.

[22] F.Goldschmied, D.Wormley and D.Rowell.
Air/Gas System Dynamics of Fossial Fuel Power Plants Volume 3: Experimental Pressure Test Data of a 500 MW Unit and of a 125 MW Unit.
Technical Report CS-1444, EPRI, 1980.

[23] F.Goldschmied, D.Wormley and D.Rowell.
Air/Gas System Dynamics of Fossial Fuel Power Plants Volume 4: Experimental Vibration and Acoustic Test Data of a 500 MW Unit.
Technical Report CS-1444, EPRI, 1980.

[24] F.Goldschmied, D.Wormley and D.Rowell.
Air/Gas System Dynamics of Fossial Fuel Power Plants Volume 5: System Excitation Sources.
Technical Report CS-1444, EPRI, 1981.

[25] Goodson,R.E. and Leonard,R.G.
A Survey Of Modeling Techniques For Fluid Line Transients.
Technical Report 71-WA/FE-9, ASME, 1971.

[26] Hoy,H.R., Roberts,A.G. and Wilkin,D.M.
Behavior of Mineral Matter in Slagging Gastification Processes.
Insitution of Gas Engineering , 1965.

[27] Karnopp,D. and Azarbauani,S.
Pseudo Bond Graph For Generalized Compartmental Models in Engineering and Physiology.
Journal Of the Franklin Institute , 1981.

[28] Karnopp,D.
Pseudo Bond Graphs For Thermal Energy Transport.
Journal Of Dynamic Systems, Measurements, and Control , 1978.

[29] Karnopp,D.
State Variables and Pseudo Bond Graphs For Compressible Thermofluid Systems.
Journal Of Dynamic Systems, Measurements, and Control , 1979.

[30] W.Kirchmeier.
Air/Gas Path Testing for Furnace Implosion Studies.
In *Power Plant Testing and Thermal Performance Analysis Workshop*, . EPRI, 1978.

[31] W.Kirchmeier.
Effects of Firing Rate and Fuel Type on Furnace Implosions.
In *Joint Power Generation Conference.* Gilbert/Commonwealth, 1980.

[32] W.Kirchmeier.
Computer Implementation of Damper Control Studies.
In *Proceedings of The Third Power Plant Dynamics, Control and Testing Symposium.* Gilbert/Commonwealth, 1977.

[33] W.Kirchmeier.
Furnace Negative Pressure Excursions.
In *Proceedings of The Second EEI Prime Movers/Architect- Engineer Information Exchange.* Gilbert/Commonwealth, 1978.

[34] W.Kirchmeier.
Air/Gas Dynamics Of Fossil Fuel Power Plant -- Implosions.
In *Symposium On Power Plant Fans -- The State Of The Art*, . EPRI, 1982.

[35] D.Koennman.
A Fresh Solution To the Implosion Problem.
In *1982 Joint Power Generation Conference*, . ASME, 1982.

[36] Kuo,T.J., Kuwata,M., Shieh,W. and Essenhigh,R.H.
Development Of Physical And Mathematical Model Of Incinerator, Part 2: Initial Testing Of A Real System.
In *In Proceedings Of 1970 National Incinerator Conference.* ASME, 1970.

[37] T.Laskowski.
Atroria No.6 Final Report Of The Steam Generator Master Trip Model Study.
Technical Report R3-80, Power Technologies Inc., 1980.

[38] R.Leithner, W.Hermann and G.Trautmann.
Flue Gas Pressure Vibration in Steam Generators When Firing System Break Down.
Combustion , 1980.

[39] Levenspial,O.
Chemical Reaction Engineering.
John Wiley and Sons, Inc., 1962.

[40] Masada,G.Y.
Modeling and Control Of Power Plant Boiler-Turbine-Generator Systems.
PhD thesis, M.E. Department, M.I.T., 1980.

[41] Smith,L.P., Dixon,R.R. and Shor,S.W.
Modular Modeling System (MMS): A Code For The Dynamic Simulation of Fossil and Nuclear Power Plants.
Technical Report CS/NP-3016-CCM RP1184-2, EPRI, 1983.

[42] Task Group under Subcommittee No.1 of the Committee on Boiler-Furnace Explosions.
Standard for the Protection of Furnace Implosions in Multiple Burner Boiler-Furnaces.
Technical Report 85G-1978, National Fire Protection Association, 1978.

[43] Paynter,H.M.
Analysis and Design of Engineering Systems.
The M.I.T. Press, 1961.

[44] Paynter,H.M.
Thermofluid Process Dynamics in Boiler Modeling.
In Berkowitz (editor), *Proceedings Of Boiler Modeling.* The Mitre Corporation, 1974.

[45] Paynter,H.M.
On An Analogy Between Stochastic Preocess And Monotone Dynamic System.
Conference On Control Technology , 1956.

[46] Ezekiel,F.D. and Paynter,H.M.
Computer Representation of Engineering Systems Involving Fluid Transients.
Trans. ASME 79:1840-1850, 1957.

[47] Paynter,H.M.
M.I.T. Class Notes for 2.155.
1981.

[48] Rao,S.T.R., Kuo,T.J. and Essenhigh,R.H.
Characterization Of Stirring Factors By Cold Model Simulation.
In *In Proceedings Of 1970 National Incinerator Conference.* ASME, 1970.

[49] Reid,W.T. and Cohen,P.
The Flow Characteristics of Coal-Ash Slags in the Solidification range.
Technical Report 66, Transaction of ASME, 1944.

[50] Rohsenow,W. and Choi,H.
Heat, Mass, and Momentum Transfer.
Prentice-Hall, Englewood, N.J., 1961.

[51] J.Roseborough.
Simulation and Control of Pulsations in Ductwork Systems.
Master's thesis, Department of M.E., M.I.T., 1983.

[52] Shearer,J.L., Murphy,A. and Richardson,H.
Introduction To System Dynamics.
Addison-Wiley Publishing Company, 1971.

[53] Shieh,W. and Essenhigh,R.H.
Combustion Of Computer Cards In A Continuous Test Incinerator: Comparison Of Theory And Experiments.
In *In Proceedings Of 1972 National Incinerator Conference.* ASME, 1972.

[54] Sidell,R.S. and Wormley,D.N.
An Efficient Simulation Method For Distributed/Lumped Fluid Network.
Journal Of Dynamic System, Mecrurement and Control 99, 1977.

[55] R.Srodawa, W.Roller and M.Higazy.
Furnace Implosion Control Role Of Simulation During Oil Fire Start Up.
In *Fourth Power Plant Dynamics, Control and Testing Symposium.* The Detroit Edison Company, 1980.

[56] Streeter,V.L. and Wylie,E.G.
Hydraulic Transients.
McGraw-Hill, 1967.

[57] Streeter,V.L., Ed. in Chief.
Handbook of Fluid Dynamics.
McGraw-Hill, 1961.

[58] Thring,M.W.
The Scince Of Flame And Furnaces.
Chapman and Hall LTD, London, 1962.

[59] Tomovic Mileta.
Dynamic Behavior Of Fan Duct Systems.
Master's thesis, Department of M.E., M.I.T., 1981.

[60] H.Vollmer, J.Undrill and H.Grim.
Draft Control System Design, Simulation and Test For a High Implosion Potential Boiler.
In N.Bloom and E.Burns (editor), *Plant Performance Testing and Evaluation Workshop,* . Science Application Inc., 1979.